Prediction and Optimization Study of the Effect of Laser Parameters on Weld Quality using Taguchi Array for Aluminium Alloy 5083

Author

Ameera Noor

Regn Number

00000119826

Supervisor

Dr. Salman Nisar

Co Supervisor

Dr. Usama Siddiqui

PAKISTAN NAVY ENGINEERING COLLEGE

NATIONAL UNIVERSITY OF SCIENCES AND TECHNOLOGY

ISLAMABAD

August, 2018

Prediction and Optimization Study of the Effect of Laser Parameters on Weld Quality using Taguchi Array for Aluminium Alloy 5083

Author

Ameera Noor

Regn Number

00000119826

A thesis submitted in partial fulfillment of the requirements for the degree of

MS Manufacturing Engineering and Management

Thesis Supervisor:

Dr. Salman Nisar

Thesis Supervisor's Signature: _____

PAKISTAN NAVY ENGINEERING COLLEGE

NATIONAL UNIVERSITY OF SCIENCES AND TECHNOLOGY,

ISLAMABAD

August, 2018

Declaration

I certify that this research work titled ***"Prediction and Optimization Study of the Effect of Laser Parameters on Weld Quality using Taguchi Array for Aluminium Alloy 5083"***
is my own work. The work has not been presented elsewhere for assessment. The material that has been used from other sources it has been properly acknowledged / referred.

Signature of Student

Ameera Noor

2015-NUST-MS-MEM-00000119826

Copyright Statement

Acknowledgements

I am most thankful to my Creator Allah Subhana-Watala without Whose will and support this work could not have completed. It was His Kindness and mercy for providing me with all the means to bring this task to completion in spite of many difficulties.

I would like to extend my thankfulness to my supervisor Dr. Salman Nisar for his guidance and support throughout the work and for providing me ample time to complete the work.

My most humble gratitude is extended to my Co-Supervisor, Dr. Usama Siddiqui who made me learn things from beginning till the very end. Successful completion of this task without his help and continuous support would indeed have been impossible.

My parents and my brother have been my lifeline with all forms of support at every step during the program. It is indeed their hard work and patience of 16 years that has made me capable to earn this degree today. I would also like to extend my gratitude to all of my teachers from school, college and University for making me capable enough to learn and excel.

At the end, I extend my appreciation to my university and office colleagues and every individual I could not name; who in any form helped me in realization of this dream.

Dedicated to my Parents, Siblings and Teachers

Abstract

Previous published works on the optimization of parameters in laser welding process have not reported weld pool shape, weld bead width and depth and HAZ width for variable thicknesses for laser power and welding speed. This work focuses on the study of parametric effect of laser power and welding speed on peak temperatures, weld bead width, aspect ratio, heat affected zone width and macroscopic pool shape for specimens having various thicknesses through transient thermal analysis for AA 5083 alloy. Taguchi array was used to design the experiments to be carried out through Finite Element (FE) simulations which have been carried out with a general purpose commercial FE code, ABAQUS. Regression models indicate that weld width and attained temperatures are more dependent on welding speed than the laser power. Specimens having 10 mm or more thickness require to be welded at least at powers higher than 3500 watt and speeds less than 120 mm/s to attain temperatures high enough to initiate welding through melting. It is concluded that combination of welding speed and laser power greater than equal to 120 mm/s and 3500-4500 Watt produces teardrop shaped weld pools which give coarse microstructure and hence undesirable.

Contents

List of Figures

List of Tables

List of Abbreviations

- AA 5083   Aluminium Alloy 5083
- ASME   American Society of Mechanical Engineers
- HAZ   Heat Affected Zone
- TMM   Thermo Metallurgical Model
- TEP   Thermo Elastic Plastic Model
- LP   Laser Power
- WW   Weld Width

Chapter 1: Introduction

1.1   Laser Welding

Laser welding process is one of the emerging manufacturing technologies and has found widespread applications in different industrial and medical sectors. Laser welding process produces fast, precise and accurate joints and is now considered to be one of the most important joining process for the sheet metals.

It is now used extensively in automotive, electronic, shipbuilding and medical industries. The advantages of the laser welding process are associated with the generation of a high intensity heat source that can weld remotely accessible areas with high precision and control. Study and evaluation of microstructure using different techniques, characterization of mechanical properties of welded joints, study of porosity and its control in laser welded joints have been used to evaluate the process of laser welding [1]. Computational modelling of this process for different materials has helped scientists and researchers to optimize and study the process cost-effectively and in lesser time. Validation of the results of computational models by the actual results obtained from laser welding process has made numerical simulations a primary way to study and improve the process for different output parameters.

1.2   Research Problem

Laser welding is a complex process where the process outputs including thermal deformation, residual stresses, grain structure and weld bead quality are affected by numerous input parameters including welding speed, laser power, defocus distance, shielding gas and diameter of the beam. The requirements of a sound weld are high aspect ratio, minimum deformation, minimum residual stresses and fine grain structure in the fusion zone for optimum mechanical properties. It is reported in literature that small bead width and increased penetration depth increases the deformation. Welding speed and laser power also effect the stresses and deformation. Increasing the welding speed and decreasing laser power reduces the deformation and stresses by creating a weld bead of small width and depth of penetration but may not join the material soundly while conversely increasing the laser power increases the deformation and stresses effecting the quality negatively. In close fit parts, small deformations can impair the functioning and become

detrimental over the period of time. Proper selection of input values for a minimum deformation part with minimal residual stresses, fine grain structure and proper joint is of utmost importance.

Extensive work has been done on numerical simulation and modelling of the laser welding process for parametric and optimization studies. Literature review has revealed that extensive work has been done for steel and its various grades in different domains of experimentation and simulation studies. Aluminium Alloy 5083 is a structural metal used in various applications [2], [3]. Not much work has been done on AA 5083 alloy. Reported work lies in the model development domain and the study of porosity content. Study of macroscopic shape for the underlying microstructure, weld width and peak temperature at various laser powers and welding speeds in relation to variable thicknesses is not reported. Parametric studies using variable thicknesses are conducted in this work to study the effect of laser power and welding speed on macroscopic weld shape, peak temperature, weld width and width of HAZ. Regression models are developed and significant parameters are determined.

Numerical simulation of the process can be used to determine Laser welding parameters for optimum weld quality. This work aims to investigate and optimise the laser welding of aluminium alloy AA-5083 for the weld quality using weld morphology and weld pool shape determined from thermal analysis.

1.3   Research Objective

The objectives of this research work are

1. Study weld pool geometry (depth of penetration, width of weld bead at the top surface, width of HAZ) in response to laser power and welding speed for varying thicknesses of work-piece.
2. Predict the optimized weld pool shape for desirous micro-structure based on macro-properties of temperature gradient and weld pool shape.
3. Predict the laser parameters for achieving optimum weld.
4. Develop Regression models for maximum attained temperature and weld width.

1.4   Research Rationale

Numerical modelling of laser welding process has been done to optimize the process parameters and determine the co-relation between various input and output parameters for numerous materials. The most cited materials are stainless steel grade AISI 304, stainless steel grade AISI 306, stainless steel grade AISI 316, medium carbon steel, copper and tin alloys.

Small number of numerical studies have been found to simulate the process of laser welding for aluminium and its alloys in 5XXX series; with majority of the studies targeting porosity study [4]–[6]. Few numerical studies have reported optimization of laser welding parameters for aluminium and its alloys. However, there has been no reported work on laser welding of structural aluminium alloy AA 5083 for developing a co-relation between input laser power and welding speed in relation to varied thicknesses, weld pool geometry, isotherm shape for optimum aspect ratio and microstructure. Thermal analysis was carried out to predict the weld pool geometry and isotherm shape in relation to grain structure in the fusion zone for multiple thicknesses.

Research work is based upon model validation using the published work on HSLA 340 alloy and AA 5083 Alloy [7], [8]. The validated model was then applied to the current study. This work differs from the paper to be reproduced for model validation based on AA 5083 in the nature of work. The published work lied in the domain of model development only while the present work focuses on parametric study using variable thicknesses to study the effect of laser power and weld speed on the selected output parameters.

1.5   Thesis Structure

Chapter 1 gives a brief review of the laser welding process and its significance and presents research rationale and research objectives. Literature review is presented in Chapter 2. Chapter 3 contains a detailed description of the laser welding process, its types and laser welding process parameters. Research methodology and development of thermal model for finite element simulation is presented in Chapter 4. Chapter 5 contains the validation studies. Parametric optimization of laser parameters and the concluded results are presented in Chapter 6. Chapter 7 contains the final conclusions and recommendations on further study.

Chapter 2: Literature Review

Welding processes entail a vast number of technological processes from simplest oxy-acetylene gas welding to complex processes like electron beam welding and laser welding. Laser welding is although a comparatively advanced welding process yet extensive work has been done in this field in different categories.

2.1   Introduction

Research work in the domain of laser welding can be broadly characterized into experimental and simulation domains. Simulation domain can be further subdivided into three major categories based upon the physical phenomena under study. These three major simulation domains are: thermal, thermo-mechanical and Multiphysics including the modelling of fluid flow and may or may not include phase transformation modelling [9], [10]. Extensive literature review has revealed that researchers have used independent experimental studies and simulation models in all the three domains for achieving various research objectives.

The major research objectives of all previous studies have been to either develop a validated model for simulation study or to study the effect of input laser parameters on weld quality. Few optimization studies reported on the development of generalized mathematical models to determine the output parameters for a set of input parameters. Being a material intensive process, the optimization and mathematical models developed for one material may not apply to other material. However, the general trend for effect of input parameters on output parameters is reported to be the same irrespective of the material.

2.2   Experimental Studies

Weld quality has been studied in response to laser parameters using various output parameters including mechanical properties, porosity and weld pool morphology. Studies to determine the effect of process parameters on weld quality in terms of various mechanical properties have been done using experimental domain. Ultimate tensile strength and weld width was analysed experimentally using pulsed laser welding for AISI 316 and AISI 304 steels in response to laser power, welding speed and pulse width [11]. Authors used RSM and ANOVA to develop mathematical functions for tensile strength and weld width analysis. It was revealed by experiments that tensile strength increased with increasing pulse width till a critical value after

which it was observed to decrease. Weld width increased with pulse width on account of more heat input. For tensile strength, pulse width was the most significantly contributing factor while weld width was significantly affected by laser power. Optimum values of process parameters were also determined for the two materials giving maximum tensile strength and minimum bead width and were confirmed by experiments. It was revealed AISI 304 requires higher line energy for optimum welding than AISI 316 grade. Study was augmented by Masoud Haroni et. al [12] by including further mechanical properties for AZ31B magnesium alloy. Effect of welding speed and laser power on shear load, micro hardness, porosity, weld bead profile and fracture surface were studied by the authors. Experimental results revealed that by increasing laser power shear load, weld bead width and penetration depth increased while pore formation decreased. When the effects of welding speed were analysed, it was revealed that welding speed had a negative effect for all the process outputs. Squillace et. al [13] used the same laser parameters to study their effect on weld morphology, fusion zone, heat affected zone, microstructure, hardness and tensile for Ti-6AL-4V material. Analysis of obtained joints clearly agreed with previous findings for fusion zone and heat affected zone. HAZ gradient was found to be inversely proportional to heat input. It was observed that specimen welded using increased laser power and welding speed showed higher tensile strengths. Results revealed that for heat input less than 25KJ/min keyhole welding mode was achieved while for heat inputs 30KJ/min conduction regime around keyhole was obtained. Welding regime dominantly affected the weld joint. The effect of welding speed using AA 5083 aluminium alloy on hardness, tensile strength and microstructure was studied experimentally [14]. Results revealed that hardness decreases with increasing speeds however tensile strength increased. Microstructure also improved with dissolution of intermetallic compound at higher speeds. Weld pool shape and morphology of weld width and weld depth have also been studied using physical welded joints. Effect of laser power, welding speed and focal position on weld width, depth of penetration and HAZ were experimentally investigated by Shanmugarajan et. al [15] for P92 material. Taguchi orthogonal array for design of experiments and Grey Relational Analysis was used for analysis. ANOVA indicated welding speed is the most contributing factor (74%) followed by Laser power (14%) and focal position (10%). Optimum values were also determined and confirmatory experiments were performed. Effect of same laser parameters were studied for dissimilar metal welding of AISI 316 and AISI 1009 stainless steel grades using experimental approach [16]. Their effect on weld pool parameters: depth of penetration and fusion zone (FZ) were analysed using Taguchi DOE. L25 array was used by

authors for experiments' layout plan. ANOVA results indicated once again that welding speed is the most contributing factor for fusion zone, laser power being the at the second number while focal position effect is insignificant for weld pool. Mathematical models were developed for depth of penetration and fusion zone using regression equations and process parameters were also determined which gave optimum penetration depth and fusion zone width. Study of deformation in relation to the bead geometry by varying laser power and welding speed for two micro-thin stainless steel sheets was done by S. Matsouka et. al [17]. Results revealed that for increased depth of penetration the deformation was more severe. Welding mode was governed by the amount of heat input producing conduction and penetration welds. It was observed that conduction mode welding produced concave shaped deformation while deformation direction reversed for penetration welding. At lower speeds, deformation was more severe for both modes than at higher speeds. The deformation was also dependent on thickness; greater the thickness greater the deformation. Welding feasibility study was conducted [18] to obtain optimum parameters for welding of 10 mm thick steel sheet. Several parameters were tested by authors for determining input parameter values within the limits used: laser power (9-15kw) and speed (1-3m/min). Optimum parameters were revealed as 1.5m/min and 12KW diode laser power. Study also revealed the development of defects at various combinations of laser power and welding speed. High heat input and low welding speed were seen prone to porosity and cracking. Laser welding and Laser Arc Welding processes were experimentally compared to determine their efficiency for plate thicknesses in a T joint configuration [19]. Results revealed that for thicknesses less than or equal to 6 mm both processes were equally efficient however for 8mm thick plates full penetration was achieved with laser arc welding process. The penetration and weld shape were influenced by the percentage of arc energy input. Microstructure and austenite retainment were correlated to the weld quality [20] by evaluating tensile strength, Vickers hardness, and light optical microscopy (LOM) and XRD techniques at multiple levels of laser power and welding speed for dual phase DP 1000 steel. Results suggested that laser parameters which gave minimum volume fraction and minimum softening of martensite with minimum HAZ width produced optimum welds.

2.3 Studies based upon Thermal Models

Mohd. Idris SHAH ISMAIL et. al [21] described the phenomenon of thermal heating in detail for micro-welding of stainless steel sheets. Authors investigated the effect of welding speed, spot diameter and laser power on weld bead morphology and temperature variation using thermal

simulation and experimental findings. The thermal modelling employed a combination of surface and volumetric heat source and thermo-physical properties. Results revealed that weld pool shape became more elliptical with increased speed and laser powers. Higher temperatures were observed in the fusion zone and decreased sharply away from it. Larger spot diameter resulted in welds of conduction mode regime while smaller diameters resulted in keyhole mode welding. An error of 8% was reported between experimental and simulation values. Similar thermal model based on conduction welding regime was developed by Piang Jiang et. al [22] for macro welding of stainless steel sheets to obtain the minimum bead width and maximum depth of penetration against a set of welding speed, laser power and focal position. Authors used a hybrid heat source model for accurate determination of output parameters; double ellipsoid model for weld width determination while rotary Gaussian heat source model for weld depth. Kriging metamodel was used for subsequent analysis and optimized values for the objective function were determined by plotting the optimal front using NSGA-II. Main effects plots constructed using analysis from kriging metamodel revealed that bead width is directly related to laser power and inversely related to welding speed and focal position. Depth of penetration was most impacted by the laser focal position and an inverse relationship existed. Welding speed also holds inverse relation with depth of penetration. Laser power was revealed as the most contributing factor for bead width and laser focal position for depth of penetration. Optimum values for the used set of input parameters came to be 1.02 mm bead width and 2.62 mm depth of penetration. Experimental comparison of optimum values indicated an error of 28% for both parameters. The use of only two thermo-physical properties in model development may have compromised the accuracy of simulation results. Simple thermal model of stainless steel was developed using definite element method [23]. Temperature dependent thermo-physical properties and super-imposed model of surface heat source with body heat source was used. Weld width and weld depth were established by the simulated model with a variation of 1 mm in width and 0.5 mm in depth when compared with experimental results.

Optimization studies employing developed mathematical models were performed using design expert software for medium carbon steel [24]. The mathematical models were developed in a previous study based on thermal modelling of the same material. Authors developed the objective function to maximize depth of penetration and minimize weld width and HAZ width against input parameters of laser power, welding speed and focal position. Response Surface Methodology was applied for optimization studies based on separate criteria of half depth and full depth penetration

welding. It was statistically revealed that half depth penetration welding will result in less distorted welds and would be more economical. However the optimized values are not backed by experimental findings. Weld of aluminium with titanium using laser power ranging from 1.8 to 2 KW and welding speed ranging from 25 mm/s to 30 mm/s was analysed using finite element simulation based on thermal model [25]. The simulation work was supported by experiments for model validation and determination of Gaussian heat source parameters. 3D conical volumetric heat source model was used by authors in the simulation along with temperature dependant properties. Comparison of temperatures was done for two values of laser power and welding speed to test the model validity. It was revealed that the developed model showed lower temperatures than those attained experimentally. The possible reason could be that the assumed efficiency of laser source was lower than the actual efficiency. Thermal model based on elastic-plastic model was developed by C.Fang et. al [26] to study the thermal field in a ITER coil case. ITER case was modelled for AISI 316L stainless steel of 3 mm width and 2 mm depth using thermo-physical properties of thermal conductivity, specific heat and density. 3D conical Gaussian heat distribution function was used to model the heat source. Initial experiments were done by authors to determine Gaussian heat source parameters as they effect the accuracy of thermal model. Temperature profile revealed rapid heating and cooling rates. It was found that temperatures decrease drastically with increasing distance from the fusion zone. Molten pool showed a reversed conical morphology. Temperature profile was matched with the one obtained by using thermo-couples from experiments. Results were in good agreement with the simulated temperatures. Thermal model was used to determine the optimum position of laser heat source to weld dissimilar metals: CuSn10 and X5CrNi18-10 [27] . Normally distributed heat source function was used to model the laser heat source. Boundary conditions of convection, radiation and evaporation were applied. Convective heat transfer co-efficient was assumed to be 100 units. Thermo-physical properties of both materials were used in model development. Three positions of laser heat source for focusing were analysed: at the interface of butt joint of two metals, 0.2 mm towards X5CrNi18-10 and 0.2mm towards CuSn10. Position of laser heat source 0.2 mm towards CuSn10 was found to be most suitable. This research finding is also proved by previously published literature. Relationship between joint strength and bond width and thickness of intermetallic compounds layer (IMC) was evaluated using steady state heat transfer analysis and experiments for aluminium alloy and steel [28]. Convection and radiation were applied without temperature dependence. Joint strength was characterized by tensile strength of the welded joints. Study was conducted of a weld in lap joint

configuration using unequal plates of Aluminium alloy 5083 and steel XF350 2mm; with steel over aluminium. Effect of power density and interaction time was studied by varying laser power and time. Results reported that thin IMC layer and wide bonding area are required for optimum joint strength. Results of experiments revealed that power density and interaction time both positively contributed towards width of bonding area and IMC layer. Maximum joint strength was observed at intermediate values of power density and interaction time. It was concluded in the study that wide bonding area and thin IMC layer are not achievable at the same time through optimization of process parameters because of their opposing behaviours towards the power density and interaction time.

2.4   Studies based upon Thermo-Mechanical Models

Thermal simulations can only predict the weld pool and its temperature profile. Thermo-Mechanical simulations are used to predict and study the deformations produced in the workpiece during welding. Thermo-mechanical model was developed by Vemanaboina et. al [29] for TIG welding to model residual stresses and temperature distributions using cylindrical heat source model for SS304 material. The model was based on temperature dependent thermal and constant mechanical properties. Results show that the temperature near the weld bead were higher as compared to HAZ and base plate. Residual stresses showed a normal distribution along the transverse direction with maximum value in the FZ. However, the assumption of constant mechanical properties at elevated welding temperatures might have compromised the accuracy of model. Temperature and stress fields were studied for AA 6061 aluminium alloy using thermo-mechanical model using cylindrical heat source [30]. Temperature and stress profiles indicate that the process achieves a quasi-static state after 2s reaching a maximum temperature of 1654 degree Celsius. Stress study revealed development of compressive stresses near the FZ while farther away the stress state was 0. Experiments were accompanied to verify the developed model. Temperature and stress fields during laser welding of spiral steel tubes were studied by Arif et. al [31] using simulation and experimental work. Heat source was modelled using temperature dependent thermal and mechanical properties. Enthalpy method was used by authors to avoid the non-convergence caused by sudden extreme changes in specific heat due to phase change. Double ellipsoid heat source model was modified by authors to depict heating phenomenon more accurately. Simulation results revealed that increasing welding speed reduced the von misses stresses because of elongated isotherms. Predicted temperatures were compared with experimental

results and excellent agreement was observed between the predicted and experimental values suggesting the use of model for parametric studies. Carbon steel was studied in butt joint configuration for temperatures and stress fields using finite element simulation and experimental work [32]. XRD technique was used by authors to measure the residual stresses and microstructure was evaluated using SEM and optical microscopy. Simulation used Gaussian heat source model and temperature dependent material properties. Results revealed that temperature decay rate in the molten zone is lower than that in the base metal region. Study revealed that almost equal values of stress were generated along the width while along the length sharp variation in stress was observed. This was because of high temperature gradients produced as the movement of laser heat source was along the longitudinal direction. Authors also examined the metallurgical changes due to welding and analysed hardness values. G.A Moratis et. al [33] worked to develop a thermo-mechanical model for aluminium. Authors have highlighted in their work that very less data is available for aluminium. Authors used two step approach for developing simulation model for the material. As the first step, model was developed for DH-36 steel and validated it using numerical equations. The developed model was then used to predict the temperatures and residual stresses for aluminium using 4KW laser and 50 mm/s welding speed. Results show that rate of heating is higher than cooling rate. Also the distortions were non-uniform in the beginning of laser welding at the site of laser entry however they became uniform and almost disappeared from transverse direction and became more concentrated in the longitudinal direction. Transverse stresses followed a normal distribution with almost diminishing values at the far ends and maximum value at the weld centre line.

2.5   Studies based upon Multiphysics models

Researchers have also used multi-physics simulations involving the modelling of fluid flow phenomenon and metallurgical changes to study the laser welding process for various objectives. Modelling of fluid flow phenomenon enables to see the shape of weld puddle and increases the results accuracy. However, the complexity and size of problem also enlarges. For this reason, researchers use the simulation type based on the research objective. Extensive literature review has revealed that fluid flow modelling is largely used for studying porosity content and flow characteristics of the molten pool. Fluid flow was modelled by Chang et. al [34] to study the porosity content and thermal fields for AA 5083 aluminium alloy. Authors analysed partial penetration welding and full penetration welding modes and their effect on porosity content and

fluid flow. Results suggested that for partial penetration welding conditions the pores formed were irregular and complex relationship existed between input parameters of laser power and welding speed and porosity content. However for full penetration welding, not only the porosity level decreased sharply but also increasing laser power and decreasing speed reduced porosity level. Fluid velocity increased with increasing laser power and welding speed. It was revealed that vortices formed in the molten pool were essentially the same for all conditions of welding. Authors used Gaussian volumetric heat source without considering the formation of keyhole and confirmatory experiments were also performed. Porosity content and its relation to laser welding speed under two sets of laser power and shielding gas for the same material were studied using extensive experiments specifically for partial penetrated joints [6]. Results revealed that at higher speeds more pores were liable to be formed because of early collapse of keyhole and entrapment of gases. Analysis of heat input for partial penetrated joints was also done using rotary Gaussian heat source for fluid flow modelling. Effect of shielding gas and welding nozzle stand-off distance on porosity content of AA 5083 aluminium alloy was also analysed experimentally [35]. Increasing gas flow rate and decreasing nozzle stand-off distance produced joints of higher quality with lower porosity content. Spatter formation for the same alloy of aluminium was studied [4] using 10 KW laser, welding speeds of 2m/min and 9m/min and leading and trailing nozzle positions using fluid flow simulation and experimental work. Fluid flow was modelled by employing multiple reflections and Fresnel absorption. Droplet-escape condition was modelled using Young Laplace Equation. Convection, conduction and evaporation were used as energy boundary conditions and were modelled using their standard equations. 3D Conical Gaussian heat source model was used to define the laser source. Results indicated that higher welding speed and trailing position of nozzle resulted in reduced spatter formation in the weld bead. Fluid flow model was used to study the weld pool shape for AZ91 magnesium alloy and was supported by experimental results [36]. Volumetric heat source model was used to define the laser heat source. The effect of welding speed and laser power was analysed on temperature gradients and velocities of the molten pool by modelling keyhole and fluid flow using finite volume method. Several assumptions were made including flat surface of weld pool and constant thermo-physical properties. Laser power varied from 700 to 2000 Watt and welding speed varied from 1 to 10m/min. Boundary conditions of surface tension and convection were defined while radiation was not considered. Conservation equations of mass, momentum and energy were modelled for fusion zone for computation of velocity and temperature distribution in the region. Boundary

conditions and governing equations were applied using control volume method to simplify the modelling process. Results revealed that higher velocities of molten pool existed in the front of keyhole while lower velocities in the rear region. It was also observed that in front of the heat source temperature gradients were higher and positive because of melting taking place while at the back they were less steep and negative because solidification was taking place. It was also highlighted by authors that temperatures decreased with increasing depth. Numerically predicted results were in good agreement with experimental findings. However at higher laser powers and lower welding speeds discrepancies were observed. Weld pool macrostructure and molten pool velocities were studied for Ti6AL4V metal alloy using fluid flow modelling for pulsed laser welding [37]. Finite volume method was employed by authors for simulating the flow. Three welding speeds were: 3, 6 and 9 mm/s using a laser of 750 Watts and pulse durations from 0.2 to 25s. The pulse of laser was modelled using its Gaussian function. It was assumed that laser is fixed while work piece was moving. Weld pool surface was assumed to be flat with laminar incompressible flow. Governing equations used to model the process included conservation of mass, conservation of momentum and conservation of energy. Boundary conditions of convection and radiation were applied at all surfaces. Results revealed that fluid velocities were higher at the edges than at the centres. It was observed that with increased welding speed, heat input was reduced thereby reducing the weld width and depth of penetration. HAZ width also reduced with decreased welding speed. When compared with experimental results; the percentage error lied in the range of 2-17%. Temperature profile and weld pool shape were also studied using fluid-flow modelling for stainless steel 304 grade [38]. Authors used volumetric heat source model for laser heat source and volume of fluid method to track free surfaces during the simulation. It was assumed that properties of liquid metal were independent of temperature. In addition to basic governing equations of energy, mass and momentum authors also incorporated volume fraction function to model the problem. Results of weld pool simulation using 2500 Watt laser and 0.05 m/s were in close agreement with experimental findings. Results indicated higher temperatures ahead of the laser. It was also characterized that recoil pressure plays a key role in keyhole formation. A Multiphysics model incorporating phenomena of heat transfer, fluid dynamics, phase transitions and electromagnetic variations was developed to study the effects of externally applied alternating magnetic field on the weld pool for 10mm thick aluminium plates [39]. It was assumed that free surfaces and keyhole have a fixed geometry to simplify modelling. Inductive heating of magnet and plasma heat effects were also neglected. CFD and EM boundary conditions were

27

applied. Results indicated that employing an alternating current magnetic field could substantially reduce sinking and gravity drop out of molten pool by balancing the hydrostatic pressure. Velocity, pressure, temperature and electromagnetic field distributions were also modelled as secondary results by the author. Numerical and experimental models were used to generate multiple input variable levels of laser power, welding speed and defocus distance to give off the same weld macrostructure for Al-Mg 5183 alloy [40]. The weld macrostructure was characterized by weld width at the top and bottom and bead penetration depth. Genetic algorithm was applied to determine the set of input parameters at various levels to produce laser beams which gave the same weld geometry. The tailored geometry parameters have different sets of input variables (laser power, welding speed and defocus distance) all giving the same weld profile. The authors determined the values of absorption and focal radius using hit and trial method using the random values generated by GA and then used the values which gave the weld width and penetration in simulation closer to experimental results. Tsirkas et. al [41] used Multiphysics simulation approach for butt joint weld using two different thicknesses of AH36 steel to predict deformation and develop a mathematical model for parametric studies of deformation. Tests for three sets of different combinations of laser power and speed were performed. 3D conical Gaussian heat source was used for modelling. Displacements were observed to be non-uniform in the beginning and became uniform at the end of the process. The efficiency of laser welding variants: autogenous laser welding (ALW), cold wire assisted laser welding (CWALW) and hybrid laser arc welding (HLAW) was compared with submerged arc welding (SAW) for residual stresses, distortions, HAZ and tensile strength using thermo-metallurgical-mechanical model and experiments [42] . Stainless steel was the medium of study. The modelling process employed temperature and phase dependent material properties. Heat source model in laser welding processes and submerged arc welding process was defined by 3D conical Gaussian distribution and double ellipsoidal distribution respectively. It was concluded that for all the analysed processes, laser welding processes were more efficient than submerged arc welding process. Good co-relation between numerical and experimental results was observed.

Mi et. al [43] compared the efficiency of thermo-metallurgical modelling (TMM) with thermo-elastic plastic model (TEP) using Q235 steel grade. The model was developed using both approaches and was compared for stresses, distortions and weld pool macro structure. The results of TMM model were compared with TEP model. The fusion zone of TEM model was smaller than the fusion zone of TEP because of lower thermal conductivity values used in the former

model. Stress and deformations were also modelled. Comparison with experiments revealed that TEM model was more accurate than TEP model as the temperature profile and phase fractions of TMM model were more close to experimental values than those obtained with TEP. It was also revealed that phase transformation have a high impact on distortions and stresses. Macroscopic results of thermo-fluid model were used to determine the grain growth orientation based on mathematical equations employing pulling velocity and temperature gradients for 2A14 aluminium alloy. Good agreement was observed between experimentally observed and simulated grain growth orientation.

2.6   Conclusion

The above done extensive literature review has revealed that not much work is done on aluminium and its alloys in the field of developing thermal and thermo-mechanical models. Thermal models although cover the simplest type of modelling technique yet they form the basis of all analysis and further modelling techniques. Once valid thermal model is established only then it is possible to proceed to thermo-mechanical or Multiphysics simulation. This work is therefore based on thermal modelling of Aluminium Alloy 5083, belonging to the 5XXX series. In this study, weld macrostructure is evaluated in response to changing laser parameters as well as specimen thickness for keyhole or penetration welding regime and weld pool shape is predicted for optimum weld and microstructural characteristics.

Chapter 3: Laser Welding Process

3.1   Introduction

High quality welding processes are required to carry out welding on bodies for critical applications like aerospace, marine structures, boilers and turbines. Advanced welding techniques in current use include Plasma welding, Metal Inert Gas (MIG) welding, Tungsten Inert Gas (TIG) welding, Electron beam welding and Laser beam welding. Correct choice of process as per the application is highly critical for service life and it depends upon the material to be welded, application and its service environment, cost, process parameters, residual distortions and stresses produced.

Fusion welding includes all those processes in which heat source melts the material underneath in either absence or presence of filler material. Coalescence is achieved when the molten pool solidifies and creates a joint between the two distinct metal pieces. Welding processes are characterized by the method by which heat is generated to fuse the two pieces and achieve coalescence. During the process of melting and solidification several critical changes take place in the workpiece. The microstructure of the fusion zone and region surrounding it changes as a result of experiencing high temperatures. Undesired residual stresses and distortions appear in the workpiece which may affect their use in the application.
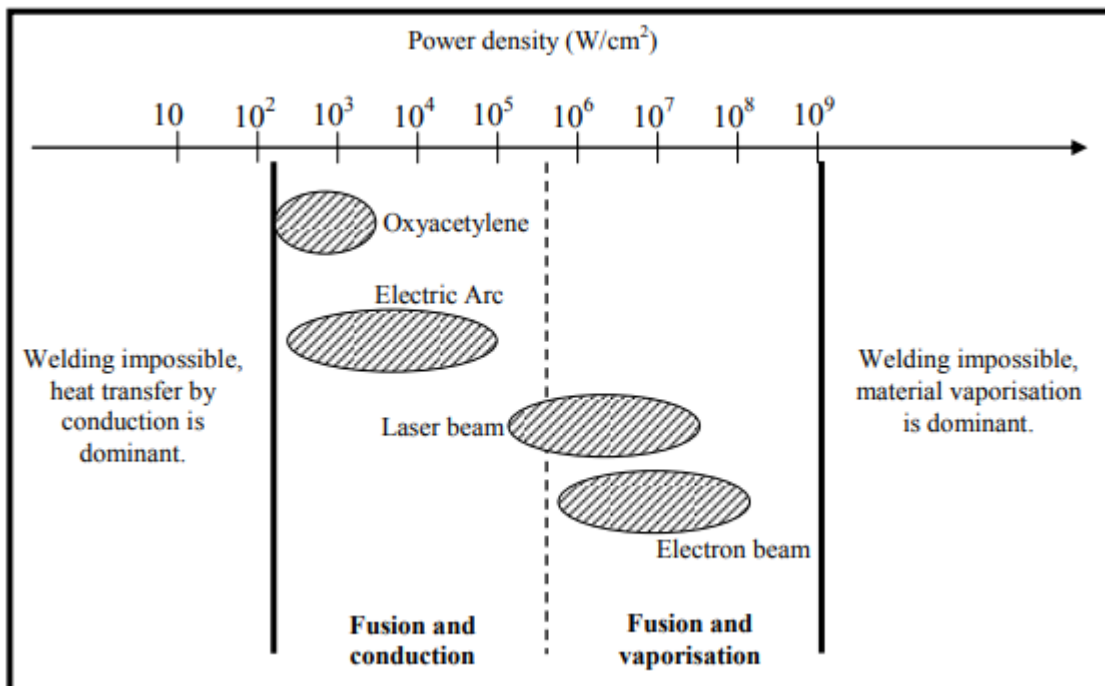
Figure 1 Welding Processes as a Function of their Power Density [44]

Laser welding process is advantageous for critical applications like in aerospace and marine sectors and for difficult to weld materials including aluminium and its alloys of 5XXX and 6XXX series. High power density of process and localized heating produce lower residual stresses, distortions and undesired changes in microstructure of the base metal. It can be seen from Figure 1 that laser welding is a high Power Density (PD) process. Other merits and demerits in comparison with commonly used advanced welding processes are presented in Table 1.

Table 1 Merits and Demerits of Laser Welding in Comparison with other Advanced Welding Processes [44]

Welding process	Welding speed	One pass penetration	Merits	Demerits
Oxy-acetylene	10 cm/min	2-3 mm	• Low cost • Portable	• Slow speed • High deformation
MIG-MAG	50-100 cm/min	3-4 mm	• Low cost	• High deformation • Groove preparation
TIG	10-50 cm/min	3-4 mm	• High quality • Portable	• High deformation • Slow speed • Larger HAZ
Laser beam	1-5 m/min	upto 10 mm (6 kW)	• High speed • Less deformation	• High installation cost • Non-portable
Electron beam	1-10 m/min	upto 80 mm (25 kW)	• High speed • Greater thickness	• Vacuum required • High cost

3.2 Introduction to Laser Welding

The term LASER stands for Light Amplification by Stimulated Emission of Radiation. Laser welding is one of the emerging manufacturing technologies in which monochromatic and coherent light beam joins two similar or dissimilar materials through coalescence. Materials weld together as heat is produced by the impinging concentrated, focused light beam directed on them. Laser welding process requires no electrodes and filler wires and thus high degree of repeatability exist. The intensity of heat produced by the laser is affected by the choice of laser type, selection of lenses used, distance between the heating source and the base material.

Laser welding takes place when the laser beam irradiates two overlapping surfaces. The focused light beam is absorbed by the surface of the material. This absorbed energy causes heating and

melting of the material underneath which results in the formation of a welded joint. The amount of energy contained in the irradiating laser beam is partly reflected and partly absorbed. The energy absorption depends upon the material properties

(absorption coefficient and heat conduction) and mode of welding achieved as a result of applied power density, surface properties of the workpiece and compatibility of wavelength of laser beam and the material to be welded. In keyhole welding reflection and absorption of the material is important only till keyhole formation initiates. Once the keyhole is formed, absorption co-efficient becomes irrelevant as the keyhole acts as a blackbody.

3.3   Modes of Welding

Power Density (PD) of a laser heat source is defined mathematically as

$$PD = \frac{LaserPower}{Areaofbeam}$$

(3.1)

Where Laser Power is in Watts and Area of beam spot is usually measured in millimetres square or centimetre square.

When the PD is less than $10^6 W/cm^2$ conduction type welds are formed while when the PD is higher than this deep penetration welds are obtained [45] formed due to keyhole generation during the welding. For this reason, deep penetration welds are also known as keyhole welds.

3.3.1 Conduction mode

Conduction laser welding is a low energy type of laser welding which is performed at a laser power enough to melt the metal. Heat is conducted from the top surface and into the metal, forming the weld nugget from the top and till the depth where heat travels as shown in Figure 2. Depth of penetration is therefore controlled by timing of exposure per unit area. Conduction type welds are wider than their depth.

3.3.2 Keyhole or Penetration mode

This type of laser welding uses a high-energy beam that vaporizes the metal. Vaporizing metal creates gas which in turn creates a keyhole or tunnel from the surface down into the metal as depicted in Figure 2. As the laser beam moves across the surface, the keyhole follows and creates a typically deep and narrow weld. The resulting weld is therefore deeper and stronger, and has a lower heat affected zone.

Formation of keyhole and its dynamics have been studied extensively. Stanciu et. al studied the mechanism of keyhole formation in detail [46]. Keyhole is formed when a high density laser beam focused on the metal melts and subsequently vaporizes. As the metal evaporates, a narrow keyhole cavity is formed by multiple internal reflections of the laser beam. The narrow cavity is produced due to the surface depression caused by the recoil force of vaporization from the liquid surface. Overall energy transfer efficiency is governed by the mechanisms of Inverse Bremsstrahlung absorption and Fresnel absorption. Inverse Bremsstrahlung absorption transfers energy from photons to electrons in the ionized plasma plume formed above and inside the keyhole region. While Fresnel absorption takes places through multiple reflections at the keyhole walls. During the entire process of laser welding, keyhole is maintained by reaching a state of equilibrium between the opening and closing forces. Material ablation and formation of ionized plasma generate the opening forces of keyhole and surface tension and hydrostatic force from the surrounding melt pool generate the closing forces. As the heat source moves, the keyhole moves along it and a weld bead is formed. Selection of optimum speed is necessary during keyhole welding- a fast pace welding would result in collapse of keyhole while a slow welding will result in a sagged weld bead.
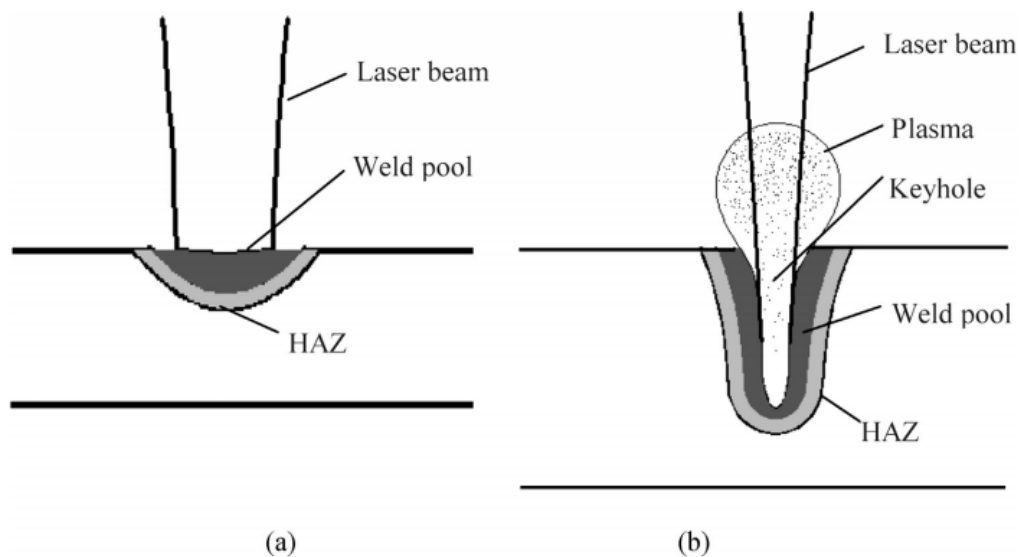
Figure 2 Modes of Welding (a) Conduction Laser Welding (b) Deep Penetration Laser Welding [36]

3.4 Modes of Emission in Laser Welding

Laser Welding Process can be executed either in continuous wave (CW) or pulsed wave (PW) mode of operation.

3.4.1 Continuous Wave (CW) Lasers

In CW Lasers, the lasers are either on or off for the entire operation. These lasers emit light beams of same power over a period of time and utilize average powers. Width of HAZ and penetration depth is higher in CW laser mode as compared to these in PW mode [47]. The laser parameters associated with CW mode of operation are laser power, beam diameter and welding speed.

3.4.2 Pulsed Wave (PW) Lasers

In PW Lasers, the laser source is excited for short pulses of small durations generally in milliseconds. These pulses are repeatable in power and duration over the operation time. Minimal heat is transferred into the part when operated in PW mode. The associated parameters are pulse duration, energy and beam diameter [47].

3.5 Types of Lasers

There are many different types of lasers [48]. Main categories in which lasers fall are Gas Lasers, Solid State Lasers, Fibre Lasers and Diode Lasers.

3.5.1 Gas Lasers

Gas lasers require high voltage, high current source to generate the laser beam. The active medium in gas state lasers is a mixture of gases. The optical cavity for these lasers has to be made from rigid lenses and mirrors due to high wavelength. Their output power can go as high as 25 KW. They can be used in pulsed or continuous mode.

3.5.1.1 CO2 Lasers

Carbon-dioxide lasers are most frequently used among the category of gas lasers. In CO_2 lasers, laser beam is generated by applying electrical energy to mixture of gases which stimulates the CO_2 gas molecule to emit photons thus producing laser beam. Wavelength lies in deep infrared region having a value of 10.6 micrometre. The mixture of gases is composed of 0–20% carbon dioxide, 10–20% nitrogen, a few percent hydrogen and/or xenon and helium. CO2 lasers are the highest-power continuous wave lasers available.

The characteristics of CO2 lasers include; high the ratio of output power to pump power, high beam quality at good dollar-per-watt ratio, a beam of infrared light with an average wavelength of 10.6 um. Because of longer wavelength, these laser beams cannot be guided through flexible glass fibres. Laser beams generated by such type of lasers follow Gaussian distribution. Their power ranges from 1.5- 6 KW and in CW mode greater than or equal to 10KW. The energy transfer efficiency of these lasers from the beam into the material is as high as 0.8. However, the energy absorption by the material is low (upto) 15% because of higher wavelengths.

CO2 lasers are frequently used in high power applications particularly welding and cutting and in low power applications of engraving.

3.5.2 Solid-State Lasers

Solid-state lasers [5] have a very low wavelength so they can be hazardous for eyes if observed without eye protection. The active or lasing material is a solid as the name suggests, it can be a pure metal or a composite material or a semiconductor etc. Nd:YAG lasers can operate both in pulsed and continuous mode but other laser types are limited to pulsed mode. Solid-State lasers have an output range of 10-20 KW.

3.5.2.1   Nd: YAG Lasers

Nd: YAG Lasers belong to the class of solid-state lasers and are optically pumped. The laser rod is a synthetic crystal of yttrium aluminum garnet (YAG). The YAG crystal is the gain medium containing the dopant: neodymium. These lasers permit operation at high average power levels. The laser rod dimensions govern the power and optical quality. The maximum rod size is 15 mm diameter and a length of 200 mm.

Their operating wavelength is 1.06μm with average powers of several hundred Watts and peak power pulses of 1-10 kW. Because of the lower wavelength, metals also have a higher surface absorptivity under the laser beams produced by ND: YAG lasers. Their overall efficiency range is 3-5%.The laser beam of such lasers can be guided through flexible glass fibre which makes it very convenient to use. In contrast, CO2 lasers use a complicated mirror system to focus and deliver the laser beam. The energy is distributed evenly (flat hat distribution).

ND:YAG Lasers are used in welding, cutting and medical applications.

3.5.3 Fibre Lasers

The laser beam in these lasers is generated within a flexible doped glass fiber of 10 to 30 feet length and 9 to 50 microns diameter. For most industrial lasers Ytterbium is used as the doping element producing 1 micron wavelength. Thulium can also be used giving a beam of 1-2 micron wavelength used for low power plastic welding applications.

The fiber core medium is pumped by diodes that produce a specific wavelength, which is absorbed by the doping element. This enables up to 50 percent conversion of input electricity to laser light. This efficiency is known as wall plug efficiency.

Fibre lasers find their applications in marking, engraving and cutting in the domain of material processing, telecommunication, spectroscopy and medicine.

3.5.4 Diode Lasers

Diode Lasers are electrically pumped semiconductor lasers in which the p-n junction of semiconductor diode acts as the laser medium. The operating range of wavelength of laser beam produced by these lasers lie in the near infrared region. These lasers are compact then the CO_2 gas lasers and Nd:YAG lasers which makes them easy to use.

Diode lasers are used in fibre optic communications, as barcode readers, for image scanning, optical data recording, combustion ignition, laser surgery, industrial sorting and industrial machining.

3.6   Laser Welding Process Parameters

Laser welding process parameters define the welding process. The main process parameters are laser power, welding speed, gas flow rate and focal distance (also known as laser focal position). Wavelength of the laser beam also plays a key role as different wavelengths respond differently to different materials based on the energy they carry. Beam divergence also controls the laser energy input into the material. Small beam divergence angles are responsible for localized heating without effecting the surrounding base metal. The weld pool macrostructure and its quality is dependent on the selection of these process parameters. The major role of shielding gas is to provide an inert welding atmosphere; protected from oxygen and water vapours present in the environment. Once laser wavelength or in other words its wavelength is selected based on compatibility with the material, key parameters left are laser power, welding speed and focal distance. Amongst these three process parameters, laser power and welding speed have a key role

in determining the amount of heat input into the weld which determines the weld macrostructure and the HAZ[12], [15], [49].

3.7   Outcomes of Welding Process

As a result of heat input to join two objects through coalescence, a weld bead is obtained as the preliminary outcome of the welding process. The macrostructure of the weld bead is characterized by weld width (WW) weld reinforcement (WR) and weld depth (DP) as given in Figure 3. From the modelling point of view, while weld width and weld depth can be modelled accurately in simplest thermal modelling of the process, weld reinforcement can only be obtained when fluid flow is modelled and thus comes under computational fluid dynamics.
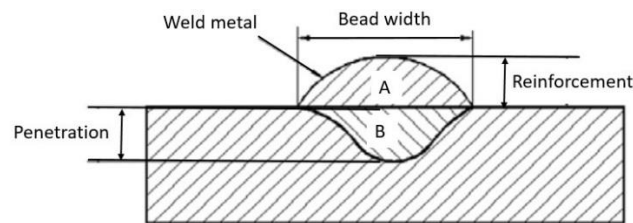
Figure 3 Schematics of Weld Bead [50]

Heat input into the subject metal produces three distinctive zones: fusion zone (FZ), heat affected zone (HAZ) and base metal (BM). Fusion zone is the actual area where welding took place and is characterized by the formation of weld bead, HAZ is the area which has undergone microstructural changes and is characterized by those regions having temperatures equal or greater than the recrystallization temperature while BM is the area that remains unaffected.

Microstructural changes are studied using various techniques including scanning electron microscopy (SEM), light optical microscopy (LOM) and x-ray diffraction techniques (XRD) [15-16]. However it is reported from literature review that macroscopic shape of weld pool can give an insight to the microstructure of the FZ and HAZ without incurring the cost and time of detailed procedures of microstructural study [51].

Thermal gradients also induce residual stresses and distortions in the workpiece. The solidification of molten pool causes shrinkage and exerts stress on the HAZ. Microstructural changes also induce stresses in the HAZ and the BM. While stresses are low in the BM they tend to increase towards the HAZ and give maximum values in the FZ. Non-uniform expansion and shrinkage produce distortions which can be controlled using fixtures and clamps.

As this work is related to the study of thermal effects through thermal modelling of the laser welding process, detailed discussion on induced residual stresses, distortions and microstructural changes is out of the scope of this report.

Chapter 4: Thermal Modelling and Research Methodology

4.1   Introduction

Modelling and simulation of laser welding is a complex task and its simulation studies have been split into three major areas which are: thermal modelling which studies the temperature evolution during welding process, thermo-mechanical modelling which studies residual stresses and distortions and Multiphysics simulations which model fluid flow phenomenon along with the study of temperature profile and stresses. The simulation and modelling techniques are chosen such that they minimize the problem size and complexity while giving the required results.

The current study is based on transient thermal analysis to study the temperature profile and macro characteristics of weld pool including the shape and aspect ratio at various levels of laser power and welding speed for multiple thicknesses of aluminium alloy 5083.

4.2   Methodology

Results obtained from simulation and modelling studies of physical processes cannot be relied upon unless they have been compared against experimental findings. Literature review has revealed that extensive work has been done in development of models where authors have simulated the process using various models of heat source and have validated the developed models by using experiments [23, 38, 51, 52]. The models are developed with various underlying assumptions and have given satisfactory results with minimal error; indicating that the simulation models can be relied upon for basing future work on them.

To optimize the laser welding parameters of 5083 alloy of aluminium the first step is to develop a satisfactory heat source model which is able to give comparable results as that of experiment. Since such a setup of laser welding is not available locally, the heat source model was developed using published papers as the benchmark studies [8], [54]; quoted onward as benchmark paper-I [54] and benchmark paper-II [8]. As a single paper could not satisfy all the criteria of selection henceforth two papers were selected. These papers were selected based on following factors:

1. The selected paper should be a recent publication.
2. Subject Material should be Aluminium Alloy 5083.
3. The paper should contain information about heat source parameters
4. Paper should be based on Thermo-Mechanical modelling

5. Paper should be based upon keyhole mode of welding and use conical Gaussian heat source

A comparative summary of the benchmarked papers and research study against common major inputs is given in Table 2. Initially the thermal model based on conical Gaussian heat source model was developed for Abaqus Standard and subroutine code was written for simulating the moving heat source to reproduce the results for benchmarked paper-I. Since the benchmarked paper-I used HSLA 340 alloy as the study material and the research study is based upon aluminium alloy 5083, the bench marking study was then extended to another paper. The heat source model developed and verified in benchmark study-I was then applied to reproduce results of second benchmarked paper of R.Spina et. al based on Aluminium Alloy 5083. The same model was applicable to both the studies as both papers simulated their experimental work using conical Gaussian heat source model and considered the formation of keyhole. Heat source model changed in terms of Gaussian model parameters, power of laser source and welding speeds for the selected papers as benchmark.

Table 2 Comparative Summary of Benchmarked Papers and Research Objective

Sr. No	Major Inputs	Research Study	Benchmarked Paper-I	Benchmarked Paper-II
01	Year of Publication	N-A	2016	2007
02	Material	Aluminium Alloy 5083	HSLA 340 Alloy	Aluminium Alloy 5083
03	Heat Source Model Used	3D Conical Gaussian Heat Source Model	3D Conical Gaussian Heat Source Model	3D Conical Gaussian Heat Source Model
04	Mode of Welding	Deep Penetration Welding	Deep Penetration Welding	Deep Penetration Welding
05	Gaussian Heat Source Parameters	To be used from Benchmarked Paper-II	Given	Not Given
06	Simulation Category	Thermal Analysis	Thermo-Mechanical Analysis	Thermo-Mechanical Analysis

07	Nature of Study	Optimization	Model Development	Parametric Study of Distortions

Upon model validation of heat source for the second benchmarked paper, the study was then extended to meet the objectives as listed in section 1.3. Hence this research work comprised of four major steps as identified in Figure 4.
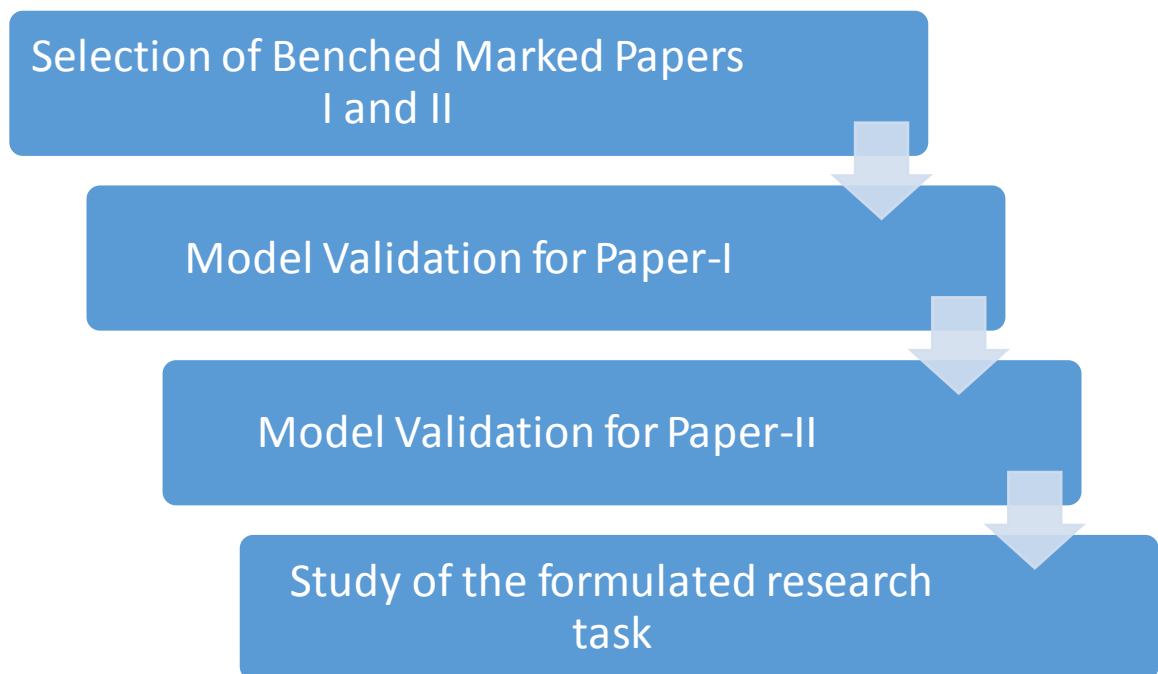
Figure 4 Major Steps of Research Problem

4.3 Physics behind Transient Thermal Analysis

Thermal modelling is primarily used to study temperature evolution during a welding process. Study of the heat affected zone and weld pool are the secondary outcomes of this modelling technique. When temperature profile and applied load varies as a function of time, the analysis is known as transient thermal analysis else it forms steady state heat transfer problem.

All heat transfers take place either through one or a combination of conduction, convection or radiation phenomena. For a laser welding process, heat energy is transferred from the incident

laser beam into the metal through conduction. This heat transfer takes place in accordance with the transient heat conduction equation which is defined as equation (4.1) below

$$\rho C_p \frac{\partial T}{\partial t} + \rho C_p u.\nabla T + \nabla.q = Q \qquad (4.1)$$

and

$$q = -k\nabla T \qquad (4.2)$$

Where

ρ is the density of material measured in kg/m^3

C_p is the Specific heat at Constant Pressure measured in J/K or $J/°C$

k is the thermal conductivity of material measured in $W/(m.K)$

u is the velocity field defined by translational motion when model is moving in the material frame measured in m/s or mm/s

Q is the total amount of heat generated by the heat source measured in $Watts$

Thermal conductivity k determines the amount of flow of heat flux q into the base metal based on the temperature difference while Specific heat C_p describes the amount of energy needed to raise the temperature by one degree per unit mass of material.

In Abaqus/Standard, the numerical analysis of any heat transfer problem is based upon the Fourier's energy conservation equation, which is expressed by equation (4.3) below

$$\int_v \rho \frac{\partial U}{\partial t} \delta T dV + \int_v \frac{\partial \delta T}{\partial x_a} \cdot \left(\lambda \frac{\partial T}{\partial x_a} \right) dV = \int_v \delta T q_v dV + \int_s \delta T q_s dS \qquad (4.3)$$

Where

ρ is density measured in kg/m^3

U is internal energy measured in J/Kg

δT is variational function of temperature measured in $°C$

λ Is thermal conductivity measured in $W/m°C$

q_v Is the heat input from the laser source measured in W/m^3

q_s is boundary heat flux measured in W/m^2

The position of moving laser source is determined at each step and depends upon the welding speed. Lagrange's coordinate system is employed for carrying out the simulations, the coordinates for the centre position of heat source are determined using equations explained in section 0.

Equation (4.3) uses the condition $t = 0 : T = T_0$ as initial condition and phenomenon of convection and radiation, which quantify the heat loss, act as boundary conditions for it [27].

In convection, heat is transferred when a fluid comes in contact with the hot object. The molecules of the fluid absorb energy and as a result they expand. Because of this expansion, the density decreases and the hot fluid molecules rise and the colder, less dense air molecules take their place. As a result, heat energy is transferred due to movement of fluid molecules. The rate of heat transfer from convection depends on the surface area and the temperature difference between source and sink. Equation (4.5) gives Mathematical definition of convection which is

$$q_h = hA(T_2 - T_1) \tag{4.5}$$

Where

q_h is heat transfer by convection measured in W

h is the heat transfer co-efficient measured in $W/m^2\,°C$

A is the surface area of the object measured in m^2

T_2 is the temperature of heat source or the object measured in $°C$

T_1 is the temperature of heat sink or the surrounding medium measured in $°C$

Radiation is defined as the transfer of thermal energy through emission of electromagnetic waves from the hot body based on the temperature difference between the object and the surrounding media. Thermal radiation depends upon the emissivity of the object, surface area of the object and the temperature difference and is defined by Stefan-Boltzmann law which is given below

$$q_r = \varepsilon A(T_2 - T_1)^4 \tag{4.6}$$

Where

q_r is the heat transfer by radiation measured in W

ε Is the Stephan-Boltzmann constant; which is $5.67 \times 10^{-8} W/m^2 K^4$

A is the surface area of the object measured in m^2

T_2 is the temperature of heat source or the object measured in $°C$

T_1 is the temperature of heat sink or the surrounding medium measured in $°C$

Additionally, the energy responsible for phase change that takes place when the base metal melts and then re-solidifies has been defined either directly or by integrating the latent heat with the specific heat [29,50].This work uses the direct specification method of latent heat of fusion and latent heat of vaporization.

4.4 Basic Algorithm and Steps of Developing Finite Element Model for Transient Thermal Analysis

The inputs used in the present study form the basic framework to obtain the time-dependant temperature field. This framework is given in Figure 5. User subroutine is the most important part of defining the finite element model as it defines the heat load for the transient analysis. This heat load is modelled using mathematical equations of the heat source model employed for study.
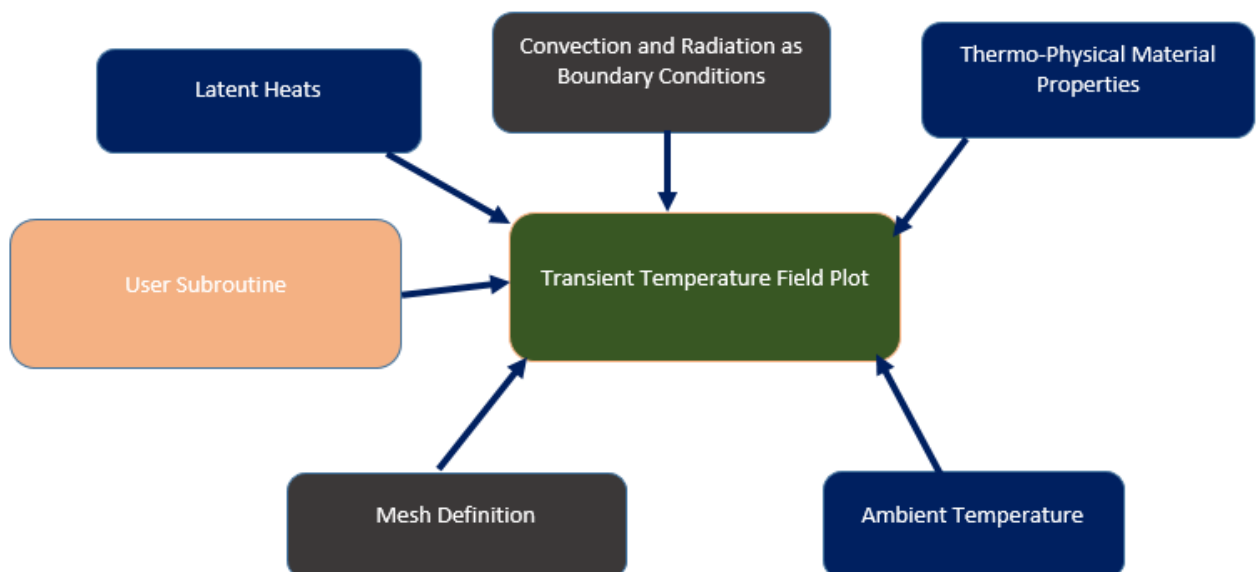
Figure 5 Basic Framework of Thermal Analysis

The sequential steps for development of finite element model are identified in

Figure 6. Initially geometry is defined in the software followed by the assignment of properties. The properties may or may not be assigned as a function of temperature. When temperature dependent properties are used, the solution accuracy increases as the material definition gets closer to the actual behaviour of material at higher temperatures. Such properties are called as thermo-physical properties. Literature review has revealed that majority of the studies have been done by employing temperature dependent properties. However, it is also reported from literature that various studies have been conducted by assuming that properties are independent of temperature effect. Applied load is modelled using subroutine DFLUX as a function of time. Conduction and convection are defined as boundary conditions while ambient temperature condition is defined by predefined field.

```
┌─────────────────────┐
│ Geometry Modelling  │
└─────────────────────┘
          ↓
┌─────────────────────┐
│ Defining Properties │
└─────────────────────┘
          ↓
┌─────────────────────┐
│ Material Allocation │
└─────────────────────┘
          ↓
┌─────────────────────┐
│   Step Definition   │
└─────────────────────┘
          ↓
┌─────────────────────┐
│ Boundary Conditions │
└─────────────────────┘
          ↓
┌─────────────────────┐
│   Predefined Field  │
└─────────────────────┘
          ↓
┌─────────────────────┐
│   User Subroutine   │
└─────────────────────┘
          ↓
┌─────────────────────┐
│      Meshing        │
└─────────────────────┘
          ↓
┌─────────────────────┐
│ Finite Element Model│
└─────────────────────┘
```
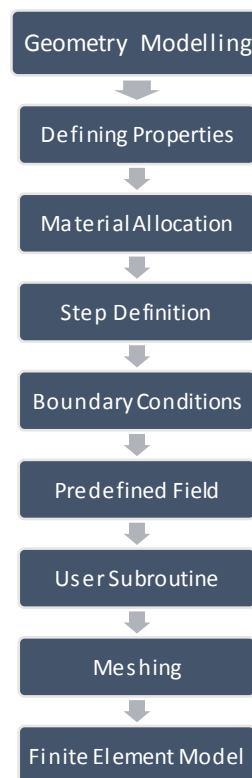
Figure 6 Sequential Steps for Developing Finite Element Model

4.4.1 Heat Source Model

Numerous heat source models [56] have been developed and experimented upon to investigate their suitability with the laser welding simulation.

As cited in literature, 3D Conical Gaussian heat source model is most suitable for modelling of deep penetration welding as it incorporates the keyhole shape formed during high density laser welding process and has been extensively used by authors for keyhole based modelling [57]–[60]. The same model is used in the present work to initially model the results of the benchmarked papers and then for the study of research problem at hand.

Figure 7 represents the profile of 3D conical heat source model where heat flux is linearly distributed in the axial direction and normally distributed in the radial direct ion.
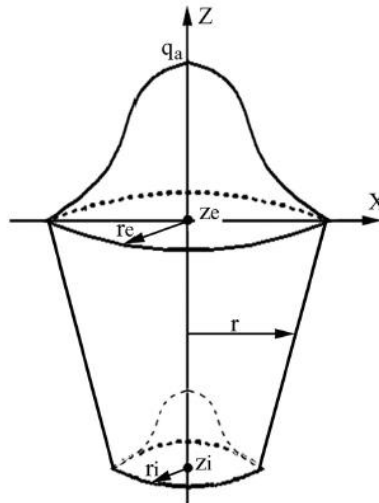
Figure 7 Heat Source Profile of Conical Gaussian Heat Source Model

Where the parameters are;

- q_a : heat source

- r_e : radius of heat source at top plane

- r_i : radius of heat source at bottom plane

- z_e : z co-ordinate of top plane

- z_i : z co-ordinate of bottom plane

- r : radius of heat source at any point along depth between z_e and z_i

Extensive literature review has revealed that authors have used different equations to model 3D Conical Gaussian heat source. These equations differ in certain parameters based on the software used, ignored factors because of simplifying assumptions made and absorption rate of the subject metal. The cone shaped welding model was used in a study of temperature and stress fields by Liu et. al [61] during laser welding of high-strength steel using equation (4.7)

$$q(r, z) = \frac{2P}{\pi r_o^2 Y} \exp(1 - \frac{r^2}{r_o^2})(1 - \frac{y}{Y}) \tag{4.7}$$

In the above equation, P corresponds to laser power, r_o is the initial radius or radius of the laser beam at the top, Y denotes depth of the model and r is the radius at depth y.

Numerical simulation of a micro-welding case was undertaken for study using steel sheets [21]. The authors used the heat source equation given as equation (4.8) to model the cone-shaped geometry. It can be seen that the equation used is not the same as equation (4.7) but is very similar to it.

$$q_v = \frac{3Q}{\pi r_o^2 h} \exp(\frac{-3r_c^2}{r_o^2})(1 - \frac{z}{h}) \tag{4.8}$$

Here, Q corresponds to laser power, r_o is the initial radius, h denotes depth of the model and r_c is the radius at depth z.

A similar equation for constant heat intensity heat source was used by the authors for study of Laser Machining [62]. It is evident from equation (4.9) that it is used for constant intensity heat source as depth multiplication factor is not present in the given equation

$$q(x, z) = \frac{2PA}{\pi r^2} \exp(\frac{-2(x^2 + z^2)}{r^2}) \tag{4.9}$$

The terms present in the above equation are laser power P, absorptivity A, radius of laser beam at top r, and $x^2 + z^2$ correspond to the radius at some time t with respect to co-ordinates of laser position.

Thus it can be seen from the above equations that even for the same shaped profile, modelling the equations used by authors differ in certain factors. These factors, as mentioned earlier, depend

47

upon matching the results of numerical simulation with experimental results or simplifying assumptions.

Benchmarked paper-I was simulated in SYSWELD, a dedicated welding simulation software where 3D Conical Gaussian heat source is available as an in-built heat source. 3D conical gaussian heat source profile, as shown in Figure 7, has been modelled in literature using equation (4.10)

$$Q(x, y, z) = Q_O \exp(-\frac{x^2 + y^2}{r^2(z)})$$ (4.10)

and

$$r(z) = r_e + \frac{r_i - r_e}{z_i - z_e}(z - z_e)$$ (4.11)

As per the software requirement, adjustment of parameter values is required to correctly model the heat source. This is termed as 'adjustment of heat source'. Adjustment factor, as used in the literature [26] was employed, after which Equation (4.10) took the form

$$Q(x, y, z) = Q_O \exp(-\frac{3(x^2 + y^2)}{r^2(z)})$$ (4.12)

For the present work, the conventional axes are not used to develop the part model. The y and z axes in above equations correspond to z and y axes in the model respectively; therefore equations (4.11) and (4.12) take the form of equations (4.13) and (4.14) respectively

$$r(y) = r_e + \frac{r_i - r_e}{y_i - y_e}(y - y_e)$$ (4.13)

$$Q(x, y, z) = Q_O \exp(-\frac{3(x^2 + z^2)}{r^2(y)})$$ (4.14)

and 'Q_o' for conical Gaussian heat source is given as

$$Q_o = \frac{3Q}{\pi r_e^2 h}$$ (4.15)

Thus the heat source was modelled in Abaqus/Standard by employing Equation (4.13), (4.14) and (4.15). The parameters used in the specified equations are given in detail for benchmarked paper-I and benchmarked paper-II in sections 5.1 and 5.3 respectively.

4.4.2 Thermo-Physical Properties

Temperature dependent material properties are used for thermal analysis to increase the accuracy of the model results. It is concluded from literature review that at-least two thermo-physical properties are necessarily used for developing model for thermal analysis [62]. These properties are thermal conductivity and specific heat. Increasing the thermo-physical properties increases the model capability to verify the experimental results from the simulation results achieved. However, non-linearity associated with the problem also increases with the increasing number of thermo-physical properties making it more complex.

For a problem to verify the experimental findings, the model inputs have to be more accurate. The thermo-physical properties associated with thermal model used in the study are extracted from the literature

These properties are:

1. Density
2. Thermal Conductivity
3. Latent heat of solidification
4. Latent heat of vaporization
5. Specific heat at constant pressure

Values and use of these properties are different for the two studies corresponding to the benchmarked papers and are given in detail in the respective sections.

4.4.3 Boundary Conditions

Boundary conditions define the external loads and conditions acting on the body. Heat transfer can take place through three modes; conduction, convection and radiation. Conduction mode is responsible for the flow of heat in solid objects. Likewise, the terms convection and radiation are used to define heat flow in fluids and act on the external surfaces as they are in contact with the surrounding media which is fluid in nature. In the present work, phenomena of convection and

radiation are modelled for heat loss from the workpiece during welding as boundary conditions using equations *(4.5) and (4.6)* described in section 4.4.

Chapter: 5 Validation Studies

5.1   Validation Study of Benchmark Paper-I

5.1.2 Characteristics of Laser Source

The laser source is defined using the specifications as given by the authors in the paper [54] . Dynamic TruDisk 4006 laser source was used by the authors having a welding power of 3400 W and was moving with a speed of 8.5m/min or 16.67mm/s. The depth of focus of used laser system is 1.1mm. Radius of the laser beam at the top surface was 0.69 mm and it varied linearly with depth to 0.3mm as defined by the profile of the heat source model.

5.1.3 Heat Source Modelling Parameters

As per Figure 7 of 3D Gaussian heat source model, the parameter values of r_e, r_i, z_e and z_i are used as given by the authors in the paper and are defined in section 4.4.1 These values are given in Table 3 below.

Table 3 Heat Source Parameters for Benchmarked Paper-I

Parameter	Value	Unit
r_e	0.69	mm
r_i	0.30	mm
z_e	0.00	mm
z_i	-2.6	mm

5.1.4 Material Properties

Two plates with different materials and thicknesses were employed in the laser welding simulation as given by the authors in their work. One plate was of HSLA 340+Z alloy and had thickness of 2.6 mm while the other plate was made of HC340LAD+Z with a thickness of 1.7 mm. The chemical composition of two materials is given in

Table 4 and Table 5. As evident from tables, both plates were alloys of stainless steel with minute differences in the chemical composition, therefore only properties of HSLA340+Z were used in the model.

Table 4 Chemical Composition of HSLA 340+Z [63]

C	Si	Mn	P	S	Nb
≤ 0.1	≤ 0.05	≤ 0.75-0.85	≤ 0.015-0.025	≤ 0.05	≤ 0.05

Table 5 Chemical Composition of HC340LAD+Z [63]

C	Si	Mn	P	S	Nb
≤ 0.11	≤ 0.5	≤ 1.0	≤ 0.025	≤ 0.03	≤ 0.09

The physical properties of HSLA340+Z were defined as a function of temperature i-e by the thermo-physical properties. Authors have defined only the properties of thermal conductivity and specific heat as a function of temperature in the paper and it is assumed that density at room temperature was used for modelling the process. However, no information about the numerical value used for density is provided in the paper. Henceforth, the properties of thermal conductivity and specific heat were used as given in the benchmarked paper [54] and are given in Table 6.

Table 6 Temperature Dependent Thermal Conductivity and Specific Heat [54]

Temperature (℃)	Thermal Conductivity (λ, W/m,℃)	Specific heat (C_P, J/Kg,℃)
20	15.0	442
200	17.5	515
400	20.0	563
600	22.5	581
800	25.5	609

1000	28.3	631
1200	31.1	654
1340	33.1	669
1390	66.2	675
2000	66.2	675
5000	66.2	675

To increase the accuracy of this study, density was also used as thermo-physical property instead of defining a value independent of temperature as assumed for the work done by authors. Keeping in view the referencing of properties for HSLA-340 from stainless steel 304, the value of density not given in the paper was also used as that of stainless steel from the work of [21]. The temperature versus density values are given in *Table 7* below.

Table 7 Temperature dependent Density values[21]

Temperature (℃)	Density (ρ, kg/m^3)
32.01	7917.677
141.76	7886.747
258.384	7839.505
361.280	7797.714
466.46	7757.732
599.08	7701.412
717.98	7648.732
841.46	7583.366
946.646	7528.891

1051.82	7478.03
1157.012	7421.753
1266.768	7367.27
1344.51	7330.947
1399.39	7298.27
5000	7298.27

The amount of energies absorbed during phase change from solid to liquid and liquid to plasma phase during welding are defined by the latent heat of solidification and latent heat of vaporization. Latent heat of vaporization was also incorporated in model definition as the keyhole shape profile is modelled. Latent heat of solidification for stainless steel is 285 KJ/Kg where the solidus and liquidus temperatures are 1400 ℃ and 1450 ℃ respectively. Latent heat of vaporization is 760 KJ/Kg [64] and its vaporization temperature is referenced from stainless steel which is 2800 ℃ [61]. The maximum temperature was assumed to be 3000 ℃.

5.1.5 Convection and Radiation

Heat losses were modelled by applying boundary conditions of convection and radiation. However, instead of applying the convection and radiation through two separate equations total heat loss co-efficient, 'α_h' was calculated using equations (5.1) and (5.2) as given in the paper [54] and was applied as a heat transfer co-efficient using surface film condition tab available in the software.

$$\alpha_h = 0.0668T , \ 0 < T < 500 \tag{5.1}$$

$$\alpha_h = 0.231T - 82.1 , \ T > 500 \tag{5.2}$$

Where T is the temperature in degree Celsius.

5.2   Modelling in Abaqus/Standard

5.2.1   Geometry

3D geometrical part was modelled in Abaqus/Standard using 'part' module. The plates used were 2.7 mm (0.0027 m) and 1.7 mm (0.0017 m) thick, 60mm wide and 400mm long. However part symmetry was utilized and quarter length was modelled for analysis only 400 mm as reduced to 100 mm. The complete geometrical information was referred from the benchmarked paper. The geometry was modelled symmetrically i-e the origin was at the top centre of the model.

The dimensions of the part are given in Figure 8 using top and side views.
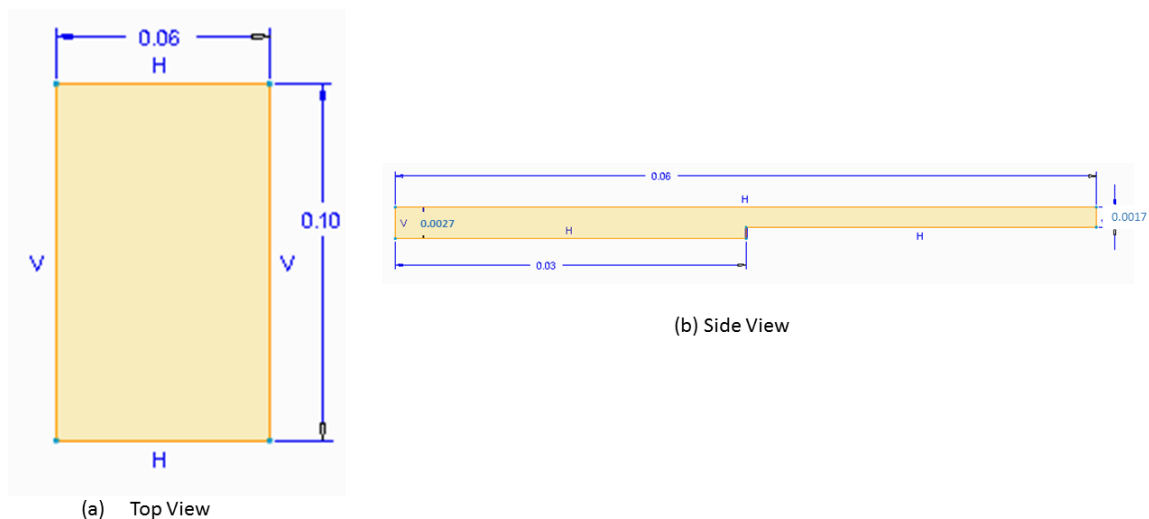
Figure 8 Part Geometry Dimensions (in metres)

5.2.2   Properties and Section Assingment

Thermo-physical properties were assigned to the model using the 'property' module. Properties assigned for thermal analysis are

1. Density
2. Thermal conductivity
3. Specific heat at Constant Pressure
4. Latent heat of solidification
5. Latent heat of vaporization

The above mentioned properties and their values were defined at temperatures ranging from 0 ℃ to 5000 ℃ and are given in section 5.1.4.

5.2.3 Steps

Two steps were created in Abaqus/Standard to perform transient analysis. These are

i.   Step-1: Initial
ii. Step-2: Welding

Step-1: Initial

The 'Initial' step is generated by default in Abaqus which signifies the unloaded condition of the model. The room temperature condition is defined in this step as a pre-defined field of 25 ℃ acting on the model. The pre-defined temperature field in 'initial' step is shown in Figure 9 below.
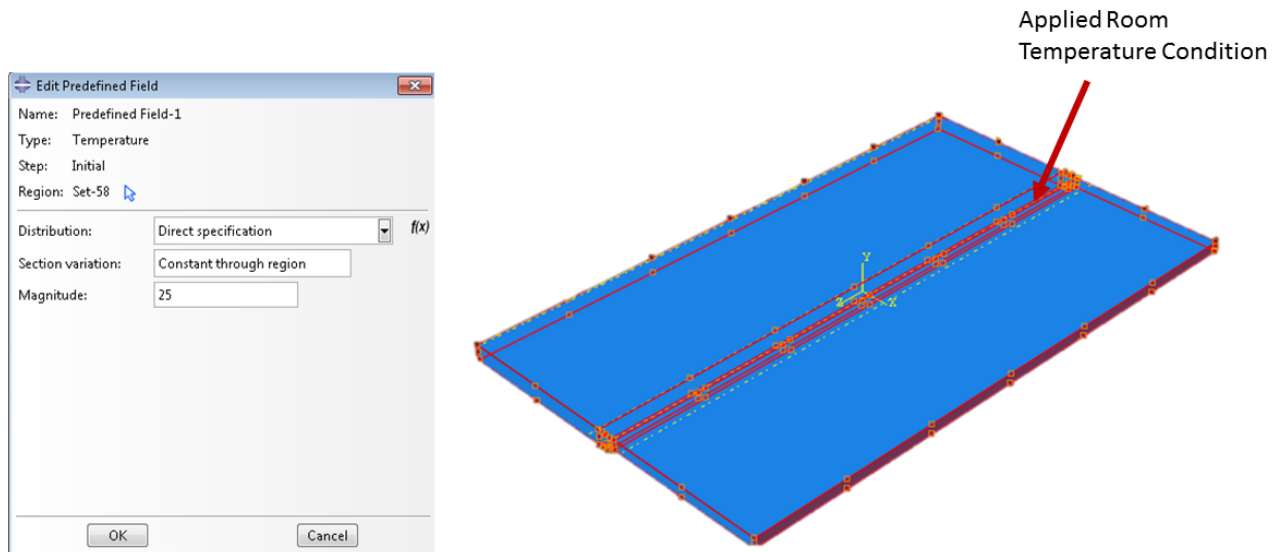
Figure 9 Assignment of Room Temperature Condition in Initial Step

Step-2: Welding

Transient thermal analysis is actually carried out in this step. The step definition includes the increment size, maximum temperature change allowed in a step and the type of solution method. Newton method was used for solving non-linear equations of transient thermal analysis.

The step details are given in Table 8.

56

Table 8 Details of Transient Analysis Step 'Welding'

Step Definition	Details
Type	Transient thermal analysis
Step- time	0.75 seconds
Maximum allowed temperature change per increment	200 ℃
Initial Increment Size	0.001
Minimum Increment Size	0.00001
Maximum Increment Size	0.001

5.2.4   Boundary Conditions

Boundary conditions of convection and radiation were applied by calculating total heat loss co-effcient 'α_h' using equations (5.1) and (5.2).

The calculated values of 'α_h' for a range from 0 ˚C to 5000 ˚C are presented in Table 9 below.

Table 9 Temperature Dependent values of Total Heat Loss Coefficient

Sr. No	Temperature	α_h
1	0	18.234
2	100	24.9164
3	200	31.59
4	227	33.4
5	300	50.263
6	400	73.363
7	500	96.46

8	600	119.563
9	700	142.663
10	800	165.763
11	900	188.863
12	1000	211.963
13	1100	235.063
14	1200	258.163
15	1300	281
16	1400	304.363
17	1500	327.4
18	1600	350.563
19	1700	373.663
20	1800	396.763
21	1900	419.863
22	2000	442.963
23	2100	466.063
24	2200	489.163
25	2300	512.263
26	2400	535.363
27	2500	558.463
28	2600	581.56
29	2700	604.66
30	2800	627.76

31	2900	650.86
32	3000	673.96
33	3100	697.06
34	5000	697.06

5.2.5 Application of Heat Flux and Modelling of Moving Laser Beam

Laser beam source for simulating the welding process was modelled using user subroutine DFLUX.

Equations (4.13), (4.14) and (4.15) as described in section 4.4.1 above were used to calculate the heat flux produced by the incident laser beam of 3400 W moving with a speed of 8.5m/min over the subject.

Moving laser characteristic was incorporated in the subroutine using triangular wave function according to which the applied heat flux moved from one end to the other end.

The user subroutine DFLUX used for simulating results of benchmarked paper-I is given as Appendix-A. The construction of subroutine is summarized block wise by Figure 10. The division of subroutine in various blocks is done for ease of explanation based on functions of its different parts.

Block-1 • Lists the variables to be called in the subroutine and their data type

Block-2 • Defines parametric values of the variables to be used

Block-3 • Defines the laser movement coordinates

Block-4 • Defines the thermal model using equations described in section 4.4.1

Block-5 • Defines wave function for laser source movement over the workpiece
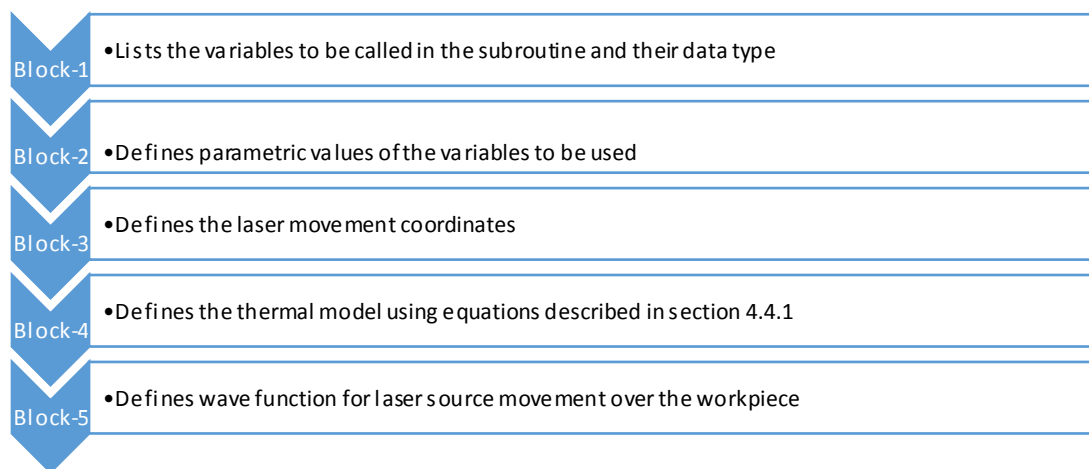
Figure 10 Construction of Subroutine

The subrountine blocks' 1, 2 , 3 , 4 and 5 are described below.

Block- 1

This block defines the constants and variables used in the model. Two data types are used in this block for defining the variables and constants. **Real** corresponds to type Real numbers which can take all the rational and irrational values or in other words any point on a number line. All the variables and constants used are described as real numbers. **Double Precision** is another data type which allows more precision with respect to saving the digits after decimal point. In double precision data type number, the number of significant places is 15 otherwise upto 6 digits are stored in the memory. The variables and constants assigned in block 1 are described in .

Table 10.

Table 10 Variables and Constants used in DFLUX subroutine

Sr. No	Variable/Constant	Description
1	x	x-cordinate (width)
2	y	Y co-ordinate (depth)
3	z	Z co-ordinate (length)
4	v	Velocity of laser heat source
5	t	Time
6	xl	Changing position of laser source wrt x axis However as laser moves on z-axis, x-cordinate doesn't change with time so xl=0
7	zl	Changing position of laser source wrt z axis

8	nom_power	$\text{nom\_power} = Q_o = \dfrac{3Q}{\pi r_e{}^2 h}$
9	re	Radius of laser beam at the top surface
10	ri	Radius of laser beam at the depth of 0.0011m
11	ye	Y co-ordinate at the top surface thus ye=0
12	yi	Y co-ordinate at the maximum depth till which heat source acts (yi=0.0011)
13	rc	Radius at the top surface calculated from the x and z co-ordinates at time t
14	r	Radius of heat source at some depth

Block-2

This block contains the values of constants of heat source profile which are **re**, **ri**, **ye**, **yi** and **nom_power.** The heat source profile is computed using equation (4.15) which is

$$Q_o = \frac{3Q}{\pi r_e{}^2 h} \tag{4.14}$$

Where

Q denotes laser power; measured in Watts

π is a constant

r_e is the radius of laser source at the top surface; measured in mm or m

h is the depth of work piece measured in mm or m

Block-3

In this section of the subroutine, the co-ordinates of point at any time 't' and the radius of laser heat source 'rc' conforming to the x and z co-ordinates and radius of heat profile 'r' corresponding to depth 'y' are calculated. The current time is denoted by 't' at which the co-ordinates of laser position are x, y and z. Change in the position of laser source along z-axis is governed by the

triangular wave function, i-e zl=triang (t) which is defined in block 5. As laser beam moves on the z-axis (as per the modelling of geometry) change in position with respect to x co-ordinates i-e xl=0. Thus from the distance between two points formula and the radius calculation using x and z co-ordinates we get 'rc' from the following equation used in the subroutine

$$r_c = \sqrt{(x-xl)^2 + (z-zl)^2} \qquad (5.3)$$

where rc is the radius at the current time, 't'.

The radius 'r' of the heat source profile changes with depth as evident from figure 2. This changing radius 'r' is calculated using equation (4.13); which is

$$r(y) = r_e + \frac{r_i - r_e}{y_i - y_e}(y - y_e) \qquad (4.13)$$

Where

$r_e = 0.00069$

$r_i = 0.0003$

$y_i = -0.0011$

$y_e = 0$

y is the depth from 0 to -0.0027

Putting in the values in above equation,

$$r(y) = 0.00069 + \frac{0.0003 - 0.00069}{-0.0027 - 0}(y - 0) \qquad (5.4)$$

Therefore, the above equation reduces to

$$r(y) = 0.00069 + 0.1625 * y \qquad (5.5)$$

Which is used in the code to calculate 'r'.

62

Block-4

This part of the subroutine deals with the actual application of laser heat source on the model through expression

$$FLUX(1)=nom\_power*exp(-3*rc**2/r**2) \qquad (5.6)$$

Where '*' means multiplication and '**' refers to raised to the power.

Which is derived from equation (4.14) ; which is

$$Q(x, y, z) = Q_O \exp(-\frac{3(x^2+z^2)}{r^2(y)}) \qquad (4.14)$$

Where

nom_power= Q_O

rc**2= $x^2 + z^2$

r**2= $r^2(y)$

'rc' and 'r' are used as given by equations (5.3) and (5.5) in block 3.

USE OF CONDITIONAL STATEMENT

Conditional statement 'IF' is used in this block for application of heat flux. The conditional statement used is IF (r>0). It implies that when radius changing with depth is greater than 0, only then the expression evaluating heat flux will apply otherwise no heat flux will act on the part model. This statement accounts for the heat source profile Gaussian parameters given by the authors that the heat flux doesn't apply equally on the whole irradiated spot in depth rather, the radius of heat flux application decreases until it reaches a depth of 2.4mm or 0.0024m. The same condition is applied using the IF statement that when the radius becomes 0 at depths greater than the specified dimensions, the heat flux doesn't act. Also, negative 'r' values signify increasing heat flux with increasing depth which is not possible.

Block-5

In this section the triangular wave function is defined which governs the movement of laser heat source on the work-piece in z direction. Length 'L' and velocity 'v' are used to determine the period which is given by the following equation

$$period = \frac{2L}{v}$$ (5.7)

5.2.6 Meshing

Initially a test simulation with uniform mesh was run to determine the accuracy of mesh and width of region affected by the laser heat source. Standard DC3D4 4-node linear tetrahedron was used for testing mesh size. The element size used for the generated mesh in Figure 11 was 0.0004 m. Simulation results revealed that this mesh size was not adequate to model the process as improper laser shape was obtained with the simulation based on this mesh. The distorted laser shape obtained with the mentioned mesh size is also shown in Figure 11(a).

(a) Distorted Laser Shape   (b) Eight Elements lie under HAZ
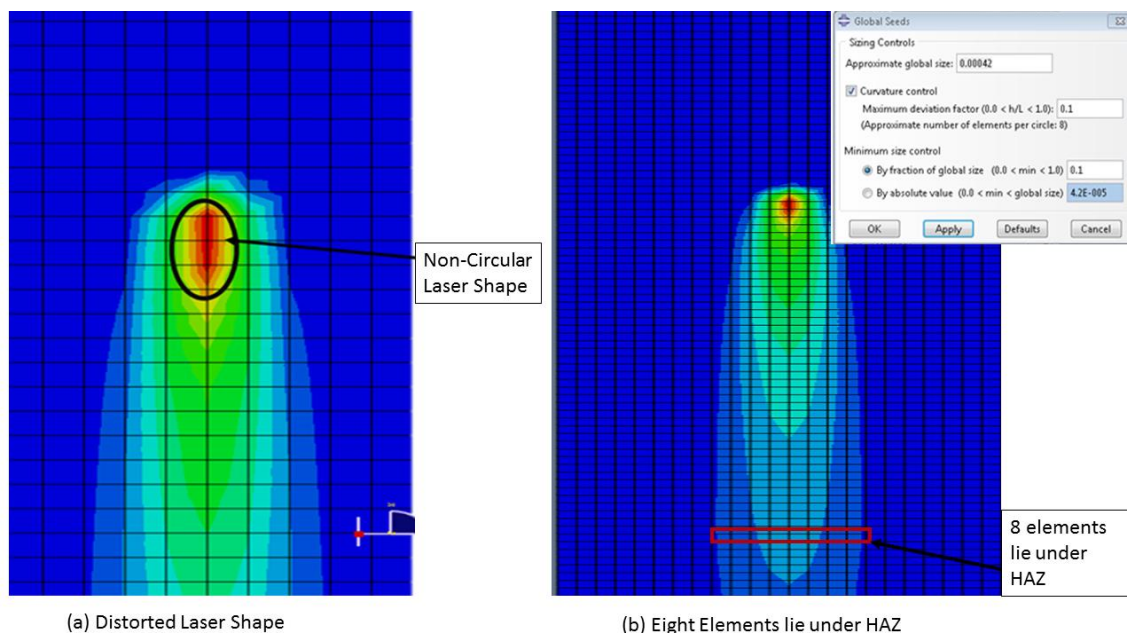
Figure 11 Distorted Laser Shape and Width of Region Underwent Temperature Change

The width of region that underwent temperature change was computed by multiplying the number of elements with the element size.

width of region underwent temperature change=0.00042×8 (5.8)

$$\text{width of region underwent temperature ch\qquad ange=0.0036} \qquad (5.9)$$

Therefore the geometry was divided into three regions for meshing to increase the accuracy of results with reduced computational time. The central region where the heat source moved was meshed using smaller sized elements and resulted in a very fine mesh while the regions around the welding region contained a coarse mesh. Based on the calculation given by equation (5.9) the welding region (centre of the model) was modelled by assigning it a width of 0.0036m. The division of geometry into three regions is highlighted in Figure 12. The geometry was divided into three regions for meshing.
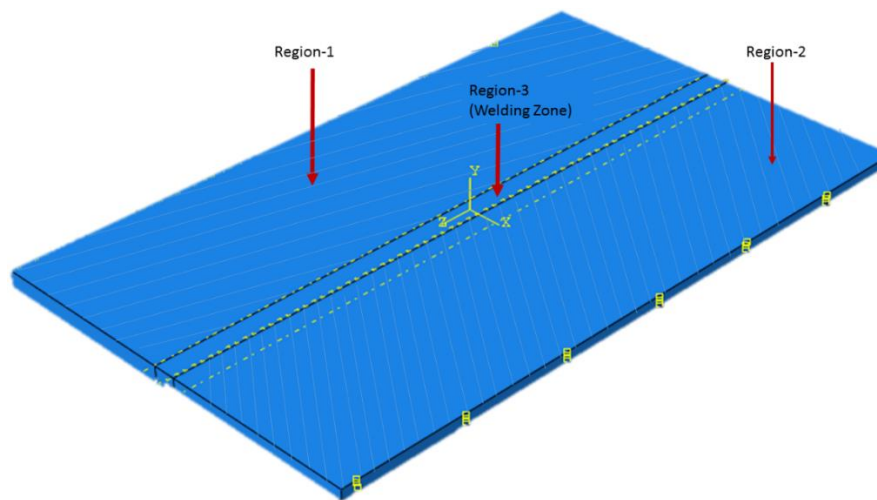
Figure 12 Division of Geometry in three regions for meshing
Regions-1 and 2 contained coarse mesh while Region-3 contained fine mesh

Combination of element types was used in order to control the mesh size and balance the computational time and accuracy of results [65]. Hex dominated shape elements of size $0.000138 \times 0.000138 \times 0.003$ m were used for meshing Region-3 or the welding region. Free mesh was generated in Regions-1 and 2 using tetrahedral shaped elements having a size of $0.001 \times 0.0025 \times 0.0025$ m^3 at the top and $0.003 \times 0.0025 \times 0.0025$ m^3 at the bottom. The growth rate of elements was set at 2. The element sizes at various edges are given by Figure 13 and Figure 14.
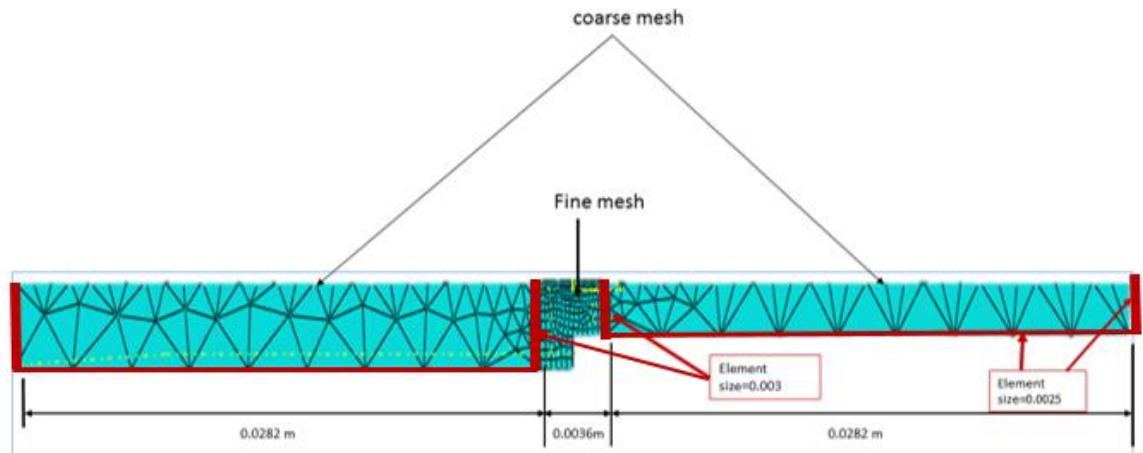
Figure 13 Element sizes defined for the vertical and horizontal edges for the welded and surrounding regions by red edges
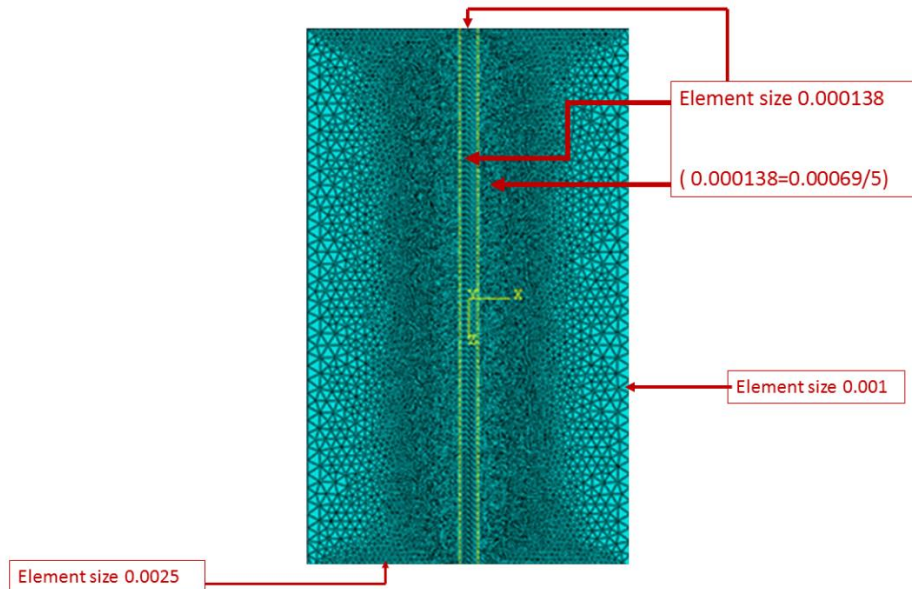
Figure 14 Element sizes of Mesh at the top surface

A total of 1094245 elements were generated with 360834 nodes. Out of these 123250 were linear hexahedral elements of type DC3D8, 1450 were linear wedge elements of type DC3D6 and 969545 were linear tetrahedral elements of type DC3D4.

5.2.3 Results and Validation

The maximum welding temperature reported from the benchmarked paper is 2937 °C as given by graph in Figure 15.
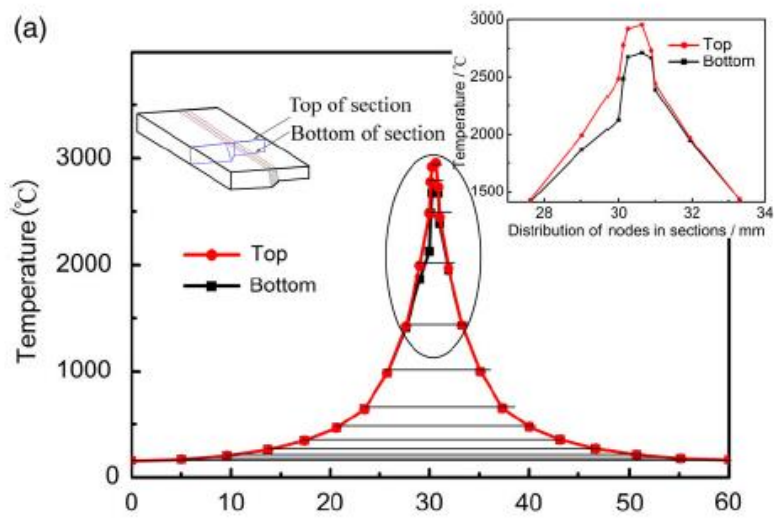
Figure 15 Temperature vs Distance Graph [54]

The temperature achieved from the simulation was $2912\,°C$. The welding tail plotted at 0.3 seconds during the process at quasi-static temperature state is given by Figure 16.
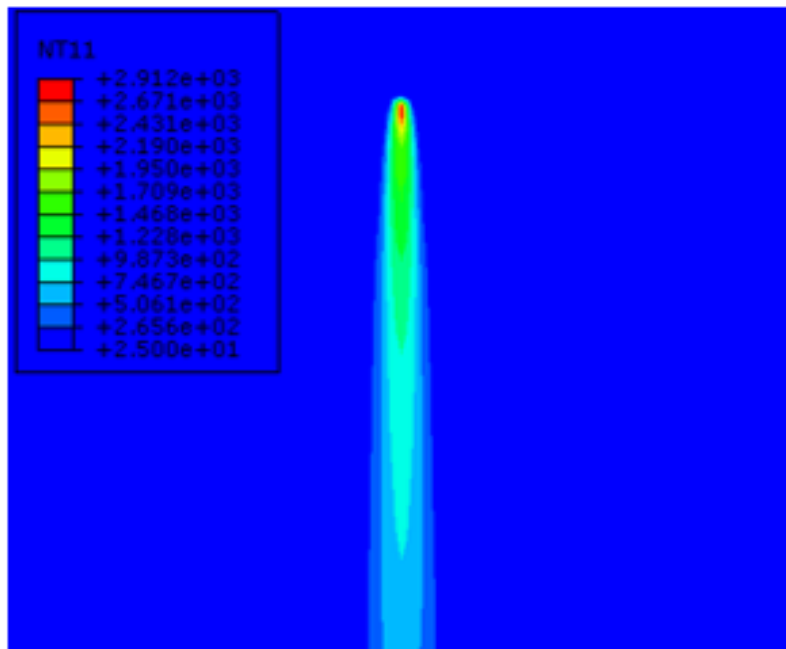
Figure 16 Welding Tail at 0.3 s showing Maximum Attained Temperature

The percentage difference between the reported value and the achieved value is given as

$$PercentageError = \frac{2937 - 2912}{2912} \times 100 \qquad (5.10)$$

$$PercentageError = 0.85\% \qquad (5.11)$$

The benchmarked paper did not report any numerical value for the width of fusion zone. However, the graphical figure indicated that the entire depth underwent fusion after the welding. Graphical comparison of the cross-section of the workpiece between the image reported from paper and the simulation is given in Figure 17 . The time or distance reference for the reported image was not given in the paper and it was therefore assumed that the measurement was done at the completion of the welding process. It is evident from the figure that the temperatures reported for the given bead cross-section bead from the reported paper and those achieved in the simulation have the same temperature distribution. The enclosed regions by bounding boxes indicated by the arrow heads in Figure 17(a) and (b) have the temperature in the region i-e $1400\,°C$. The peak temperature in Figure 18(b) is reported 2916 C as the image was captured during the process. The maximum temperature is comparable to the maximum reported temperature as mentioned above.
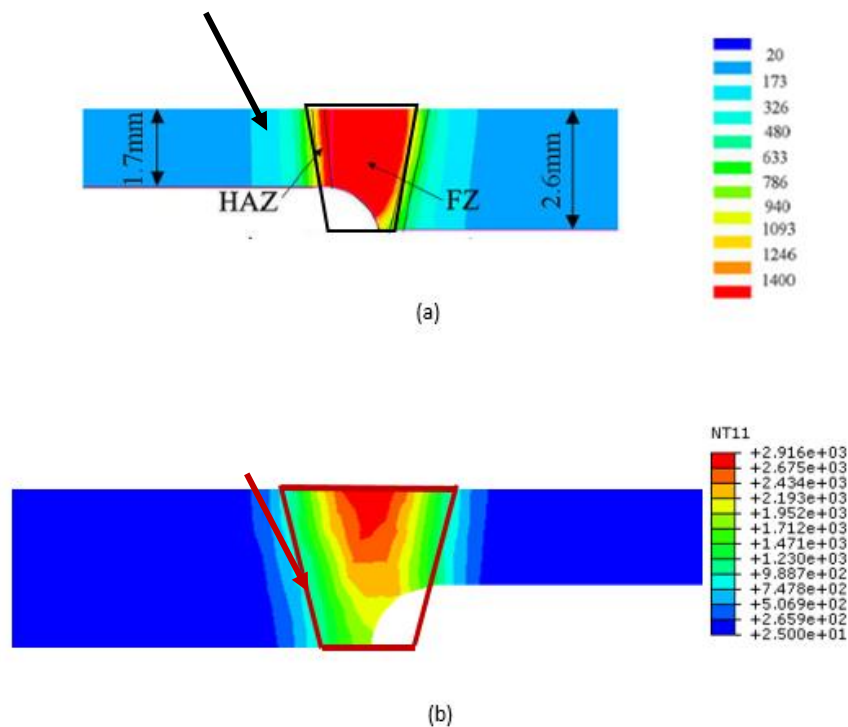
Figure 17 Comparison of Reported and Achieved Results for the Cross-Section where (a) Reported Results from Paper [54] (b) Achieved Results

The reported results were achieved with a percentage error of 0.85 % and the developed model was thus verified to be used for further study. The model was then extended to validate the results of benchmarked paper-II with variations in laser and heat source model parameters.

5.3   Validation Study of Benchmark Paper-II

5.3.1 Characteristics of Laser Source

Laser source of 2500 Watt was used by authors for laser welding of Aluminium Alloy 5083 [8]. CO_2 laser was employed for performing the welding having a focal length of 200mm. The laser beam had a diameter of 25 mm at the exit with a divergence of 0.5mrad. The velocity with which laser source traversed is given as 100mm/s or 0.1 m/s.

5.3.2 Heat Source Modelling Parameters

Authors have assumed the Conical Gaussian heat source distribution along thickness of workpiece with the formation of a stable keyhole. Based on this assumption, the same heat source model was employed for this paper as used for benchmark study-I as given in section 4.1. Unlike benchmarked paper-I, parameters to model the heat source i-e r_e, r_i, z_e and z_i were not given in the paper and thus they were determined using hit and trial method to capture the temperature profile as in the paper.

The final values of the heat source parameters that were determined are given in Table 11 below.

Table 11 Gaussian Heat Source Parameters for Benchmark Paper-II

Parameter	Value	Unit
r_e	0.6	mm
r_i	0.54	mm
z_e	0.00	mm
z_i	-3.0	mm

5.3.3 Material Properties

Model material AA 5083 alloy was used for the welding simulation of two plates butt welded together. AA 5083 alloy is a structural alloy used particularly in applications of ship building and industrial applications because of its resistivity to extreme environments. The alloy composition of this material is given in Table 12[66].

Table 12 Composition of Aluminium Alloy 5083[66]

Si	Cu	Mn	Mg	Ti	Al
0.5	0.1	0.5	4.5	0.15	Balance

For simulating the welding process, temperature dependent properties of thermal conductivity, specific heat and density were used. Latent heat of vaporization was also used along with latent heat of fusion. The values of these properties were referenced from published literature. Literature survey revealed that for Aluminium Alloy 5083 the thermo-physical properties were given upto 580 degree Celsius. Values of temperature dependant Thermal Conductivity were determined using the formula given in TALAT Lectures [67]. These values are given in below.

Table 13 below.

Table 13 Temperature dependent Thermal Conductivity of Aluminium Alloy 5083[67]

Temperature ($°C$)	Thermal Conductivity ($W / m\,°C$)
20	142
40	144
60	146
80	148
100	150
120	152

140	154s
200	160
250	165
300	170
350	175
400	180
600	240
1000	240

The values of Density and Specific heat are given in

Table 14 as referenced from the published literature [68]. The values of specific heat at temperatures higher than $580\,^\circ C$ were given in [67] and are accordingly used in the simulation to increase the degree of accuracy of results.

Table 14 Temperature Dependent Density and Specific Heat of Aluminium 5083 [66-67]

Temperature ($^\circ C$)	Density (Kg/m^3)	Specific Heat ($J/Kg^\circ C$)
-20	2673.9	924.1
80	2642.7	984.2
180	2629.4	1039.6
280	2611.5	1081.2
380	2589.3	1136.6
480	2567	1178.2
580	2549.2	1261.4
600	2549.2	1040
700	2549.2	1060

1000	2549.2	1000
2000	2549.2	1000

Other physical properties used in simulation are summarized in Table 15.

Table 15 Miscellaneous Thermal Properties of Aluminium Alloy 5083 [69]

Property/Units	Value
Latent Heat of Fusion (KJ/Kg)	397
Latent Heat of Vaporization (KJ/Kg)	9492
Liquidus Temperature ($°C$)	574
Solidus Temperature ($°C$)	657
Vaporization Temperature ($°C$)	2425

5.3.4 Convection and Radiation

Heat transfer conditions of convection and radiation were defined for the model as used by the authors in the paper. Constant conditions of convection and radiation were defined based on the assumption of free convection and radiation as no reference was given to their temperature dependency in the paper.

For defining convection and radiation; the values of emissivity, heat transfer co-efficient, Stephan-Boltzmann constant and absolute zero temperature values were defined. The values of these properties and their units are given in Table 16 below [70].

Table 16 Constants used for defining Boundary Conditions[70]

Emissivity of Aluminium Alloy 5083	0.02
Heat Transfer Co-efficient	0.05
Stephan-Boltzmann Constant	5.67E-008

Absolute Zero Temperature	-273

5.4 Modelling in Abaqus/Standard

The part was modelled and simulated in Abaqus/Standard following the same steps and interface modules of the software as explained in detail for modelling of benchmark paper-I, section 5.2.

5.4.1 Geometry

3D geometrical part of $50\,mm \times 58\,mm \times 3\,mm$ was modelled. The modelling dimensions used by authors in their work were $108\,mm \times 58\,mm \times 3\,mm$. Instead of modelling complete length of $108\,mm$, a smaller workpiece was modelled as the temperature profile to be achieved for model validation was independent of the length of workpiece. Figure 18 below shows top and front views of the model with dimensions.
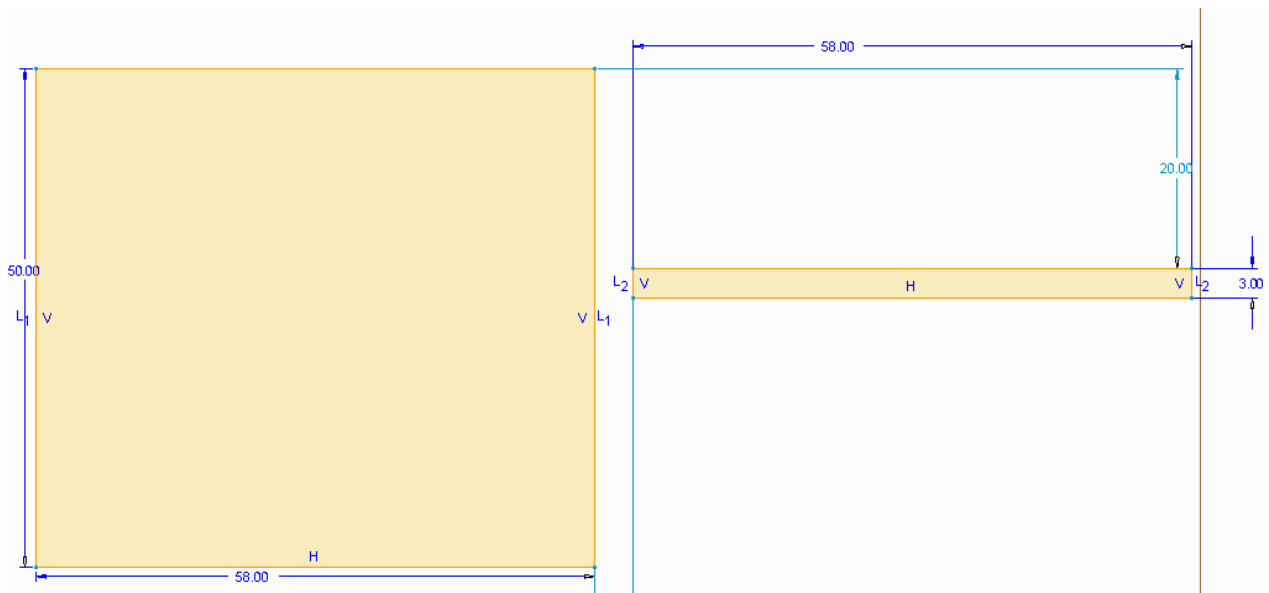
Figure 18 Modelling Dimensions for Geometry in Benchmark Study-II

5.4.2 Properties and Section Assingment

Density, thermal conductivity and specific heat were defined as thermo-physical properties for thermal analysis and were assigned to the model through section assignment. Latent heat of fusion, latent heat of vaporization, solidus temperature, liquidus temperature and boiling temperature were also defined. The values of these properties are given in section 5.3.3.

5.4.3 Steps

Two steps were defined to carry out the transient thermal analysis. Transient analysis was performed under the welding step.

iii.   Step-1: Initial

iv.   Step-2: Welding

5.4.3.1   Step-1: Initial

The room temperature condition was defined in this step as a pre-defined field of $20°C$ acting on the model.

5.4.3.2   Step-2: Welding

The step definition includes the increment size,maximum temperature change allowed in a step and the type of solution method. Newton method was used for solving non-linear equations of transient thermal analysis. The step details are given in Table 17

Table 17 Step Details for Transient Thermal Analysis for Benchmark Study-II

Step Definition	Details
Type	Transient thermal analysis
Step- time	0.5 Seconds
Maximum allowed temperature change per increment	400 ℃
Initial Increment Size	0.001
Minimum Increment Size	0.00001
Maximum Increment Size	0.001

5.4.4 Boundary Conditions

Boundary conditions of convection and radiation were applied by defining the interaction conditions using surface film condition and surface radiation. Surface film condition defines the phenomenon of convection using heat transfer coefiicient while surface radiation condition defines heat transfer through radiation using emissivity and Stephan-Boltzmann constant.

5.4.5 Application of Heat Flux and Modelling of Moving Laser Beam

User subroutine DFLUX was employed for simulating the moving laser heat source and is attached as Appendix-B.

Same Equations i-e (4.13), (4.14) and (4.15) as described in section 4.4.1 were used to calculate the heat flux. However, the values of parameters defining the laser source changed in accordance to those used by the authors of benchmark paper-II.

Block wise construction of the subroutine is the same as given in Figure 10.

Block- 1

The constants and variables used in the model are the same as given in .

Table 10 provided in section 5.2.5.

Block-2

This block contains the values of constants used for modelling heat source profile. These are **re**, **ri**, **ye**, **yi** and **nom_power** $Q_\circ$**,** which is computed using equation (4.15); given as

$$Q_o = \frac{3Q}{\pi r_e^{\ 2} h}$$

Block-3

Following parameters are calculated in this part of the sub-routine:

The co-ordinates of point at any time 't'
The radius of laser heat source 'rc' conforming to the x and z co-ordinates
Radius of heat profile 'r' corresponding to depth 'y'

As explained earlier, the radius at any instant of time is given by equation (5.3) which is:

$$r_c = \sqrt{(x - xl)^2 + (z - zl)^2}$$

where rc is the radius at the current time, 't'.

The radius 'r' of the heat source profile changes with depth as evident from Figure 7. This changing radius 'r' is calculated using equation (4.13); which is

$$r(y) = r_e + \frac{r_i - r_e}{y_i - y_e}(y - y_e)$$

Where

$r_e = 0.0006$

$r_i = 0.00054$

$y_i = -0.003$

$y_e = 0$

y is the depth from 0 to -0.003

Block-4

This part of the subroutine is the same as for the benchmark paper-I as it is based on equations of the heat source model.

Block-5

The explanation for this block given for benchmark paper-I holds good for benchmark paper-II. The only difference lies in the scanning speed of the laser heat source over the workpiece.

Meshing

For the thermal analysis, combination of element types was used in order to control the mesh size and refinement to balance the computational time and accuracy of results [65].

The geometry was divided into two regions for meshing. The central region over which the laser source traversed contained a fine mesh of hexahedral elements of uniform size of 9E-4 units while the peripheral region were meshed with tetrahedral elements with a growth rate of 1.37 towards the periphery to balance the computational time.

Authors have not reported any specific mesh size used for the model except that the mesh consisted of about 20,000 elements. However, the model in present case consisted of 747650 elements and 474315 nodes while the simulation took 26 hours to complete. 747650 elements were used for reporting results as this set of elements was selected after performing mesh sensitivity analysis.

5.2.1.1 Results and Validation of Developed Model

Temperature profile for model validation was achieved with peak temperature of 1048 °C. The simulation was run for 0.1 seconds until the maximum temperature was achieved and no further variation in temperature was observed.

For validation of developed thermal model, a comparison of temperature profile for the lateral view is given in Figure 19. Maximum temperature obtained from the study is 1048 °C and that reported by the authors is 980 °C; percentage error being 6.48 %.

(a)

(b)
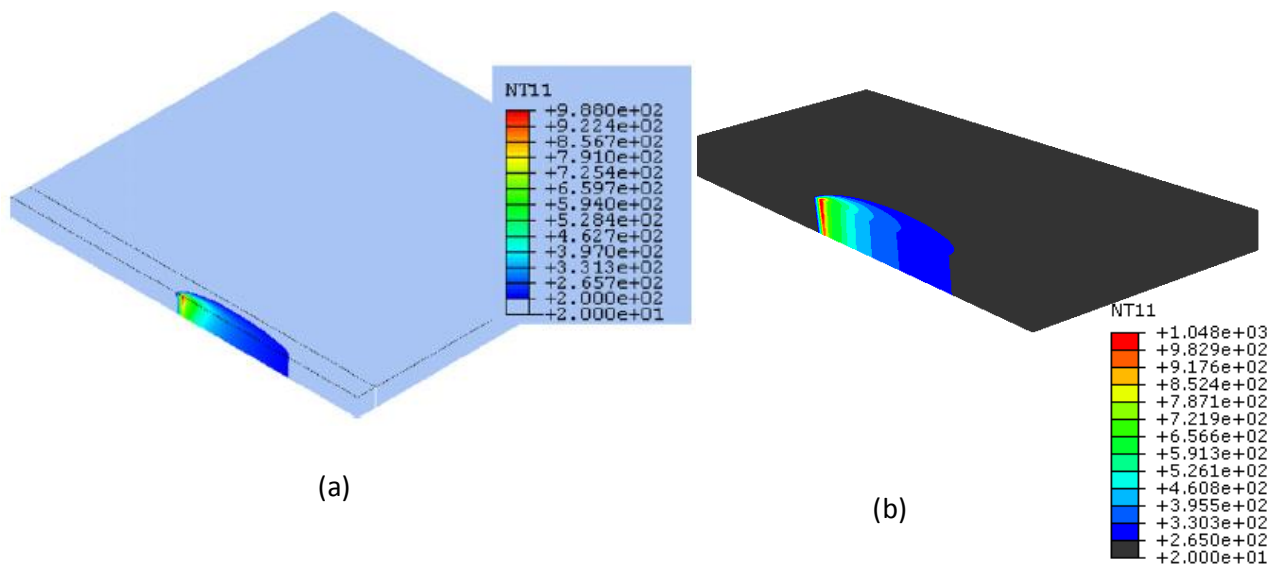
Figure 19 Comparison of Reported and Achieved Temperatures for Lateral View Benchmarked Paper-II where (a) Reported Temperatures [8] *(b) Achieved Temperatures*

Comparison of cross-sectional view at the end of the process and top view of the weld at intermediate time during welding between the simulated and reported results is given by Figure 20 and Figure 21 respectively. The similarity in shape of the welded regions is evident as given by the cited figures and minimal percentage error indicate that the model is sufficiently accurate to model the process.
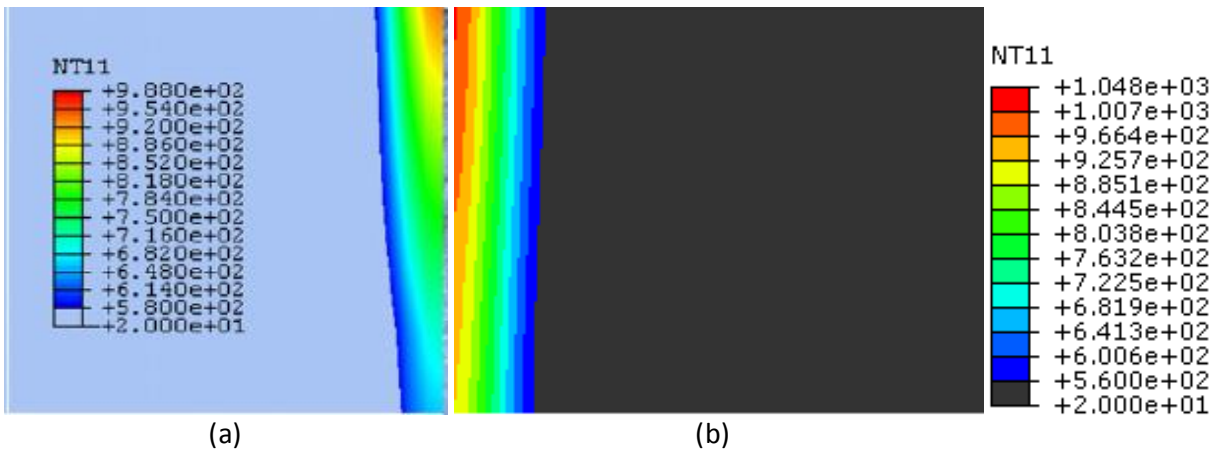
Figure 20 Comparison of Cross-Sectional Weld View for Benchmarked Paper-II where (a) Results Reported by Paper [8] (b) Achieved Results
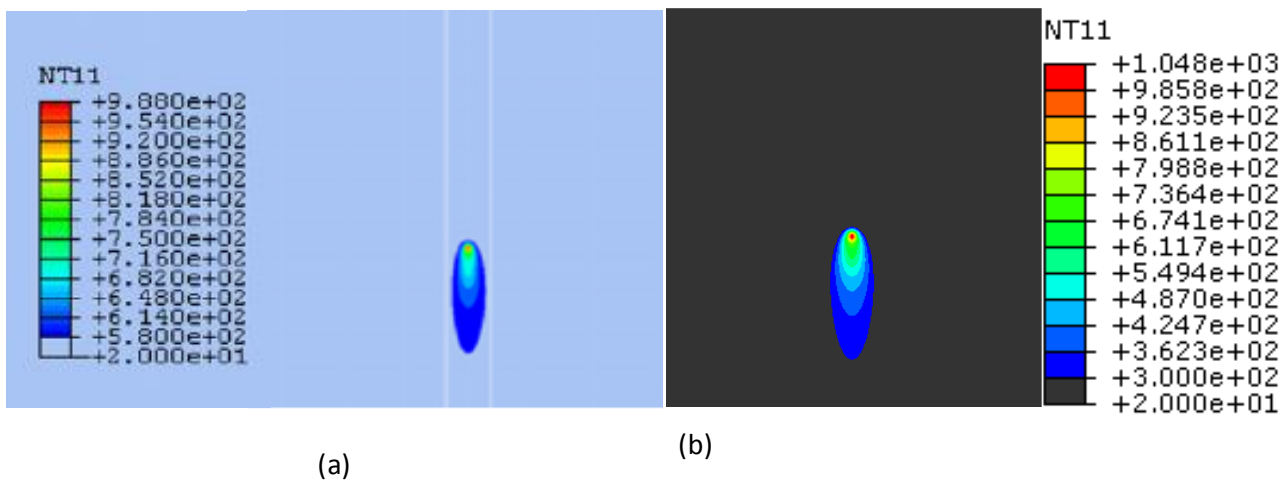
Figure 21 Comparison of Results for the Top View for Benchmarked Paper-II where (a) Results Reported from Paper [8] (b) Achieved Results

Based on reproduced results of benchmarked paper-I and benchmarked paper-II with percentage error of 0.8 % and 6.48 percent respectively it is concluded that thermal model presented in section 4.4.1 and subroutine DFLUX is adequate to model the process of laser welding.

Based on the above validated model, the parametric optimization studies for AA 5083 were carried out as given in the next chapter.

Chapter 6: Parametric Optimization Studies for AA 5083 for Laser Welding Process

The thermal model as explained in detail in Chapter 5 and user subroutine DFLUX was used to simulate the laser welding process for optimization studies.

6.1 Input and Output Parameters

The optimization studies were carried out for determining the weld aspect ratio, heat affected zone and weld pool shape for desired micro-structure against varying laser power, welding speed and specimen thickness. The input and output parameters are given in Table 18.

Table 18 Input and Output Parameters of Study

Input Parameters	Output or Response Parameters
Laser Power (Watts)	Peak Temperatures (˚C)
Welding Speed (mm/s)	Aspect Ratio
Specimen Thickness (mm)	Width and Depth of Weld Bead (mm)
	Macroscopic Pool Shape
	Width of Heat Affected Zone (HAZ) (mm)

It is reported from literature that out of all the process parameters, Laser power and welding speed are the two most important factors which govern the heat input model, penetration model and welded zone width [12], [15], [16], [71]. Laser Power and welding speed parameters provide the most flexibility to model laser welding simulation and are thus used extensively in simulation studies.

Various parametric studies have revealed the obvious behaviour between the laser power and welding speed and the attained temperatures. However, no reported work was found to predict the accurate and precise relationship between the input and output parameters marked in this study for deep penetration welding using AA 5083 aluminium alloy.

The values of laser power, welding speed and specimen thickness used in the study are given in Table 19 below. These values were selected to cover a broad range of levels based on values reported in literature and used in practice [6, 32, 33, 68, 69].

Table 19 Parametric Values of Laser Power, Welding Speed and Specimen Thickness

Parameters	Level 1	Level 2	Level 3	Level 4	Level 5
Laser Power (kW)	2.5	3.5	4.5	5.5	6.5
Welding Speed (mm/s)	60	80	100	120	140
Thickness (mm)	2	4	6	8	10

6.2 Optimization Study Matrix

The optimization studies were carried out according to the study mapped using Taguchi Design of Experiments [15], [16].Taguchi designs cover all interactions of the factor set in the most fool proof and cost effective way. The experiment set consists of every combination of the factor level without duplication and hence becomes cost effective and time saving. It is in wide use to design experiments for investigation and optimization research works and provides valid insights to the research problem. Table 20 below presents the design study matrix of simulation cases formulated using MINITAB software. The sample space contained 25 experiments with varying input parameters at 5 different levels.

Table 20 Optimization Study Matrix

Simulation Case	Level of Laser Power	Level of Welding speed	Specimen Thickness
1	1	1	1
2	1	2	2
3	1	3	3
4	1	4	4
5	1	5	5

6	2	1	2
7	2	2	3
8	2	3	4
9	2	4	5
10	2	5	1
11	3	1	3
12	3	2	4
13	3	3	5
14	3	4	1
15	3	5	2
16	4	1	4
17	4	2	5
18	4	3	1
19	4	4	2
20	4	5	3
21	5	1	5
22	5	2	1
23	5	3	2
24	5	4	3
25	5	5	4

6.3 Thermal Modelling for Optimization Studies

The optimization studies were carried in accordance with the experiments laid out in Table 20. The explanation for thermal modelling is given in detail in Chapter 4 and Chapter 5. The basic assumptions for thermal modelling are listed below:

i. The ambient environment temperature is 20 $°C$.
ii. Intensity of laser source is high enough that keyhole is formed.
iii. 100% laser energy incident on the workpiece is absorbed as keyhole acts as blackbody.
iv. The surfaces of the workpiece are subjected to free convection and radiation.

Validated Gaussian Heat source parameters to be used in the thermal modelling equations were borrowed from Chapter 5; section 5.3.2 and are summarized in Table 21 below.

Table 21 Heat Source Parameters used in Research Study

Heat Source Parameters	Value (m)
r_e	0.0006
r_i	0.00054
y_e	0.0
* y_i	-0.002

*where the parameter y_i correspond to the thickness of workpiece. For each simulation case, y_i changed according to the thickness values given in Table 19.

6.4 Material Properties

Material properties for Aluminium Alloy 5083 were used as given in section 5.3.3.These properties included density, specific heat, thermal conductivity, latent heat of fusion and latent heat of vaporization.

6.5 Boundary Conditions

Boundary conditions of free convection and radiation were applied as given in section 5.4.4 for benchmarked study-II.

6.6 Simulation Cases

For the 25 simulation cases, the framework of thermal modelling remained the same including the key assumptions, boundary conditions, physical properties and thermal modelling equations as explained in chapters 4 and 5. However, thickness, input laser power and scanning velocity of laser source on the workpiece changed with every case as given in Table 20.

The size of the workpiece selected for study was $50mm \times 40mm \times thickness$. The geometry was modelled by applying symmetric boundary condition therefore only half width i-e 20mm was modelled. The five values of thicknesses used in the study are given in Table 19.

For each simulation case thickness, heat input and step time changed (as the welding speed changed) while all other properties and boundary conditions remained the same. Simulation case-1 is explained in detail step-wise below.

6.6.1 Simulation Case-1

6.6.1.1 Geometry

For the first case, lowest level of thickness i-e 2mm was used. The dimensions are given using top and front views by Figure 22. As mentioned earlier, since symmetric boundary condition was applied therefore only half width i-e 20 mm was employed for modelling to save the computational time.
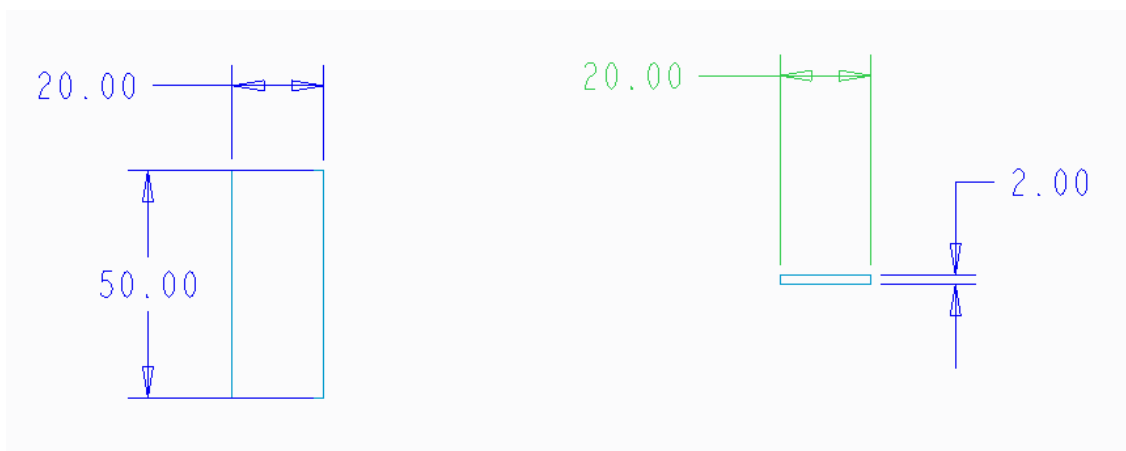

Figure 22 Geometrical Dimensions for case-1 (units: mm)

6.6.1.2 Material Properties

Thermo-physical material properties for AA 5083 alloy were used as given in section 4.6.3.

6.6.1.3 Step Definition

Step definition contained the details of time stepping which are governed by the scanning speed. For simulation case-1, the welding speed was $60mm/s$ or $0.06m/s$. Using the length of workpiece as $0.05m$, the step time became

$$t = \frac{0.05}{0.06} = 0.84s \tag{6.1}$$

6.6.1.4 Boundary Conditions

Free Convection and radiation were applied as boundary conditions as given in section 4.6.5.4.

6.6.1.5 Heat Input

For case-1, lowest level of laser power was used i-e $2500W$. The thermal model used in the subroutine (attached as appendix C) is based on equations (4.13), (4.14) and (4.15). The detailed calculations for heat input as used in the subroutine based on these equations are given below.

The total heat input for the process is given by equation (4.14); which is

$$Q(x, y, z) = Q_O \exp(-\frac{3(x^2+z^2)}{r^2(y)}) \tag{4.14}$$

Where $Q_\circ$; nominal input power; is given by equation (4.15) as;

$$Q_o = \frac{3Q}{\pi r_e^2 h} \tag{4.15}$$

And $r(y)$ is given by equation (4.13) as;

$$r(y) = r_e + \frac{r_i - r_e}{y_i - y_e}(y - y_e) \tag{4.13}$$

Putting in the values of heat source parameters from Table 21 and $y_{i=}-0.002$ for case-1; $r(y)$ becomes;

$$r(y) = 0.0006 + \frac{0.00054 - 0.0006}{-0.002 - 0}(y - 0)$$

Therefore $r(y)$ becomes;

$$\Rightarrow r(y) = 0.0006 + 0.03(y) \tag{6.2}$$

Putting in the values of parameters in equation (4.15); where

$$Q = 2500$$

$$h = 0.002$$

$$\Rightarrow Q_o = \frac{3 \times 2500}{\pi \times (0.0006)^2 \times 0.002}$$

$$\tag{6.3}$$

$$\Rightarrow Q_O = 3.315727981E12 \tag{6.4}$$

Putting the values of Q_O from equation (6.3) in equation (4.14) above;

$$\Rightarrow Q(x, y, z) = 3.315727981E12 \exp\left(\frac{-3(x^2 + y^2)}{r^2(y)}\right) \tag{6.5}$$

The equation (6.5) above is expressed as 'FLUX (1)=nom_power*exp(-3*rc**2/ro**2)' in the subroutine and corresponds to the given expression as follows.

$$\text{nom\_power} = 3.315727981E12 \tag{6.6}$$

$$\text{rc**2} = x^2 + y^2 \tag{6.7}$$

$$\text{ro**2} = r^2(y) \tag{6.8}$$

The detailed explanation of the subroutine is given in chapter 4.

6.6.1.6 Meshing

The geometry was divided into two regions for meshing: region-01 being the area over which laser heat source actually traversed and region-02 being the area around it. Region 01 contained extremely fine mesh of hexahedral elements of size 0.09mm while region 02 contained non-unform tetrahedral mesh with a growth rate of 1.37 and element size 0.9mm as shown in

Figure 23.The problem size consisted of 585720 elements and 37002 nodes.
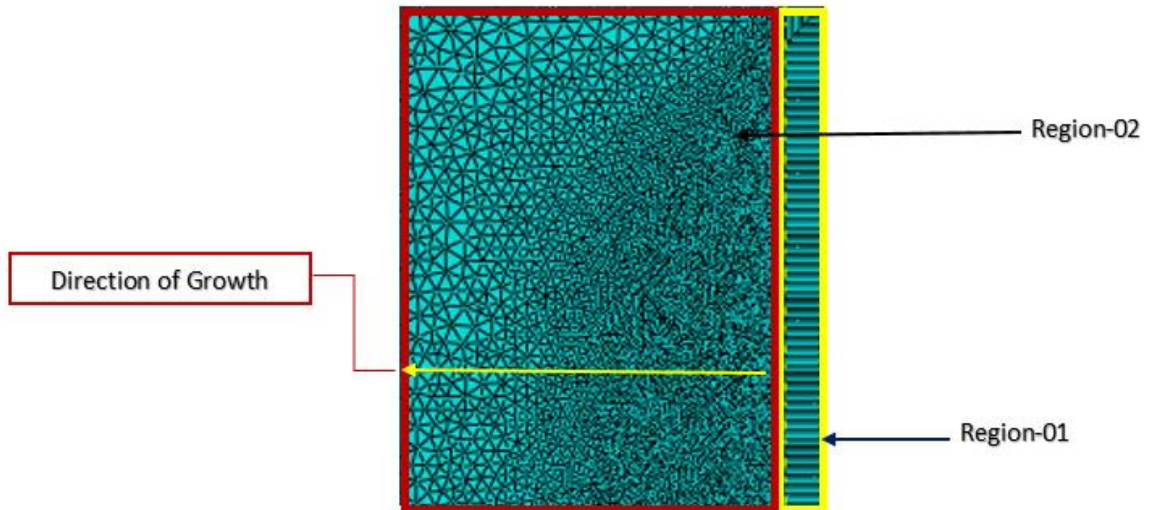
Figure 23 Element Size Distribution in the Mesh

6.7   Detailed Analysis Case-I Results

Results of Case-I are discussed in detail as a base case. All other cases can be studied relative to this discussion. Results of other cases are dicussed with respect to their effect on output parameters as per the objectives of the work.

6.7.1 Temperature Profile

Simulation result of the first case revealed that laser welding carried using Laser Power 2500 Watts at a speed of 60 mm/s achieved quasi-static temperature condition at 0.27 seconds. The maximum temperature that was recorded at this time was 1887 $°C$, after which the temperature became constant.The temperature profiles corresponding to different times during the process are shown in Figure 24 for the half work-piece.

Figure 24 Temperature Profiles at various instants

It can be seen from Figure 24 that region arround the laser source experienced high temperatures but the regions farther away re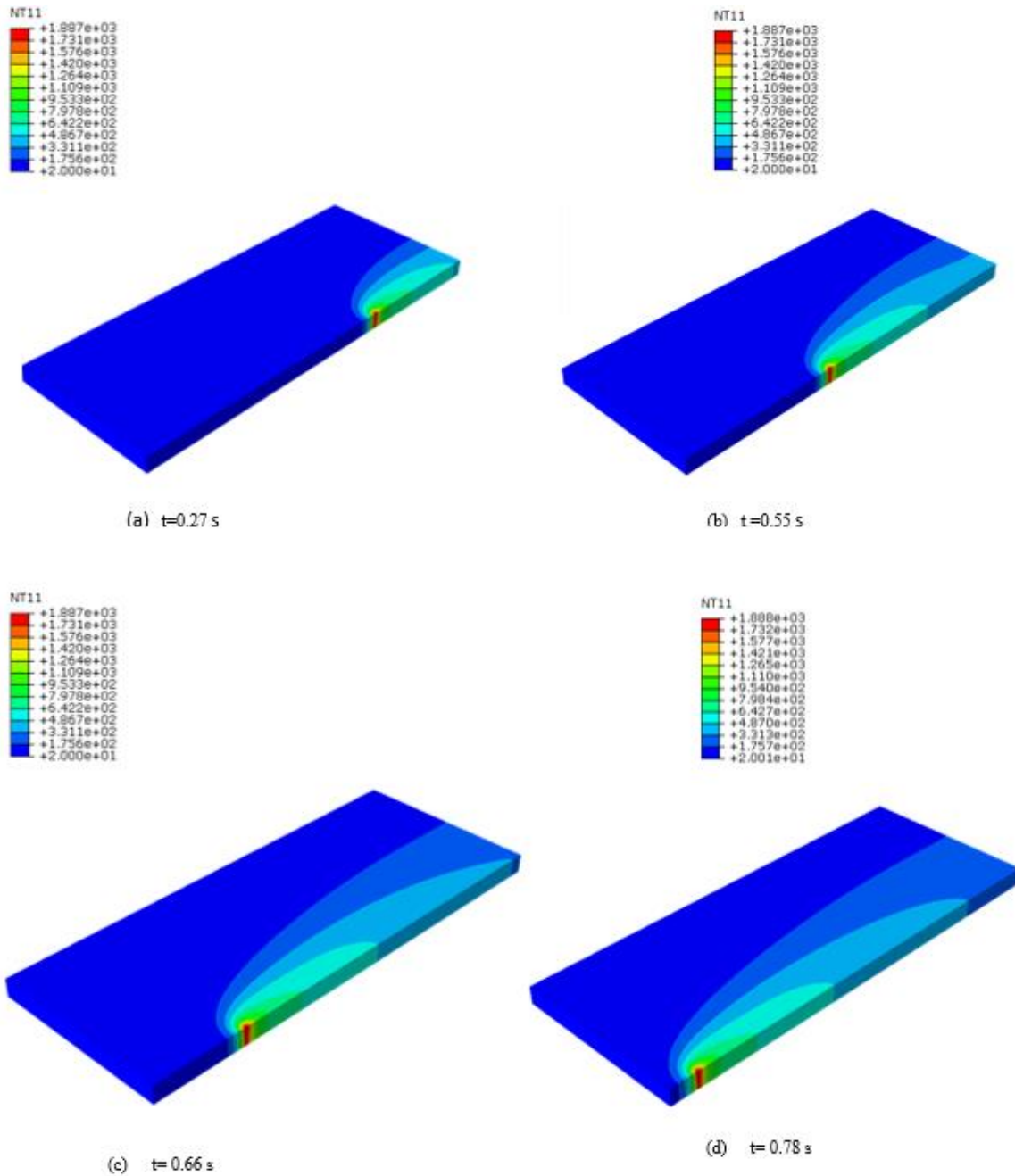mained at room temperature. This confirms the fact that laser welding is a highly localized welding process. The Weldpool captured at 0.78 seconds along with the temperature distribution inside the molten region is given by Figure 25.
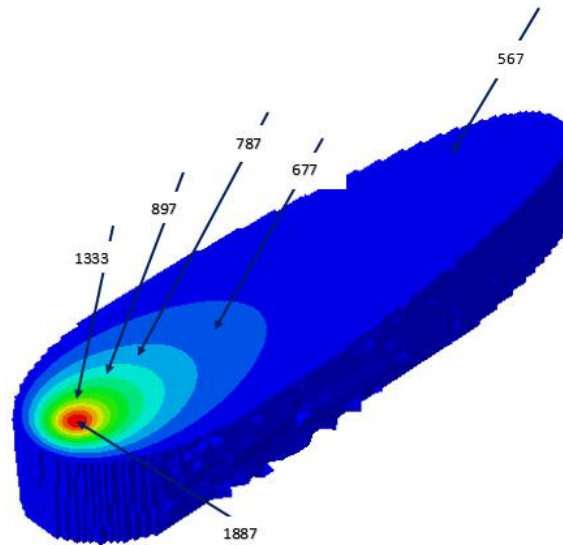
Figure 25 Weld pool shape and temperature distribution inside the molten region

The effect of changing laser parameters on the temperature profile is dicussed in detail in section 6.8.1. The maximum temperature attained from each simulation is given in Table 22.

6.7.2 Weld-Aspect Ratio

Weld aspect ratio is defined as the ratio of weld bead width to penetration depth. It is reported in the literature that weld aspect ratio can be used to predict cracking tendency [74]. Welds with high aspect ratios are desired because of narrow heat affected zone and lager depths ensuring good joint integrity. Low aspect ratio gives a poor joint because of higher heat affected zone and lower or sometimes incomplete penetration.

Laser welding is characterized for high aspect ratio because of the localized heat effect. The aspect ratio is one of the output parameters of this optimization study. Aspect ratio was determined by dividing the weld bead width by the depth of penetration. Weld bead width and penetration depth were characterized by the area having temperatures greater than or equal to the melting point of AA 5083, that being $576°C$. Figure 26 shows the weld bead width and penetration depth used to determine the aspect ratio which is given for this case by equation (6.9) below.

(a) Top view at t=0.78 s   (b) Cross-sectional view at t=0.78 s
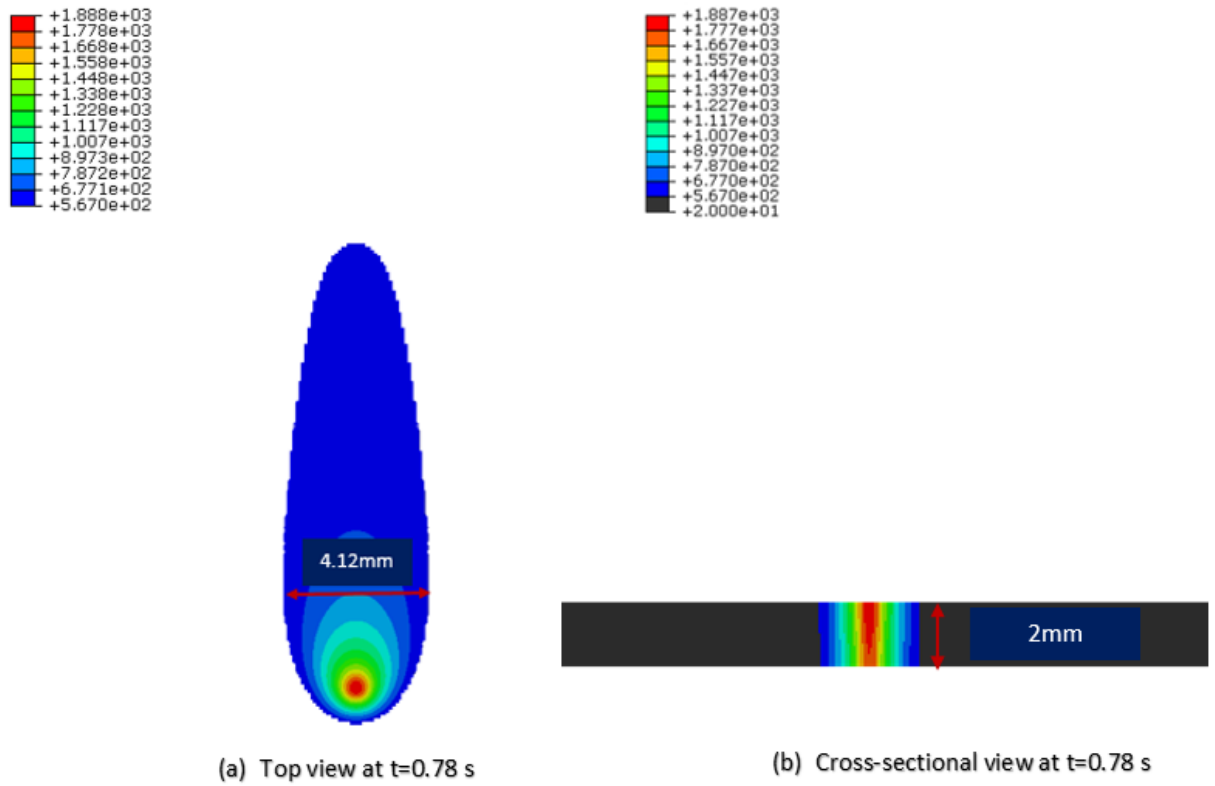
Figure 26 Width of Weld Bead and Depth of Penetration characterized by the molten region at or above 567 degree Centigrade

$$WeldAspectRatio = \frac{WidthofFusionZone}{DepthofPenetration} \qquad (6.9)$$

$$WeldAspectRatio = \frac{4.12mm}{2mm} \qquad (6.10)$$

$$WeldAspectRatio = 2.06 \qquad (6.11)$$

Table 20 summarizes the weld aspect ratios achieved for the complete study against different input parameters employed.

6.7.3 Macroscopic Shape of Weld Pool

Figure 25 shows the weldpool macro shape to be elliptical for the first simulation case. It is reported from literature that the macroscopic shape of weldpool can be used to predict that whether the microstructure in the fusion zone has a favourable growth or not. Elliptical or Circular weldpools are favourable over teardrop shaped weldpools because they support the growth of

desired fine grain columnar structure [75] unlike tear drop shapes which have such a temperature gradient that it supports the growth of coarse structure. The present experimental framework is used to predict the effect of laser power and welding speed using varying thicknesses on the weldpool shape and is presented in section 6.8.3.

6.7.4 Heat Affected Zone (HAZ)

The Heat affected zone is defined as the region that has undergone microstructural changes due to heat input. Recrystallization temperature is the temperature at which the material undergoes microstructural phase transformations and is generally 0.3 to 0.5 times of the melting point for a particular metal. For mild steel, it is reported that phase transformations begin at 723℃ therefore the region where temperature is higher than this experiences metallurgical phase transformations and is termed as HAZ (https://www.quora.com/What-is-the-heat-affected-area-in-welding). Therefore based on the analogy above, HAZ is characterized by the regions at or above the recrystallization temperature but below the melting point in this work. Recrystallization temperature is taken as 450℃ for aluminium alloy 5083 from the Al-Mg phase diagram as given in Figure 27 [76]. The recrystallization temperature was referred from the Al-Mg phase diagram for AA 5083 alloy as the major alloying element in this alloy is magnesium as evident from the chemical composition given in Table 12.
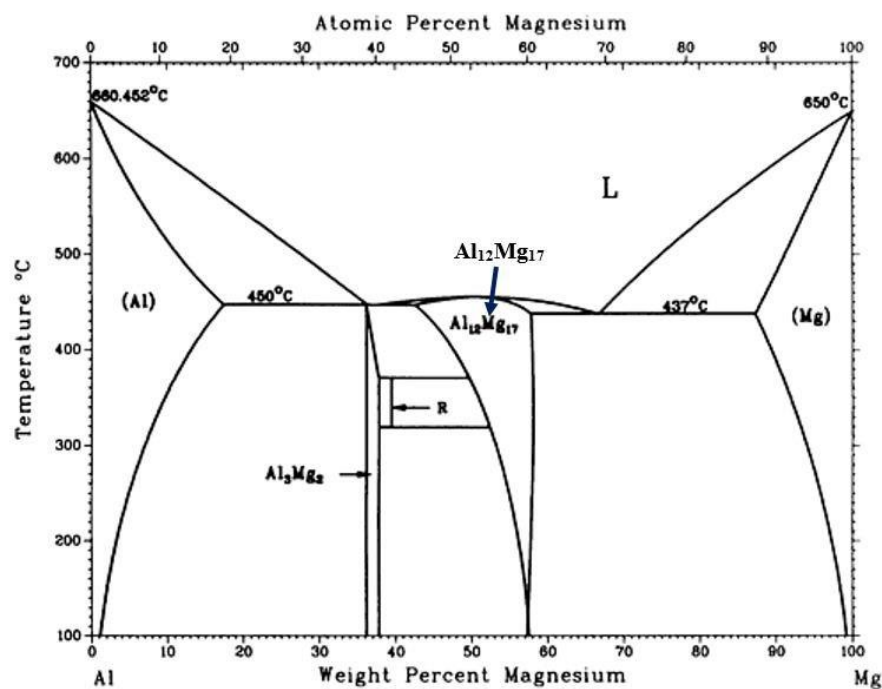

Figure 27 Aluminium-Magnesium Phase Diagram [76]

The HAZ for a 2 mm thick work-piece welded at 2500 Watt laser power at a speed of 60mm/s is given in Figure 28 having width and volume of 6.78mm and 163.6mm^3 respectively. The volume and width of the region were measured using the querying module of Abaqus. The empty region inside the HAZ given in Figure 28 indicates the presence of molten material forming the weld bead.
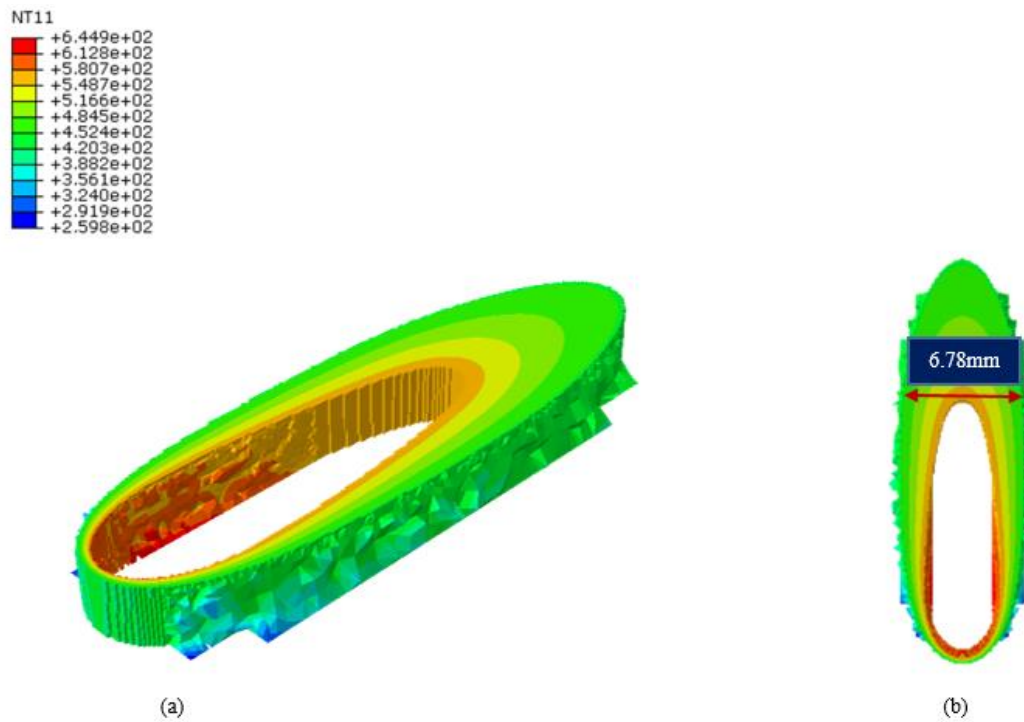
Figure 28 (a) isometric view of the HAZ; (b) top view of the HAZ showing the width in millimetres at 0.78 s

6.8   Study of Effect of Input Parameters on Output Parameters

The output parameters of study (as outlined in section 1.3) obtained from simulations conducted according to the scheme given in Table 20 are summarized in (6.12)

Table 22. The results obtained were analysed group wise for each output parameter. The group for analysis consisted of all the simulation cases having the same thickness level and variable levels of employed laser power and welding speed to gauge their influence on the output parameters.

Laser power and welding speed are the factors that are responsible for the overall heat input into the workpiece. This total heat input is termed as net heat input H_{net} or the line energy and is given

by equation (6.12) .Line energy is ultimately responsible for the various desired as well as undesired effects of welding [18] . The laser power and welding speed used in each simulation case was initially used to calculate line energy and the obtained value was then used to analyse the effect of heat input on the various output parameters.

$$H_{net} = \frac{LaserPower}{WeldingSpeed} \qquad (6.12)$$

Table 22 Summary of Output Parameters against the Input Parameters used in the Study

Case	Laser Power (Watts)	Welding Speed (mm/s)	Specimen thickness (mm)	Temperature (˚C)	Weld bead width (mm)	Weld bead width depth (mm)	Width of HAZ (mm)	Volume of HAZ (cubic mm)
case1	2500	60	2	1888	4.13	2	6.78	81.7899
case2	2500	80	4	884.7	4.50	4	2.12	7.94218
case3	2500	100	6	633	0.531	6	1.24	3.37855
Case4	2500	120	8	600	0.24	8	0.94	6.4
case5	2500	140	10	351.3	Fusion not achieved	Fusion not achieved	Fusion not achieved	Fusion not achieved
case6	3500	60	4	1183	1.93	4	3.16	21.5669
case7	3500	80	6	857	1.24	6	2.30	13.1881
case8	3500	100	8	651	0.531	8	1.24	5.16442
case9	3500	120	10	536	Fusion not achieved	Fusion not achieved	Fusion not achieved	Fusion not achieved
case10	3500	140	2	1851	2.64	2	6.55	41.3068

case11	4500	60	6	1187	2.30	6	3.83	48.1623
case12	4500	80	8	837	1.24	8	2.12	15.5749
case13	4500	100	10	662	0.531	10	1.41	6.99564
case14	4500	120	2	2545	4.13	2	7.53	116.863
case15	4500	140	4	1174	1.58	4	2.46	15.7605
case16	5500	60	8	1031	2.12	8	3.36	4798000
case17	5500	80	10	824	1.24	10	2.15	18.3071
case18	5500	100	2	2960	6.07	2	8.38	184.736
case19	5500	120	4	1545	2.29	4	3.34	37.8207
case20	5500	140	6	989.2	1.24	6	2.12	17.6803
Case21	6500	60	10	1021	4.4	10	6.4	56
case22	5500	80	2	3394	9.06	2	8.89	178.04
case23	6500	100	4	1989	3.16	4	36	92.2923
case24	5500	120	6	1254	1.78	6	3.01	75.5
Case25	6500	140	8	857	2.4	8	4.4	10.8

The simulation cases categorized into groups and the corresponding line energy values are given in Table 23.

*Table 23 Categorization of Cases into Groups for Analysis and Line Energy Values*

Case	Laser Power (Watts)	Welding Speed (mm/s)	Line Energy (W.s/mm)	Specimen thickness (mm)	Peak Temperature	Weld bead width (mm)	Width of HAZ (mm)	Volume of HAZ (cubic mm)
case1	2500	60	41.67	2	1888	4.13	6.78	81.7899
case10	3500	140	25	2	1851	2.64	6.55	41.3068
case14	4500	120	37.5	2	2545	4.13	7.53	116.863
case18	5500	100	55	2	2960	6.07	8.38	184.736
case22	5500	80	68.75	2	3394	9.06	8.89	178.04
case2	2500	80	31.25	4	884.7	4.50	2.12	7.94218
case6	3500	60	58.33	4	1183	1.93	3.16	21.5669
case15	4500	140	32.14	4	1174	1.58	2.46	15.7605
case19	5500	120	45.83	4	1545	2.29	3.34	37.8207
case23	6500	100	65	4	1989	3.16	36	92.2923
case3	2500	100	25	6	633	0.531	1.24	3.37855
case7	3500	80	43.75	6	857	1.24	2.30	13.1881
case11	4500	60	75	6	1187	2.30	3.83	48.1623
case20	5500	140	39.28	6	989.2	1.24	2.12	17.6803
case24	5500	120	45.83	6	1254	1.78	3.01	75.5
Case4	2500	120	20.83	8	600	0.24	0.94	6.4
case8	3500	100	35	8	651	0.531	1.24	5.16442
case12	4500	80	56.25	8	837	1.24	2.12	15.5749
case16	5500	60	91.67	8	1031	2.12	3.36	4798000
Case25	6500	140	46.42	8	857	2.4	4.4	10.8

| case5	2500	140	17.85	10	351.3	Fusion not achieved	Fusion not achieved	Fusion not achieved
case9	3500	120	29.167	10	536	Fusion not achieved	Fusion not achieved	Fusion not achieved
case13	4500	100	45	10	662	0.531	1.41	6.99564
case17	5500	80	68.75	10	824	1.24	2.15	18.3071
Case21	6500	60	108.33	10	1021	4.4	6.4	56.2

6.8.1 Effect of Input Process Parameters on Temperature Profile

The relationship between Line energy and obtained temperatures for various thicknesses of the work piece is presented by graphs for thicknesses 2 mm, 4 mm, 6 mm, 8 mm and 10 mm in

Figure 29 (a-e) respectively. The graphs clearly indicate an increasing trend of peak temperatures with an increase in the line energy. The r-squared values also support the trend indicated by the plot of data. However, the unusual dip is also observed in the graphs of 2 mm and 4 mm thick aluminium plates. This dip is observed for the 2 mm thick plate corresponding to the line energy value of 41.67 Watts/mm where the input laser power and welding speed were 2500 W and 60 mm/s respectively and at the line energy value of 58.33 Watts/mm having 3500 W laser power and 60 mm/s welding speed for the 4 mm thick plate.
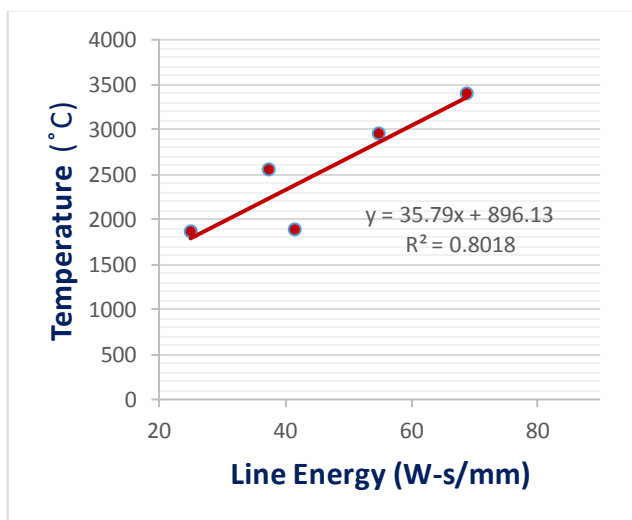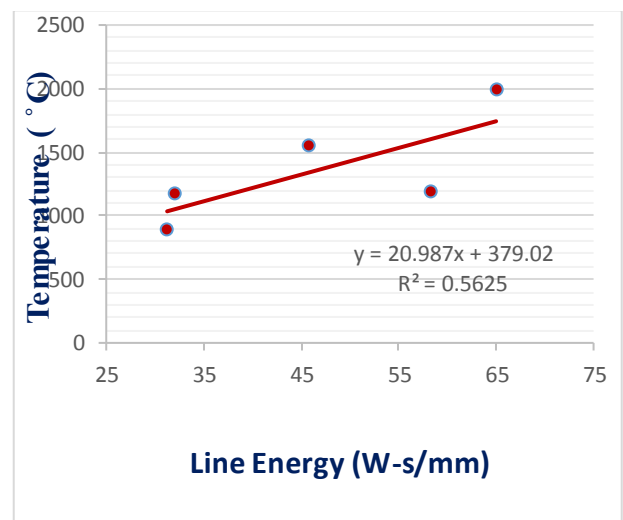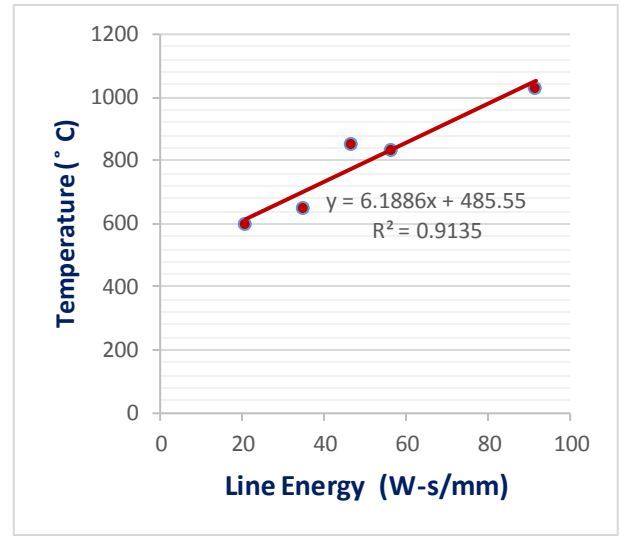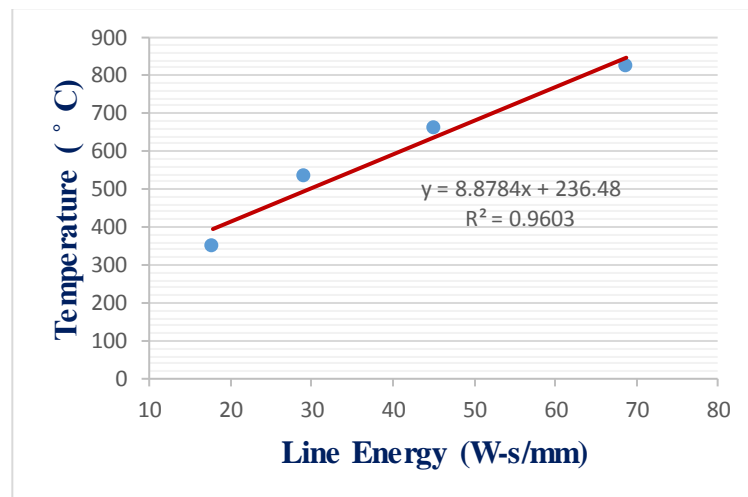

(a)   (b)
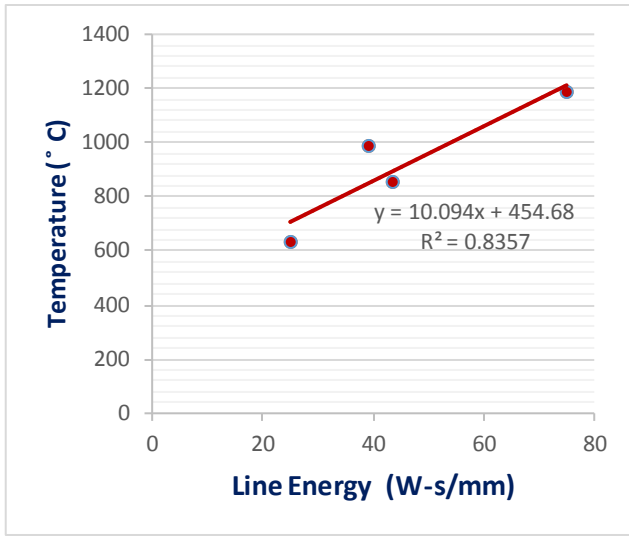
(c)

(d)

(e)

Figure 29   Line Energy-Temperature Graphs for variable thicknesses where
2 mm (b) 4 mm (c) 6 mm (d) 8 mm (e) 10 mm

This unusual behaviour can be attributed to the opposite individual behavioural effect of laser power and welding speed on the heat input. As the laser power increases, the incident power per unit area also increases and therefore the heat input increases. However when the welding speed is increased, the contact time per second of the incident laser beam decreases and thus the net heat input decreases. Thus we can say that positive correlation exists between laser power and temperature and negative correlation exists between welding speed and temperature. This

behaviour is evident from the Laser Power, Temperature (LP-T) and Welding Speed, Temperature (WS-T) Graphs given in Figure 30 and Figure 31 respectively. The graphs clearly indicate that as the power increases the temperatures increase and decrease with increase in the welding speed. R-square values of the fitted trend lines indicate the strength in the observed trends. It can be noted from the graphs in Figure 30 that multiple variable input parameters may give the same output parameters. For instance, for the 6 mm and 8 mm thick aluminium plates, the laser powers of 2500 watt and 3500 watt result in similar temperatures. This can be attributed to the variation in welding speed. For the heat input for welding carried out at a certain speed using 2500 Watt power, the same heat input may be achieved by decreasing the speed when using increased power laser source to balance the net heat input. The same results were achieved by [40] by tailoring the laser beam for variable input parameters for achieving same output parameters.

Comparison of graphs of line energy as a combined factor and laser power and welding speed as separate parameters indicate that the effect of laser power and welding speed is more pronounced when studied as separate entities as compared to the study of their combined effect in the form of line energy. Graphs of Line energy are more scattered and only exhibit a general trend while the graphs of laser power and welding speed have less scatter. This is also indicated by the respective R squared values given for each graph. For this reason, laser power and welding speed is used for analysis of effect of variation and trend determination between the input and output parameters instead of line energy.
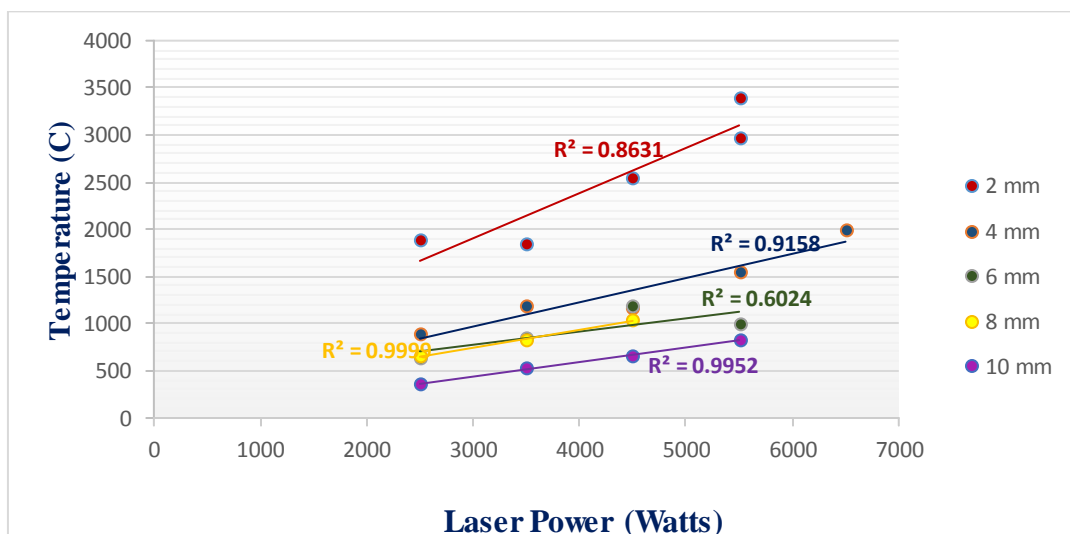

Figure 30 Laser Power-Temperature Graph for Variable Thickness values
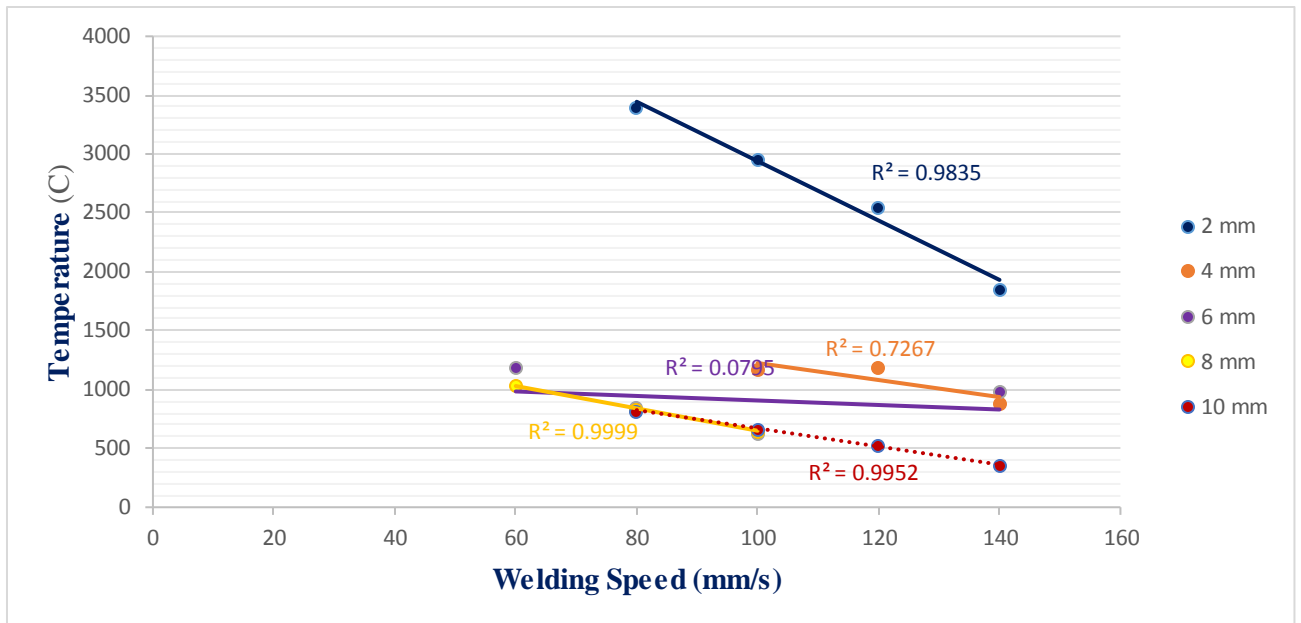
97

Figure 31 Welding Speed-Temperature Graph for Variable Thicknesses

6.8.2 Effect of Input Process Parameters on Weld Aspect Ratio

Weld aspect ratios obtained for all the simulation cases are calculated using equation (6.9) and are summarized in Table 24 against the input parameters. For all the simulation cases the heat intensity was high enough to fuse the plates in the entire thickness except for the cases 5 and 9 where the heat input was not enough for 10 mm thick plates. The fusion in the entire depth is indicative of the deep penetration welding and validates the assumption made for modelling the laser welding process.

Table 24 Weld Aspect Ratios for the Simulation Cases

Case	Laser Power (Watts)	Welding Speed (mm/s)	Line Energy (Watt/mm)	Specimen thickness (mm)	Temperature	Weld bead width (mm)	Depth of Weld (mm)	Aspect Ratio
case1	2500	60	41.67	2	1888	4.13	2	2.065
case10	3500	140	25	2	1851	2.64	2	1.32
case14	4500	120	37.5	2	2545	4.13	2	2.065
case18	5500	100	55	2	2960	6.07	2	3.03
case22	5500	80	68.75	2	3394	9.06	2	4.53

98

case2	2500	80	31.25	4	884.7	4.50	4	1.12
case6	3500	60	58.33	4	1183	1.93	4	0.48
case15	4500	140	32.14	4	1174	1.58	4	0.39
case19	5500	120	45.83	4	1545	2.29	4	0.57
case23	6500	100	65	4	1989	3.16	4	0.79
case3	2500	100	25	6	633	0.531	6	0.09
case7	3500	80	43.75	6	857	1.24	6	0.21
case11	4500	60	75	6	1187	2.30	6	0.38
case20	5500	140	39.28	6	989.2	1.24	6	0.21
case24	6500	120	45.83	6	1254	1.78	6	0.29
Case4	2500	120	20.83	8	600	0.24	8	0.03
case8	3500	100	35	8	651	0.531	8	0.06
case12	4500	80	56.25	8	837	1.24	8	0.155
case16	5500	60	91.67	8	1031	2.12	8	0.265
Case25	6500	60	108.33	8	857	2.4	8	0.3
case5	2500	140	17.85	10	351.3	Fusion not achieved	N/A	N/A
case9	3500	120	29.167	10	536	Fusion not achieved	N/A	N/A
case13	4500	100	45	10	662	0.531	10	0.05
case17	5500	80	68.75	10	824	1.24	10	0.12
Case21	6500	140	46.42	10	1021	4.4	10	0.44

The effect of laser power on the weld aspect ratios is presented in Figure 32 for all the thickness values. An increasing general trend between laser power and weld aspect ratio is depicted by the plotted graphs. For the cases of 2 and 4 mm thick plates it is observed that weld aspect ratios

increase more rapidly at powers higher than 4000 Watt. This indicates that powers greater than 4000 Watt result in wider beads for the given thickness of the workpiece. For thicknesses higher than 4 mm, the rapid increase in the width of molten pool at higher powers is less significant because of the higher thickness values. This is indicative that the economical laser powers should be used considering the thickness of plate. Similarly, the weld aspect ratio of 0.53 mm for 10 mm thick plates is indicative of a very narrow weld bead which is again undesirable.

Trend deviations are identifiable from the graphs of 4 mm and 6 mm thick plates. These points are indicated in the respective graphs given in Figure 32 (b) and (c). Higher weld aspect ratio was observed for the low laser power and low aspect ratio was observed for higher laser power for 4 and 6 mm thick plate respectively. This is explained by the welding speeds employed with these laser powers to carry out the welding process. For the case of 2 mm plate, Higher weld aspect ratio was achieved with 2000 W because of low welding speed here i-e 60 mm/s. Slow traverse of laser source resulted in longer irradiation times resulting in wider molten region. A decrease in weld aspect ratio was observed at highest employed laser power for 6 mm plate. This trend deviation is attributed to the high welding speed i-e 140 mm/s used for this case. As a result of reduced interaction time, the net heat input resulted in comparatively reduced molten region.
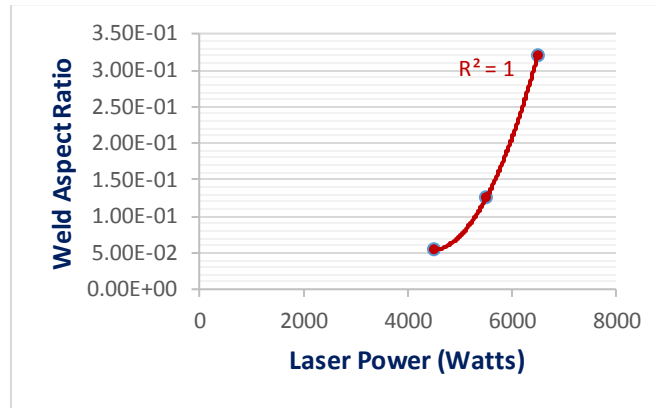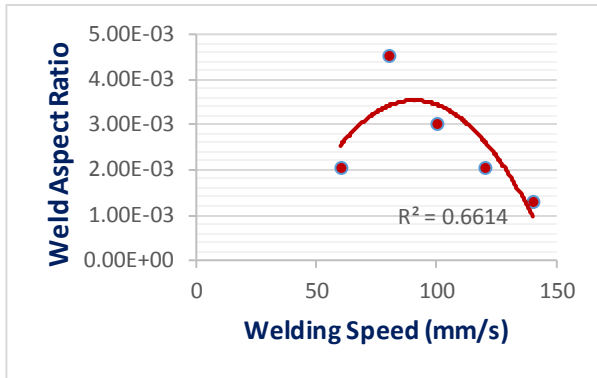

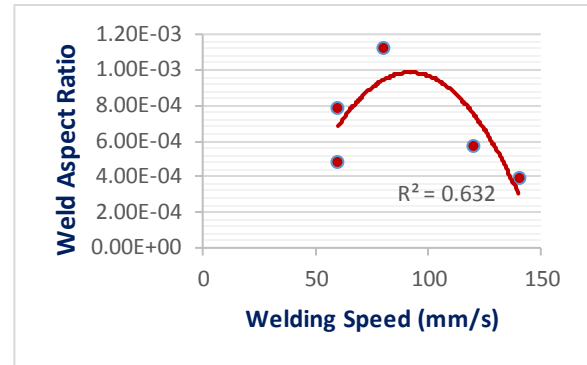(a)   (b)
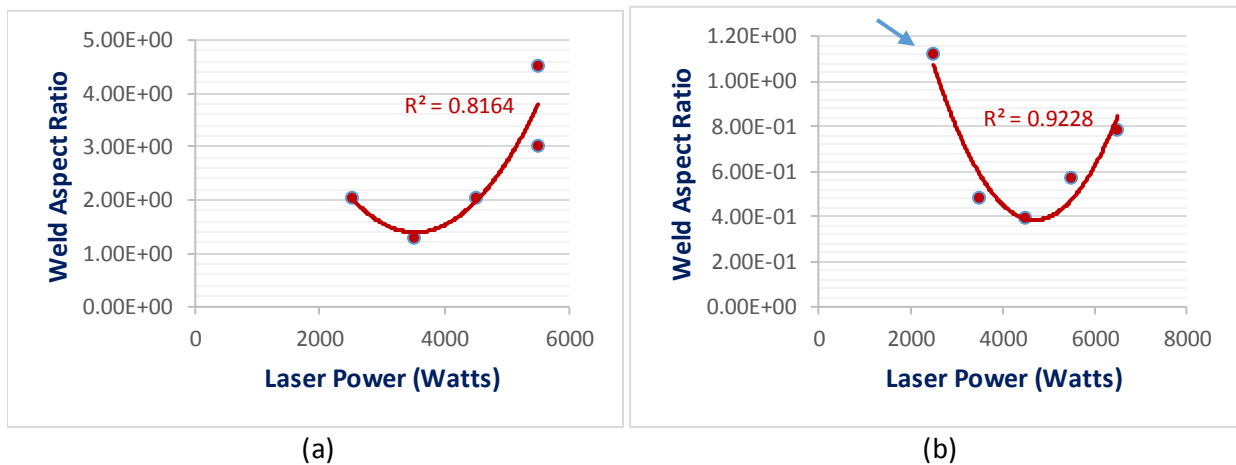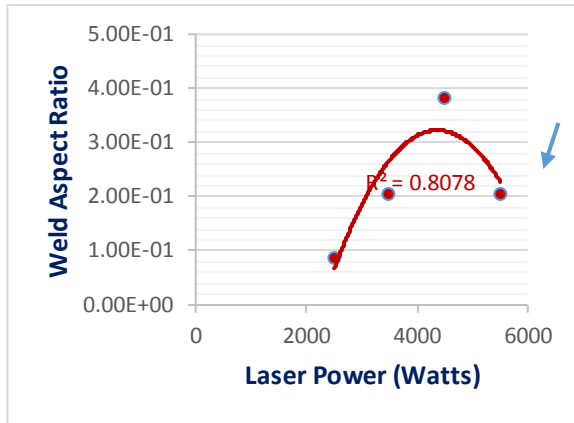
(c)
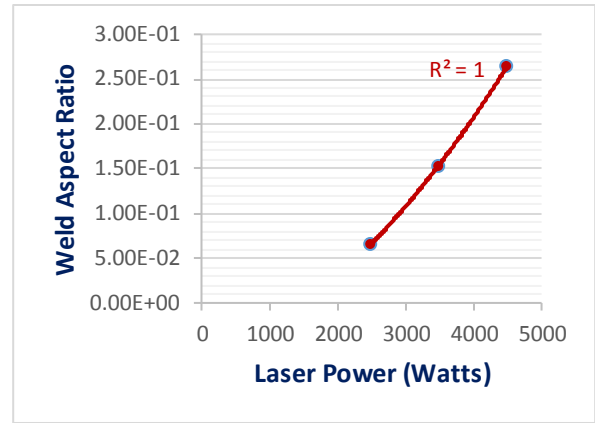
(d)

(e)

Figure 32 Weld Aspect Ratio- Laser Power Graphs for Variable Thicknesses (a) 2 mm (b) 4 mm (c) 6 mm (d) 8 mm (e) 10 mm

The increase of welding speed resulted in a weld of low aspect ratio as given by the graphs plotted between welding speed and aspect ratio for the employed thickness. Reduced irradiation time corresponds to lower heat input per unit time and thus the weld aspect ratio decreases. For the cases of 2 mm and 4 mm thick plates, the speed of 60 mm/s is shown to have irregular behaviour in Table 24 which is not supporting the general trend. The general decreasing trend is evident otherwise. Graphs were thus plotted by removing the data point corresponding to 60 mm/s for the respective cases and are given in Figure 33.

(a)

(b)

(c)

(d)

(e)

Figure 33 Weld Aspect Ratio- Welding Speed Graphs for Variable Thicknesses (a) 2 mm (b) 4 mm (c) 6 mm (d) 8 mm (e) 10 mm
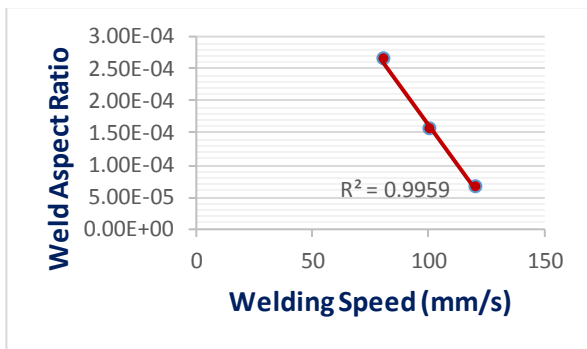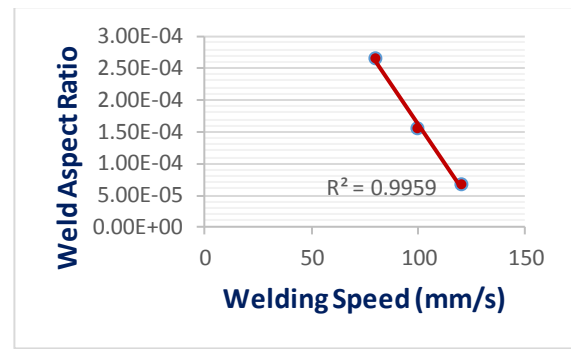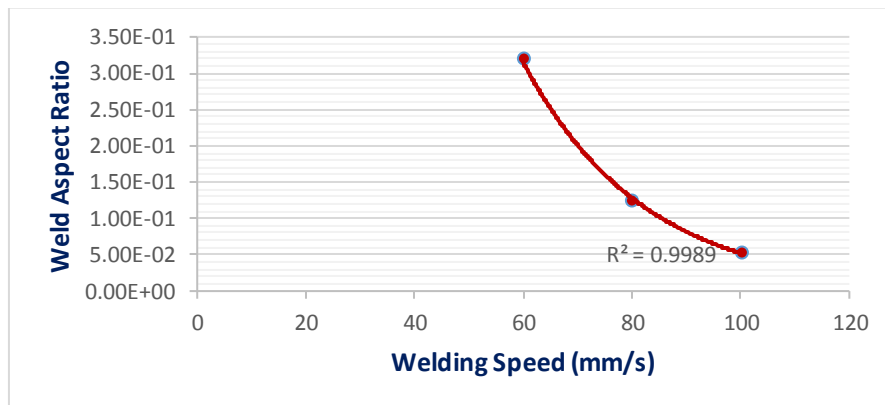
From the two input parameters, it is generally observed that welding speed has a clear and significant effect on the aspect ratio as compared to that of laser power. For a given thickness, an

increase in the aspect ratio of weld bead corresponds to the increase in the width of fusion zone or the weld bead width and vice versa.
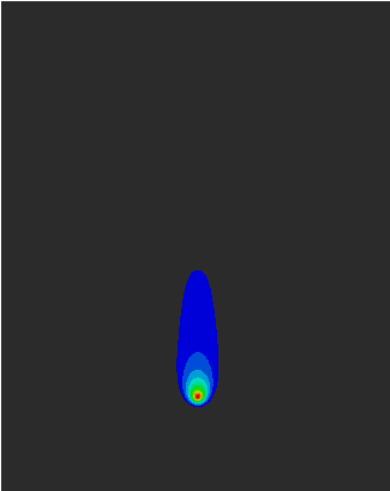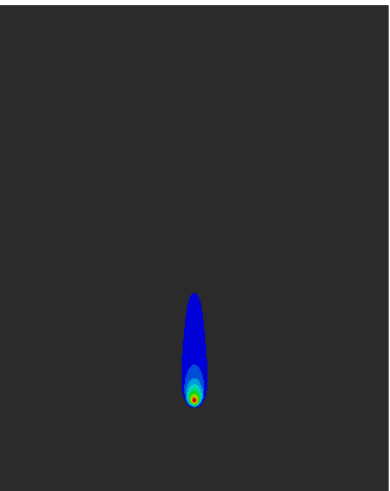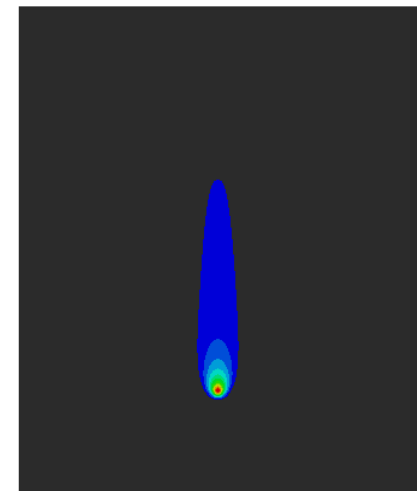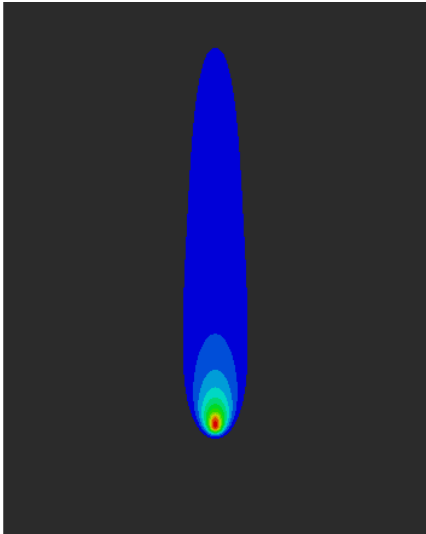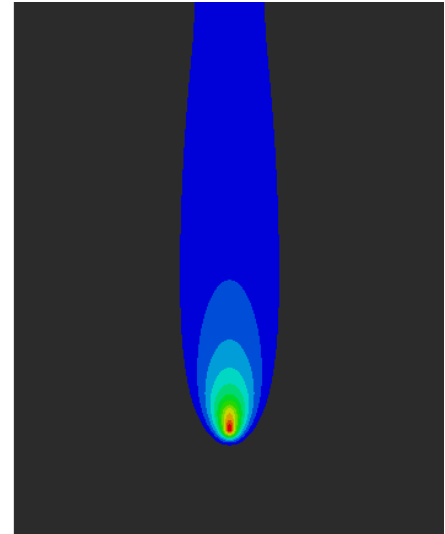
6.8.3 Effect of Input Process Parameters on Macroscopic Weld Pool Shape

The macroscopic shapes of weld pool with the classification into circular, elliptical and tear-drop categories are given in

Figure 34. All the images are captured at the end of complete simulation and at a distance of 80% of the total length modelled i-e 0.04 m or 40 mm. For all the cases, only the molten pool shape is plotted with minimum temperature 567 ˚C. Maximum achieved temperature varied with the used parameters and is given with each case in the figure. The grey coloured region indicate the non-welded base metal region.

The analysis to investigate the behavioural trend between input parameters and the weld pool shape was done for each specific thickness separately. Laser Power and welding speed were analysed separately to study their effect on the macro shape of the weld pool. It is observed that tear dropped shaped weld pools were obtained for welding speeds 120 mm/s and 140 mm/s when the Laser powers were 3500-4500 Watt as observed in cases 10, 14 and 15. However when Laser Power was increased beyond 4500 Watt, elliptical weld shape was observed at the same speeds as given by case 19 and 20.

Weld pools of circular shape are observed at low laser powers and low welding speeds. As the welding speed increases, the weld shape tends to become elliptical.

Thickness 2 mm		
Case-1	Case-10	Case-14
Macroscopic Shape: Elliptical Laser Power (W) = 2500 Welding Speed (mm/s) = 60 Line Energy (W-s/mm)= 41.67 Maximum Temperature (˚C) =1886	Macroscopic Shape: Tear Drop Laser Power (W) = 3500 Welding Speed (mm/s) = 140 Line Energy (W-s/mm)= 25 Maximum Temperature (˚C) =1851	Macroscopic Shape: Tear Drop Laser Power (W) =4500 Welding Speed (mm/s) = 120 Line Energy (W-s/mm)= 37.5 Maximum Temperature (˚C) =2545
Case-18		Case-22
Macroscopic Shape: Elliptical Laser Power (W) = 5500 Welding Speed (mm/s) =100 Line Energy (W-s/mm)= 55 Maximum Temperature (˚C) =2960		Macroscopic Shape: Undefined Laser Power (W) = 6500 Welding Speed (mm/s) = 80 Line Energy (W-s/mm)= 81.25 Maximum Temperature (˚C) =3393

Thickness 4 mm

Case-2
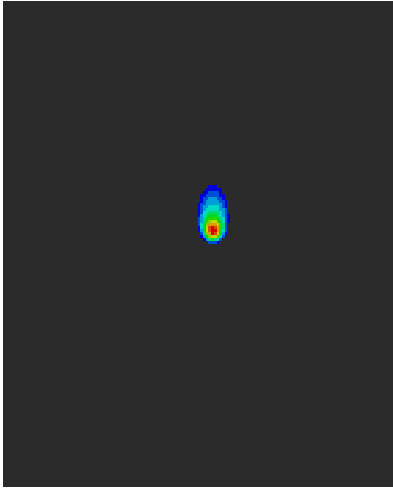
Macroscopic Shape: Circular

Laser Power (W) = 2500
Welding Speed (mm/s) = 80
Line Energy (W-s/mm)= 31.25
Maximum Temperature (˚C) =834

Case-6

Macroscopic Shape: Elliptical

Laser Power (W) = 3500
Welding Speed (mm/s) = 60
Line Energy (W-s/mm)= 58.33
Maximum Temperature (˚C) =1181

Case-15

Macroscopic Shape: Tear Drop

Laser Power (W) = 4500
Welding Speed (mm/s) = 140
Line Energy (W-s/mm)= 37.5
Maximum Temperature (˚C) =1172

Case-19

Macroscopic Shape: Elliptical

Laser Power (W) = 5500
Welding Speed (mm/s) = 120
Line Energy (W-s/mm)= 45.83
Maximum Temperature (˚C) =154

Case-23

Macroscopic Shape: Elliptical

Laser Power (W) = 6500
Welding Speed (mm/s) = 100
Line Energy (W-s/mm)= 65
Maximum Temperature (˚C) =1985

Thickness 6 mm

Case-3	Case-3 Zoomed Image	Case-11

Macroscopic Shape: Circular

Laser Power (W) =2500
Welding Speed (mm/s) = 100
Line Energy (W-s/mm)= 25
Maximum Temperature (˚C) =633

Macroscopic Shape: Elliptical

Laser Power (W) =4500
Welding Speed (mm/s) = 60
Line Energy (W-s/mm)= 75
Maximum Temperature (˚C) =1186

Case-7 (Zoomed Image)	Case-20 (Zoomed Image)

Macroscopic Shape: Circular

Laser Power (W) = 3500
Welding Speed (mm/s) = 80
Line Energy (W-s/mm)= 43.75
Maximum Temperature (˚C) =857
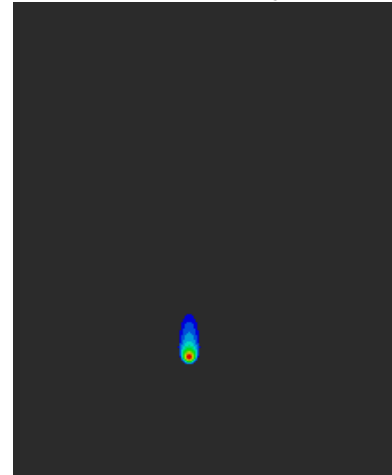
Macroscopic Shape: Elliptical

Laser Power (W) = 5500
Welding Speed (mm/s) = 140
Line Energy (W-s/mm)= 39.2
Maximum Temperature (˚C) = 989

Thickness 8 mm
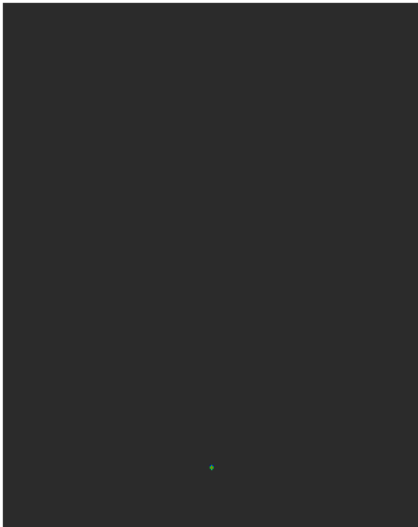
Case-4

Macroscopic Shape: Circular

Laser Power (W) = 2500
Welding Speed (mm/s) = 120
Line Energy (W-s/mm)= 21
MaximuM Temperature (˚C) =602

Case-4 (Zoomed Image)
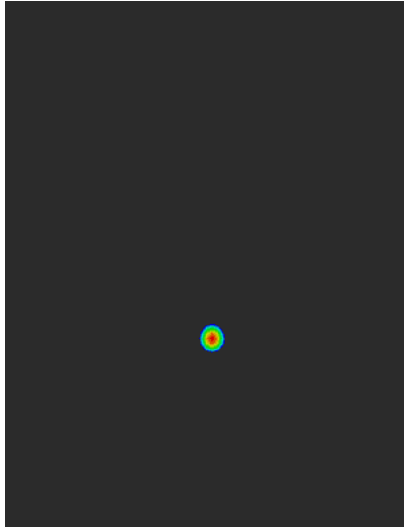
Case-8 (Zoomed Image)
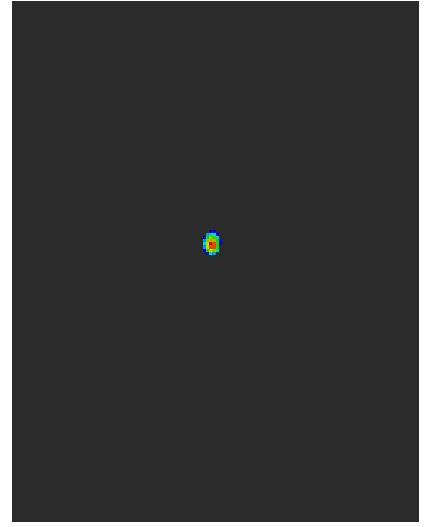
Macroscopic Shape: Circular

Laser Power (W) = 3500
Welding Speed (mm/s) = 100
Line Energy (W-s/mm)= 35
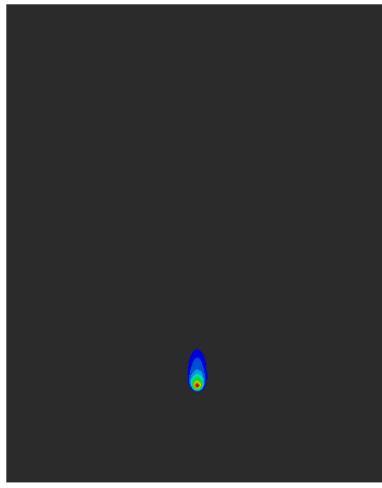Maximum Temperature (˚C) = 651

Case-12
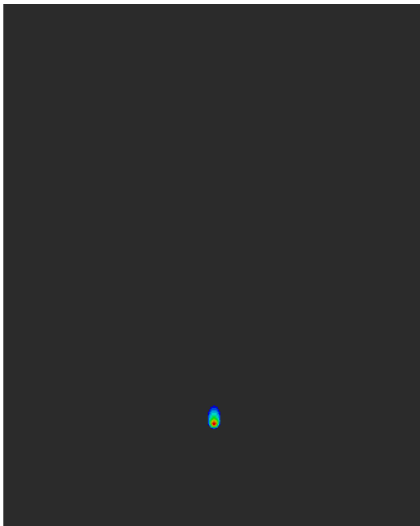
Macroscopic Shape: Elliptical

Laser Power (W) = 4500
Welding Speed (mm/s) = 80
Line Energy (W-s/mm)= 56.25
Maximum Temperature (˚C) =837

Case-16
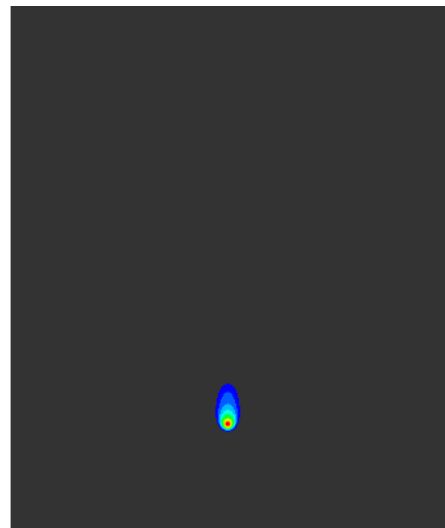
Macroscopic Shape: Elliptical

Laser Power (W) = 5500
Welding Speed (mm/s) = 60
Line Energy (W-s/mm)= 91.67
Maximum Temperature (˚C) =1103

Thickness 10 mm		
Case-5	Case-9	Case-13

Macroscopic Shape: Not Welded

Laser Power (W) = 2500
Welding Speed (mm/s) = 140
Line Energy (W-s/mm)= 17.8
Maximum Temperature (˚C) =351

Macroscopic Shape: Not Welded

Laser Power (W) = 3500
Welding Speed (mm/s) = 120
Line Energy (W-s/mm)= 29.167
Maximum Temperature (˚C) =535

Macroscopic Shape: Circular

Laser Power (W) = 4500
Welding Speed (mm/s) = 100
Line Energy (W-s/mm)= 45
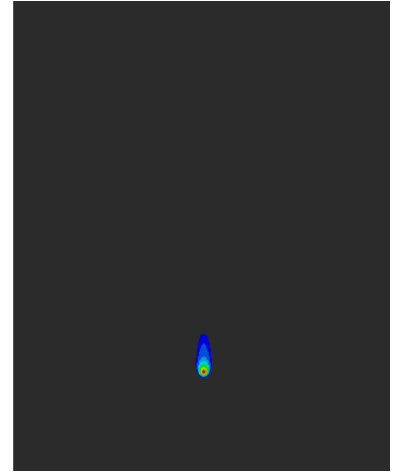Maximum Temperature (˚C) = 6

Case-17	Case-21

Macroscopic Shape: Elliptical

Laser Power (W) =4500
Welding Speed (mm/s) = 80
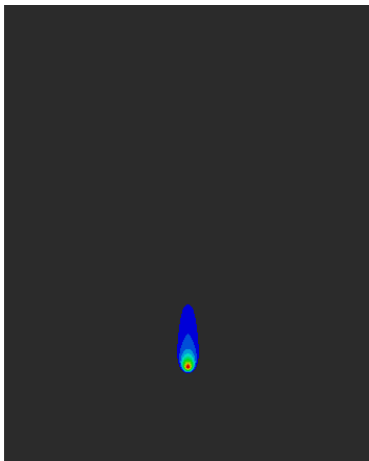Line Energy (W-s/mm)= 56.25
Maximum Temperature (˚C) =823
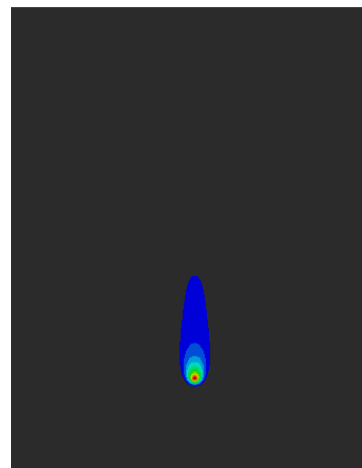
Macroscopic Shape: Elliptical

Laser Power (W) =6500
Welding Speed (mm/s) =140
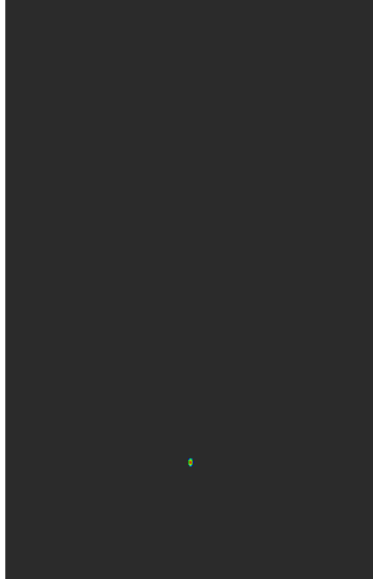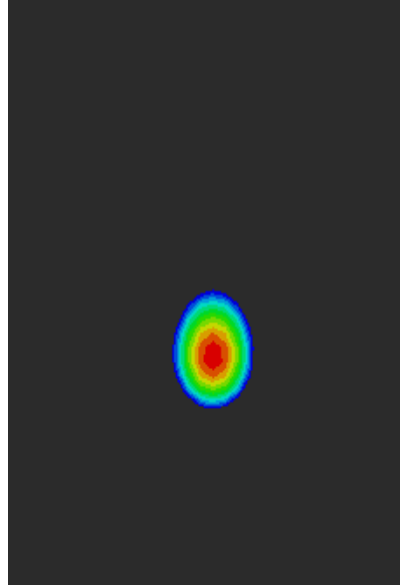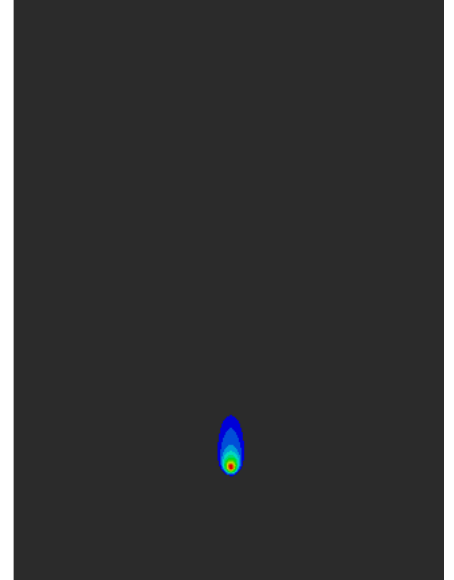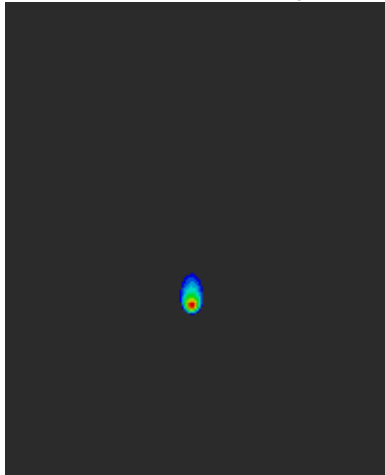Line Energy (W-s/mm)=46.42
Maximum Temperature (˚C) = 1200

Figure 34 Macroscopic Shapes of Weld Pools given by Top Views

6.8.4 Effect of Input Process Parameters on Heat Affected Zone (HAZ)

The widths of HAZ were measured and compared against laser powers and welding speeds for the thickness values used. It was concluded that when laser power is increased width of HAZ increased and opposite effect was observed with the welding speed. This is again explained by the heat input and irradiation time. As the heat input increases either through increased power source or longer irradiation times, width of HAZ increases along the molten pool and as the heat input is decreased the HAZ decreases. Laser Power and HAZ width graphs are given in Figure 35. The increasing trend between the input and response parameter is evident. R-squared values also support the direct relation between laser power and width of HAZ.

The fitted lines correspond to second order polynomial indicating a non-linear relation between HAZ width and laser power. As the laser power increases more heat energy is conducted into the work piece and surrounding regions and as a result the HAZ increases with increasing the power of laser source.
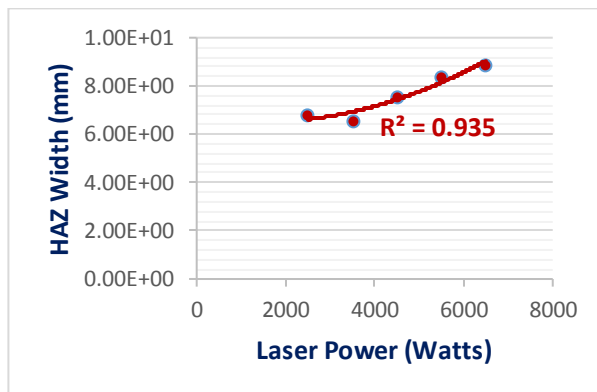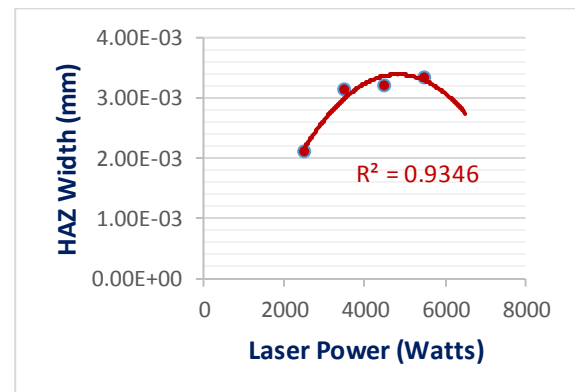
(a)   (b)
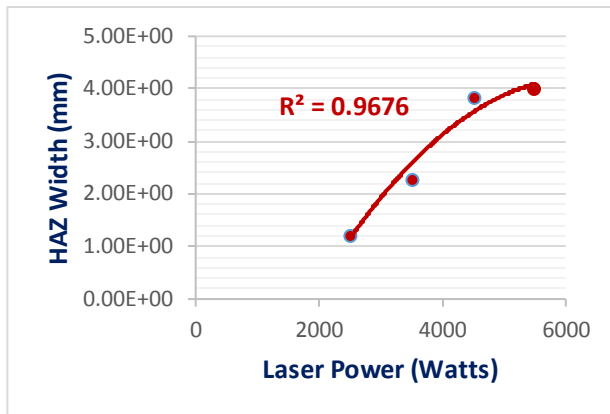
(c)
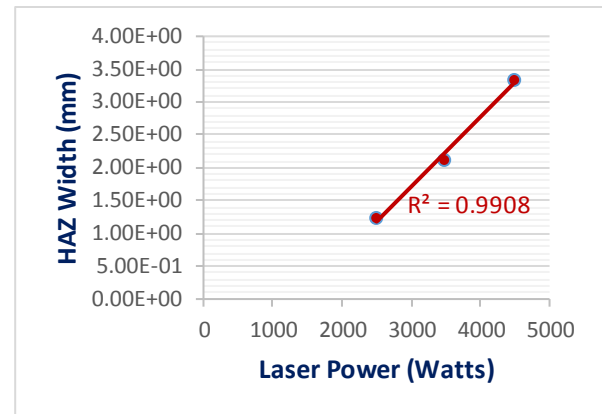
(d)
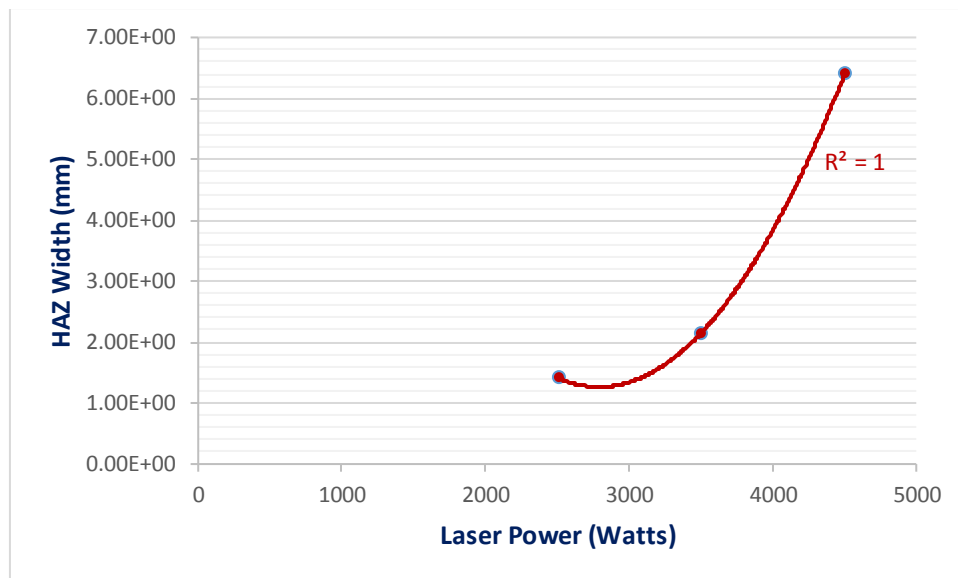
(e)

Figure 35 Laser Power- HAZ Width graphs for the Variable Thicknesses used (a) 2 mm (b) 4 mm (c) 6 mm (d) 8 mm (e) 10 mm

Graphs given in Figure 36 give the indirect relation between welding speed and HAZ width due to decreased heat input because of reduced interaction time. The fitted regression lines correspond to second order polynomial indicating that the behaviour between HAZ width and Welding speed is non-linear. Initially the width of HAZ decreases with an increase in speed after which it begins to increase. For the present case, it is attributed to the use of higher laser powers at increasing speed for the cases of 4 mm, 6 mm, 8 mm and 10 mm thicknesses indicating that the laser power is a more dominant effect for HAZ width. This is indicated by the graph obtained for 2 mm thick sheet. The associated Laser powers are more responsible for the trend in HAZ width as compared

to speed. For instance, at the data point corresponding to 60 mm/s the laser power used was 2500 Watt and for the speed of 80 mm/s the Laser Power used was 3500 Watt. The graph indicates that the width at (80, 3500) is greater than at (60, 2500) indicating that an increase of the Laser Power has a more dominant effect. However, to study the independent behaviour of welding speed on HAZ width a more detailed study is required with constant laser power and variable speed for each thickness.
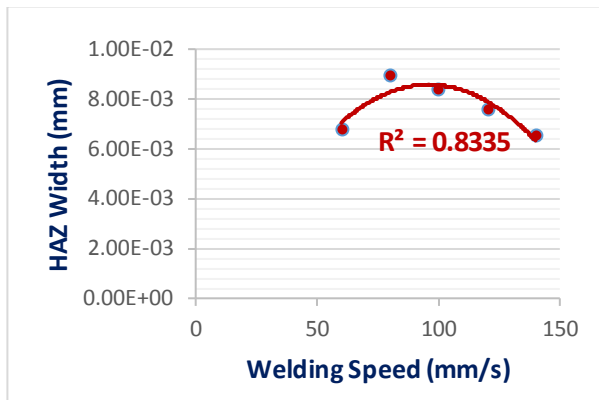
(a)
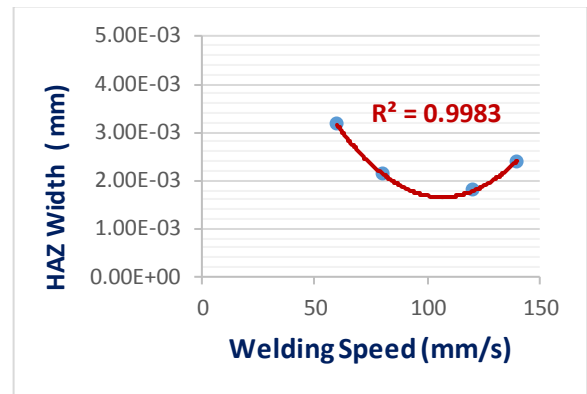
(b)
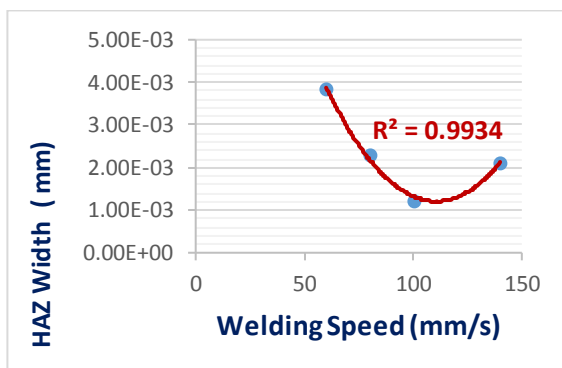
(c)
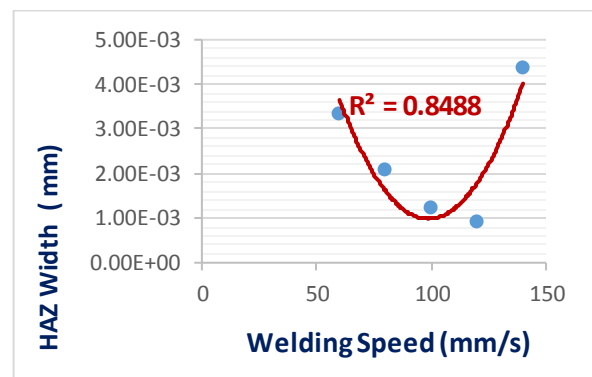
(d)
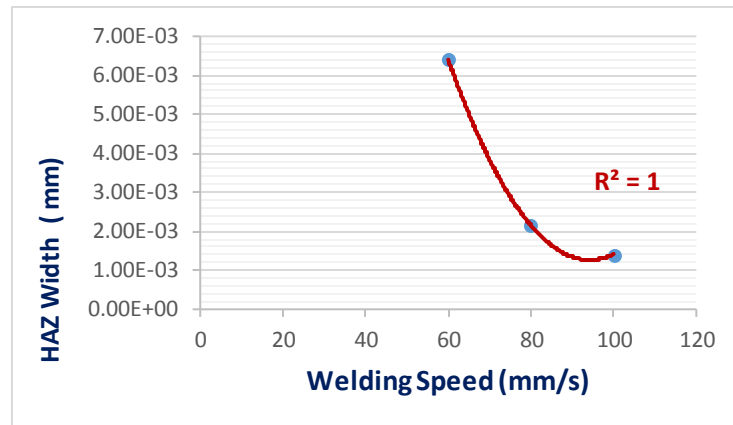
(e)

Figure 36 Welding Speed- HAZ width Graphs for Minimum and Maximum Thicknesses (a) 2 mm (b) 4 mm (c) 6 mm (d) 8 mm (e) 10 mm

Regression models were developed for weld width and peak temperature to quantitatively analyse the effect of laser welding on these parameters one by one. The models were developed for each thickness separately. Results of regression analysis and ANOVA for the weld width achieved are given in Table 25-28 for 2-8 mm thicknesses.

Table 25 Regression Statistics and ANOVA for 2 mm thickness

Regression Statistics				
Multiple R	0.945108741			
R Square	0.893230532			
Adjusted R Square	0.786461063			
Standard Error	0.001143779			
Observations	5			
ANOVA				
	df	*SS*	*MS*	*F*
Regression	2	2.19E-05	1.09E-05	8.365973
Residual	2	2.62E-06	1.31E-06	
Total	4	2.45E-05		
	Coefficients	*Standard Error*	*t Stat*	*P-value*
Intercept	0.003354795	0.00252	1.331126	0.314608
LP	1.52751E-06	4.42E-07	3.456839	0.074458
WS	-4.71857E-05	1.82E-05	-2.58989	0.122325

Table 26 Regression Statistics and ANOVA for 4 mm thickness

Regression Statistics				
Multiple R	0.998301			
R Square	0.996605			
Adjusted R Square	0.993209			
Standard Error	6.12E-05			
Observations	5			
ANOVA				
	df	SS	MS	F
Regression	2	2.2E-06	1.1E-06	293.5169
Residual	2	7.48E-09	3.74E-09	
Total	4	2.2E-06		
	Coefficients	Standard Error	t Stat	P-value
Intercept	0.000782	0.00011	7.112744	0.019199
LP	5.4E-07	2.23E-08	24.15785	0.001709
WS	-1.2E-05	1.12E-06	-10.4746	0.008992

Table 27 Regression Statistics and ANOVA for 6 mm thickness

Regression Statistics				
Multiple R	0.993442727			
R Square	0.986928452			
Adjusted R Square	0.960785357			
Standard Error	0.000144388			
Observations	4			
ANOVA				
	df	SS	MS	F
Regression	2	1.57407E-06	7.87034E-07	37.75102
Residual	1	2.0848E-08	2.0848E-08	
Total	3	1.59492E-06		
	Coefficients	Standard Error	t Stat	P-value
Intercept	0.001090522	0.000304873	3.57697421	0.173546
LP	5.06946E-07	6.97462E-08	7.268429822	0.087041
WS	-1.88631E-05	2.63616E-06	-7.15550857	0.088397

Table 28 Regression Statistics and ANOVA for 8 mm thickness

Regression Statistics				
Multiple R	0.987299544			
R Square	0.97476039			
Adjusted R Square	0.94952078			
Standard Error	0.0002133			
Observations	5			
ANOVA				
	df	SS	MS	F
Regression	2	3.51422E-06	1.75711E-06	38.6202637
Residual	2	9.09941E-08	4.5497E-08	
Total	4	3.60521E-06		
	Coefficients	Standard Error	t Stat	P-value
Intercept	-0.001133057	0.000463652	-2.443764725	0.134481954
LP	5.91157E-07	6.74515E-08	8.76418538	0.012770131
WS	-2.21047E-06	3.37257E-06	-0.655425065	0.579508459

R-squared obtained from regression analysis is used for statistical evaluation of the strength of model i-e it indicates the goodness of data fit around the regression line. R squared is also termed as coefficient of multiple determination when used in multiple regression analysis. The p values or probability values are indicative of the significance level of significance of the independent variables or the used factors. Lower p values are indicative of higher probabilities that the values of the variables will fall within the range and are thus desired As a rule of thumb, p values <0.05 are desired and lower the values the better is the model prediction. Standard Error indicated the variation in the model. Other indicative factors of ANOVA are the degree of freedom (df), Sum of Squares (SS) and Mean Sum of Squares (MS).

R squared values for the models developed for weld width are 0.89, 0.99 , 0.98 and 0.974 for the 2 mm , 4 mm, 6 mm, and 8 mm thick plates respectively indicating that the developed models fairly describe the trend for weld width as laser power and welding speed input factors. The coefficients of equations indicate the positive correlation of Laser Power and negative correlation of welding speed. Based on the values of coefficients, a unit change in the value of laser power will bring a greater change in the width of weld bead than a unit change in the value of welding speed. It can thus be said that Laser power has a significant effect on weld width than welding speed based on the values of coefficients.

The p values obtained for the factors used as independent variables (laser power and welding speed) are less than or near 0.05. An increase in number of observations may improve the results. Regression model for 10 mm thickness is not developed as only three data points were available. The regression equations developed for weld width (WW) for the thicknesses used are given from equations (6.13) to (6.16). The actual and predicted values of weld bead widths and the percentage error corresponding to each thickness value is given in Table 29.

$$2 \text{ mm} \quad WW = 0.0033 + (1.5275E-6 \times LP) - (4.718E-5 \times WS) \tag{6.13}$$

$$4 \text{ mm} \quad WW = 0.000782 + (5.4E-7 \times LP) - (1.2E-5 \times WS) \tag{6.14}$$

$$6 \text{ mm} \quad WW = 0.00109 + (5.0694E-7 \times LP) - (1.886E-5 \times WS) \tag{6.15}$$

$$8 \text{ mm} \quad WW = -0.001133 + (5.91157E-7 \times LP) - (2.2104E-6 \times WS) \tag{6.16}$$

Table 29 Actual and Predicted Values of Weld Bead

Laser Power (Watts)	Welding Speed (mm/s)	Thickness (mm)	Weld Width Measured (mm)	Predicted (mm)	Percentage Error
2500	60	2	0.0041274	0.004288	3.744213435
3500	140	2	2.64E-03	0.0020411	-29.34519
4500	120	2	0.0041269	0.0045122	8.538501601
5500	100	2	0.0060746	0.0069833	13.01184978
5500	80	2	0.0090564	0.0079269	-14.2491658
2500	80	4	0.0012308	0.001172	-5.01296928
3500	60	4	0.001934	0.001952	0.920081967
4500	140	4	0.0015824	0.001532	-3.28955614
5500	120	4	0.0022924	0.002312	0.846885813
6500	100	4	0.0031648	0.003092	-2.35446313
2500	100	6	0.0005305	0.0004714	-12.5509955
3500	80	6	0.0012379	0.0013555	8.676949136
4500	60	6	0.0022989	0.0022397	-2.64696782
5500	140	6	0.0012379	0.0012378	-0.00735174
2500	120	8	8.20E-05	7.96E-05	-2.96E+00
3500	100	8	0.0005305	7.15E-04	2.58E+01
4500	80	8	0.0012379	1.35E-03	8.33E+00
5500	60	8	0.0021221	1.99E-03	-6.87E+00
6500	140	8	0.0024	2.40E-03	2.69E-03

ANOVA results and statistics from regression analysis carried out for peak temperature as the dependent and laser power and welding speed as independent factors are presented in Table 30-33 for variable thicknesses. R squared values for all the regression models are higher than 0.95 indicative of a good model fitting. Positive correlation is indicated between laser power and peak temperature and negative correlation between welding speed and peak temperature. The

coefficient values of laser power and welding speed for the regression models indicate that welding speed has a strong effect on peak temperatures than the laser power and a unit change in welding speed will decrease the maximum achieved temperature as it has a higher impact than the laser power and corresponding unit increase in the attained temperature.

Table 30 Regression and ANOVA Statistics for 2 mm thickness for Maximum Temperature

Regression Statistics				
Multiple R	0.986695926			
R Square	0.97356885			
Adjusted R Square	0.9471377			
Standard Error	154.439091			
Observations	5			
ANOVA				
	df	SS	MS	F
Regression	2	1757094.334	878547.1672	36.83414633
Residual	2	47702.86567	23851.43284	
Total	4	1804797.2		
	Coefficients	Standard Error	t Stat	P-value
Intercept	1090.858209	340.2999358	3.205578651	0.085080901
LP	0.499537313	0.059665026	8.372363937	0.013967854
WS	-7.112686567	2.460052051	-2.891274827	0.101701646

Table 31 Regression and ANOVA Statistics for 4 mm thickness for Maximum Temperature

Regression Statistics				
Multiple R	0.996072			
R Square	0.992159			
Adjusted R Square	0.984318			
Standard Error	53.18845			
Observations	5			
ANOVA				
	df	SS	MS	F
Regression	2	715925	357962.5	126.5327
Residual	2	5658.023	2829.011	
Total	4	721583		
	Coefficients	Standard Error	t Stat	P-value
Intercept	434.1367	95.64066	4.539248	0.045263
LP	0.299927	0.019422	15.44288	0.004167
WS	-4.28667	0.971084	-4.41431	0.047678

Table 32 Regression and ANOVA Statistics for 6 mm thickness for Maximum Temperature

Regression Statistics				
Multiple R	0.99421654			
R Square	0.98846653			
Adjusted R Square	0.96539959			
Standard Error	43.2743188			
Observations	4			
ANOVA				
	df	SS	MS	F
Regression	2	160495.3633	80247.68	42.85209
Residual	1	1872.666667	1872.667	
Total	3	162368.03		
	Coefficients	Standard Error	t Stat	P-value
Intercept	608.533333	91.37271049	6.659902	0.094881
LP	0.18557333	0.020903482	8.877628	0.07141
WS	-4.57133333	0.790077352	-5.78593	0.108953

Table 33 Regression and ANOVA Statistics for 8 mm thickness for Maximum Temperature

Regression Statistics				
Multiple R	0.975040573			
R Square	0.95070412			
Adjusted R Square	0.90140824			
Standard Error	54.39990809			
Observations	5			
ANOVA				
	df	SS	MS	F
Regression	2	114146.1	57073.05	19.28567
Residual	2	5918.7	2959.35	
Total	4	120064.8		
	Coefficients	Standard Error	t Stat	P-value
Intercept	685.4	118.2494345	5.796222	0.028499
LP	0.0894	0.017202761	5.19684	0.03509
WS	-2.925	0.86013807	-3.40062	0.076662

The regression equations developed for maximum temperature attained with laser power and welding speed as the input variables are given in equations (6.17) to (6.20).

2 mm	$T = 1090 + (0.4995 \times LP) - (7.1126 \times WS)$	(6.17)
4 mm	$T = 434.1367 + (0.2999 \times LP) - (4.2867 \times WS)$	(6.18)
6 mm	$T = 608.53 + (0.1855 \times LP) - (4.57 \times WS)$	(6.19)
8 mm	$T = 685.4 + (0.0894 \times LP) - (2.925 \times WS)$	(6.20)

The predicted and actual values and the corresponding percentage errors are given in Table 34.

Table 34 Actual and Predicted Values of Temperature

Laser Power (Watts)	Welding Speed (mm/s)	Thickness (mm)	Maximum Temperature Attained (°C)	Predicted Temperature (°C)	Percentage Error
2500	60	2	1888	1911.994	1.254920256
3500	140	2	1851	1842.486	-0.462093063
4500	120	2	2545	2484.238	-2.445900916
5500	100	2	2960	3125.99	5.309997793
5500	80	2	3394	3268.242	-3.847879074
2500	80	4	884.7	840.9507	-5.202362041
3500	60	4	1183	1226.5847	3.55333798
4500	140	4	1174	1183.5487	0.806785559
5500	120	4	1545	1569.1827	1.541101619
6500	100	4	1989	1954.8167	-1.748670348
2500	100	6	633	615.28	-2.879989598
3500	80	6	857	892.18	3.943150485
4500	60	6	1187	1169.08	-1.532829233
5500	140	6	989.2	988.98	-0.022245141
2500	120	8	600	557.9	-7.546155225
3500	100	8	651	705.8	7.764239161
4500	80	8	837	853.7	1.956190699
5500	60	8	1031	1001.6	-2.935303514
6500	140	8	857	857	0

Regression models for 10 mm thick plates of aluminium alloy 5083 need a separate study for detailed analysis of effect of laser power and welding speed on the output parameters.

For 2 mm thick plate, 2500 Watt Laser Power with 60 mm/s speed gave weld bead of 4 mm width having a aspect ratio of 2. Increasing laser power is not recommended as it would result in extremely high peak temperatures resulting in undesirable distortions and thermal stresses. Increased Speed is also not recommended as it would decrease the heat input and would also

adversely affect the mechanical strength because of increased porosity content [6]. Weld pool macroscopic shape is also observed to be elliptical at these welding parameters.

Results indicate that for 10 mm thick plate of aluminium alloy 5083 Laser Power higher than 5500 Watt and welding speeds lower than 80 mm/s are to be used. Lower laser powers and higher welding speeds will not be able to develop enough line energy to attain the temperatures required for welding as indicated by the results of simulation cases 9 and 13. Also higher welding speeds result in increased porosity which has detrimental effects on the mechanical strength of the weld. Although welding initiated at 4500 Watts power and 80 mm/s speed but the width of weld bead obtained was not satisfactory. At 5500 Watt and 80 mm/s the peak temperature obtained was 834° C with the width of weld bead 1.24 mm. 1.24 mm is also very narrow and therefore it is recommended to use powers higher than 5500 Watt.

Weld pools of elliptical shape are desired as they favour the growth of fine columnar structures [75]. It is concluded that elliptical weld pools are formed when welding speeds are lower than 100 mm/s for all the specimen thicknesses.

Chapter: 7 Conclusions and Future Recommendations

7.1 Conclusions

The effect of laser power and welding speed for variable thicknesses was analysed for the maximum attained temperature, width of weld bead, HAZ and macroscopic weld pool shape. Regression models were developed for maximum attained temperature and width of weld bead. Macroscopic shape analysis was more like qualitative analysis and hence had no numerical values. For the width of HAZ, the results need to be supported by experimental evidence to be sure of their significance. As experimental setup is not available for experimental evidence of HAZ width the models were not worked upon. The indicative parameters indicate the adequacy of model to describe the behaviour of the model.

Following conclusions are drawn from the study

a. Laser power and welding speed have the opposite effect on net Heat Input. Increased laser power increases the heat input per unit area while decreased speed increases the heat input per unit time for the irradiated area.

b. When laser power is increased weld aspect ratio, fusion zone and HAZ increases. Increase in weld aspect ratio also signifies increase in the width of weld bead for a given thickness while an increase in speed has the opposite effect.

c. For 10 mm thick sheets, laser powers higher than 3500 W and speeds less than 120 mm/s are at least required. Powers lesser than 3500 W and speeds higher than 120 mm/s are not able to attain the welding temperatures.

d. A combination of mid ranged laser powers and higher welding speeds i-e 3500-4500 Watt and speeds equal to or greater than 120 mm/s produce tear drop weld shapes which are undesirable.

e. Desirous Elliptical Weld Pools are produced when welding speeds of 60-100 mm/s are used in combination with low to medium power values according to the specimen thickness used.

f. For weld width and attained temperatures, welding speed is the significant parameter. This is evident from the regression coefficients of the model.

120

The general effect of input parameters on the response parameters was observed to be the same for all specimen thicknesses. However with the increasing thickness, heat conduction in depth increased which reduced the peak welding temperatures attained. It is concluded that for each thickness value the set of recommended laser parameters will differ greatly. Wider the better weld bead criteria is reported from literature as tensile strength increases with increase in the width of weld bead [11]. For each thickness, the best welding parameters from the simulation studies are recommended in Table 35 based on wider the better weld bead, elliptical weld pool shape and higher aspect ratio. Corresponding widths of HAZ are also given.

Table 35 Recommended Values of Laser Parameters for each Specimen Thickness

Specimen Thickness (mm)	Laser Power (Watts)	Welding Speed (mm/s)	Weld bead Width (mm)	Aspect Ratio	Peak Temperature (C)	Weld Pool Shape	HAZ Width (mm)
2	2500	60	4.13	2.06	1888	Elliptical	6.78
4	2500	80	4.5	1.12	884.7	Elliptical	2.12
6	4500	60	2.3	0.4	1187	Elliptical	3.83
8	5500	60	2.12	0.265	1031	Elliptical	3.36
10	6500	60	4.4	0.44	1021	Elliptical	6.4

7.2 Future Recommendations

The present study will provide a strong foundation for extending the research in the area of modelling and simulations for laser welding process. However, Non-availability of laser welding experimental setup in Pakistan is a major bottle neck to extend this work into further studies from experimental point of view.

1. Future Work may be based upon detailed study for each specimen thickness value and predictive thermal model development for attaining a desired value of weld bead width with a certain aspect ratio.

2. Developed thermal model may be extended to thermo-mechanical model for study of stress and distortions.

3. Effect of different laser beam shapes on temperature and stress variations may also be studied.

4. Advanced statistical tools may be used to carry out detailed study of interaction effects of the used laser parameters.

5. Advanced model may be developed considering the metallurgical as well as fluid flow effects for a more detailed study.

References

[1]   X. He, "Finite Element Analysis of Laser Welding: A State of Art Review," *Mater. Manuf. Process.*, vol. 6914, no. September, p. 120813105610000, 2012.

[2]   W. S. Miller *et al.*, "Recent development in aluminium alloys for the automotive industry," *Mater. Sci. Eng. A*, vol. 280, no. 1, pp. 37–49, 2000.

[3]   S. Ferraris and L. M. Volpone, "Aluminium Alloys in Third Millennium Shipbuilding : Materials ," pp. 1–11, 2005.

[4]   D. Wu, X. Hua, F. Li, and L. Huang, "International Journal of Heat and Mass Transfer Understanding of spatter formation in fiber laser welding of 5083 aluminum alloy," *Int. J. Heat Mass Transf.*, vol. 113, pp. 730–740, 2017.

[5]   B. Chang, C. Allen, J. Blackburn, and P. Hilton, "Thermal and fluid flow characteristics and their relationships with porosity in laser welding of AA5083," *Phys. Procedia*, vol. 41, pp. 471–480, 2013.

[6]   M. M. Atabaki, N. Yazdian, and R. Kovacevic, "Partial penetration laser-based welding of aluminum alloy (AA 5083-H32)," *Opt. - Int. J. Light Electron Opt.*, vol. 127, no. 16, pp. 6782–6804, 2016.

[7]   T. Jiang, K. Wang, Z. M. Zhang, W. Fan, and Y. Zeng, "Finite element analysis of laser beam-welded butt joints," *Mater. Sci. Technol.*, vol. 0836, no. April 2015, p. 160113085516002, 2016.

[8]   R. Spina, L. Tricarico, G. Basile, and T. Sibillano, "Thermo-mechanical modeling of laser welding of AA5083 sheets," *J. Mater. Process. Technol.*, vol. 191, no. 1–3, pp. 215–219, 2007.

[9]   X. He, "Numerical Studies on Laser Welding Process," *Appl. Mech. Mater.*, vol. 440, no. 2014, pp. 158–164, 2018.

[10]   M. Dal and R. Fabbro, "An overview of the state of art in laser welding simulation," *Opt. Laser Technol.*, vol. 78, pp. 1–13, 2015.

[11]   N. Kumar, M. Mukherjee, and A. Bandyopadhyay, "Comparative study of pulsed Nd:YAG laser welding of AISI 304 and AISI 316 stainless steels," *Opt. Laser Technol.*, vol. 88, pp. 24–39, 2017.

[12]   M. Harooni, B. Carlson, R. Kovacevic, and D. Street, "Effect of process parameters on the weld quality in laser welding of AZ31B magnesium alloy in lap joint configuration," pp. 509–519, 2012.

[13]   A. Squillace, U. Prisco, S. Ciliberto, and A. Astarita, "Journal of Materials Processing Technology Effect of welding parameters on morphology and mechanical properties of Ti – 6Al – 4V laser beam welded butt joints," *J. Mater. Process. Tech.*, vol. 212, no. 2, pp. 427–436, 2012.

[14] K. Subbaiah, M. Geetha, B. Shanmugarajan, and S. R. K. Rao, "Effect of Welding Speed on CO2 Laser Beam Welded Aluminum- Magnesium Alloy 5083 in H321 Condition," vol. 685, pp. 259–263, 2013.

[15] B. Shanmugarajan, R. Shrivastava, P. Sathiya, and G. Buvanashekaran, "Optimisation of laser welding parameters for welding of P92 material using Taguchi based grey relational analysis," vol. 12, pp. 343–350, 2016.

[16] E. M. Anawa and A. G. Olabi, "Using Taguchi method to optimize welding pool of dissimilar laser-welded components," *Opt. Laser Technol.*, vol. 40, no. 2, pp. 379–388, 2008.

[17] S. Matsuoka, Y. Okamoto, and A. Okada, "Influence of weld bead geometry on thermal deformation in laser micro-welding," *Procedia - Soc. Behav. Sci.*, vol. 6, pp. 492–497, 2013.

[18] J. A. Alcock and B. Baufeld, "Journal of Materials Processing Technology Diode laser welding of stainless steel 304L," *J. Mater. Process. Tech.*, vol. 240, pp. 138–144, 2017.

[19] A. Unt, E. Lappalainen, and A. Salminen, "Autogeneous laser and hybrid laser arc welding of T-joint low alloy steel with fiber laser systems," *Phys. Procedia*, vol. 41, pp. 140–143, 2013.

[20] P. H. O. M. Alves, M. S. F. Lima, D. Raabe, and H. R. Z. Sandim, "Laser beam welding of dual-phase DP1000 steel," *J. Mater. Process. Tech.*, 2017.

[21] M. Idris, S. Ismail, Y. Okamoto, Y. Uno, and R. July, "Numerical Simulation on Micro-welding of Thin Stainless Steel Sheet by Fiber Laser," no. 1, pp. 9–14, 2010.

[22] P. Jiang, C. Wang, Q. Zhou, X. Shao, L. Shu, and X. Li, "Optimization of laser welding process parameters of stainless steel 316L using FEM, Kriging and NSGA-II," *Adv. Eng. Softw.*, vol. 99, pp. 147–160, 2016.

[23] H. Guoming, Z. Jian, and L. Jianqang, "Materials & Design Dynamic simulation of the temperature field of stainless steel laser welding," vol. 28, pp. 240–245, 2007.

[24] K. Y. Benyounis, A. G. Olabi, and M. S. J. Hashmi, "Optimizing the lasubbaser-welded butt joints of medium carbon steel using RSM," *J. Mater. Process. Technol.*, vol. 164–165, pp. 986–989, 2005.

[25] M. N. M Behlouva, E Babalova, "Simulation model of Al-Ti dissimilar laser welding-brazing and its experimental verification Simulation model of Al-Ti dissimilar laser welding-brazing and its experimental verification," in *IOP Conference Series: Materials Science and Engineering 179 012007*, 2017.

[26] C. Fang *et al.*, "Thermal analysis of laser welding for ITER correction coil case," *Fusion Eng. Des.*, vol. 100, pp. 357–363, 2015.

[27] Z. Saternus, W. Piekarska, M. Kubiak, and T. Domański, "Numerical estimation of

temperature field in a laser welded butt joint made of dissimilar materials," vol. 02043, 2018.

[28] S. Meco, L. Cozzolino, S. Ganguly, S. Williams, and N. Mcpherson, "Laser welding of steel to aluminium : Thermal modelling and joint strength analysis," vol. 247, no. July 2016, pp. 121–133, 2017.

[29] H. Vemanaboina, S. Akella, and R. K. Buddu, "Welding Process Simulation Model For Temperature and Residual Stress Analysis," *Procedia Mater. Sci.*, vol. 6, no. Icmpc, pp. 1539–1546, 2014.

[30] C. Su, J. Zhou, Y. Ye, S. Huang, and X. Meng, "Study on fiber laser welding of AA6061-T6 samples through numerical simulation and experiments," vol. 174, pp. 732–739, 2016.

[31] A. F. M. Arif, A. S. Al-Omari, B. S. Yilbas, and Y. N. Al-Nassar, "Thermal stress analysis of spiral laser-welded tube," *J. Mater. Process. Technol.*, vol. 211, no. 4, pp. 675–687, 2011.

[32] B. S. Yilbas, A. F. M. Arif, and B. J. Abdul Aleem, "Laser welding of low carbon steel and thermal stress analysis," *Opt. Laser Technol.*, vol. 42, no. 5, pp. 760–768, 2010.

[33] G. A. Moraitis and G. N. Labeas, "Residual stress and distortion calculation of laser beam welding for aluminum lap joints," vol. 8, pp. 260–269, 2007.

[34] B. Chang, C. Allen, J. Blackburn, and P. Hilton, "Thermal and fluid flow characteristics and their relationships with porosity in laser welding of AA5083," *Phys. Procedia*, vol. 41, pp. 478–487, 2013.

[35] T. Sibillano, A. Ancona, V. Berardi, E. Schingaro, G. Basile, and P. M. Lugara, "A study of the shielding gas influence on the laser beam welding of AA5083 aluminium alloys by in-process spectroscopic investigation," vol. 44, pp. 1039–1051, 2006.

[36] K. Abderrazak, S. Bannour, H. Mhiri, G. Lepalec, and M. Autric, "Numerical and experimental study of molten pool formation during continuous laser welding of AZ91 magnesium alloy," *Comput. Mater. Sci.*, vol. 44, no. 3, pp. 858–866, 2009.

[37] M. Akbari, S. Saedodin, and D. Toghraie, "Optics & Laser Technology Experimental and numerical investigation of temperature distribution and melt pool geometry during pulsed laser welding of Ti6Al4V alloy," *Opt. Laser Technol.*, vol. 59, pp. 52–59, 2014.

[38] R. Wang, Y. Lei, and Y. Shi, "Optics & Laser Technology Numerical simulation of transient temperature field during laser keyhole welding of 304 stainless steel sheet," *Opt. Laser Technol.*, vol. 43, no. 4, pp. 870–873, 2011.

[39] M. Bachmann, V. Avilov, A. Gumenyuk, and M. Rethmeier, "Numerical simulation of full-penetration laser beam welding of thick aluminium plates with inductive support," vol. 035201.

[40] R. Rai and T. Debroy, "Tailoring weld geometry during keyhole mode laser welding

using a genetic algorithm and a heat transfer model," vol. 39, pp. 1257–1266, 2006.

[41]   S. Tsirkas, P. Papanikos, and T. Kermanidis, "Numerical simulation of the laser welding process in butt-joint specimens," *J. Mater. Process. Technol.*, vol. 134, no. 1, pp. 59–69, 2003.

[42]   E. Dezhparvar, N. Yazdian, B. Craft, S. Smith, and R. Kovacevic, "Numerical simulation and experimental validation of residual stress and welding distortion induced by laser-based welding processes of thin structural steel plates in butt joint configuration," *Opt. Laser Technol.*, vol. 104, pp. 170–182, 2018.

[43]   G. Mi, L. Xiong, C. Wang, X. Hu, and Y. Wei, "A thermal-metallurgical-mechanical model for laser welding Q235 steel," *J. Mater. Process. Technol.*, vol. 238, pp. 39–48, 2016.

[44]   M. Zain-ul-Abdein, "Experimental Investigation and Numerical Simulation of Laser Beam Welding Induced Residual Stresses and Distortions in AA 6056-T4 Sheets for Aeronautic Applications," 2009.

[45]   H. Zhao, D. R. White, and T. Debroy, "Current issues and problems in laser welding of automotive aluminium alloys," vol. 44, no. 6, pp. 238–266, 1999.

[46]   S. Elena-manuela, U. T. Brasov, and O. Dontu, "MECHANISM OF KEYHOLE FORMATION," 2017.

[47]   E. Assuncao and S. Williams, "Comparison of continuous wave and pulsed wave laser welding effects," *Opt. Lasers Eng.*, vol. 51, no. 6, pp. 674–680, 2013.

[48]   C. A. Walsh, "LASER WELDING - Literature Review," no. July, p. 21, 2002.

[49]   E. M. Ã. Anawa and A. G. Olabi, "Using Taguchi method to optimize welding pool of dissimilar laser-welded components," vol. 40, pp. 379–388, 2008.

[50]   A. Tahaei *et al.*, "Metallurgical Characterization of a Weld Bead Coating Applied by the PTA Process on the D2 Tool Steel," vol. 21, no. 2, pp. 209–219, 2016.

[51]   A. Internationational, "Weld Solidification *," in *Welding Handbook*, vol. 6, 1997.

[52]   M. M. Atabaki, N. Yazdian, and R. Kovacevic, "Partial penetration laser-based welding of aluminum alloy (AA 5083-," 2016.

[53]   P. H. Chang and T. L. Teng, "Numerical and experimental investigations on the residual stresses of the butt-welded joints," *Comput. Mater. Sci.*, vol. 29, no. 4, pp. 511–522, 2004.

[54]   P. Jiang, C. Wang, Q. Zhou, X. Shao, L. Shu, and X. Li, "Advances in Engineering Software Optimization of laser welding process parameters of stainless steel 316L using FEM , Kriging and NSGA-II," *Adv. Eng. Softw.*, vol. 99, pp. 147–160, 2016.

[55]   P. Okon, G. Dearden, and M. Sharp, "Laser Welding of Aluminium Alloy 5083," no.

May 2014, 2002.

[56] J. Goldak, *Computational welding mechanics*. .

[57] A. Métais, S. Matteï, I. Tomashchuk, and S. Gaied, "Modelling of Transport Phenomena in Laser Welding of Steels," 2015.

[58] I. Tomashchuk, I. Bendaoud, P. Sallamand, E. Cicala, S. Lafaye, and M. Almuneau, "Multiphysical modelling of keyhole formation during dissimilar laser welding," no. 3, 2016.

[59] V. Dhinakaran, S. Khope, N. Siva Shanmugam, and K. Sankaranarayanasamy, "Numerical Prediction of Weld Bead Geometry in Plasma Arc Welding of Titanium Sheets Using COMSOL," no. January, 2016.

[60] Y. Ai *et al.*, "The prediction of the whole weld in fiber laser keyhole welding based on numerical simulation," *Appl. Therm. Eng.*, vol. 113, pp. 980–993, 2017.

[61] W. Liu, J. Ma, F. Kong, S. Liu, and R. Kovacevic, "Numerical Modeling and Experimental Verification of Residual Stress in Autogenous Laser Welding of High-Strength Steel," *Lasers Manuf. Mater. Process.*, vol. 2, no. 1, pp. 24–42, 2015.

[62] A. M. Sifullah, Y. Nukman, and M. A. Hassan, "3D FEM Simulation to Predict the Heat Affected Zone during Laser Machining on Stainless," pp. 3–6, 2015.

[63] T. Jiang *et al.*, "Finite element analysis of laser beam-welded butt joints Finite element analysis of laser beam-welded butt joints," vol. 0836, no. January, 2016.

[64] S. Shanmugam, "Numerical and Experimental Investigation of Laser Beam Welding of Aisi 304 Stainless Steel Sheet," *Adv. Prod. Eng. Manag.*, vol. 3, pp. 93–105, 2008.

[65] K. Ho-Le, "Finite element mesh generation methods: a review and classification," *Comput. Des.*, vol. 20, no. 1, pp. 27–38, 1988.

[66] A. Haboudou, P. Peyre, A. B. Vannes, and G. Peix, "Reduction of porosity content generated during Nd: YAG laser welding of A356 and AA5083 aluminium alloys," *Mater. Sci. Eng. A*, vol. 363, no. 1–2, pp. 40–52, 2003.

[67] SteinarLundberg, "Material Aspects of Fire Design 2502 Material Aspects of Fire Design Contents," 1997.

[68] M. M. El-Sayed, A. Y. Shash, and M. Abd-Rabou, "Finite element modeling of aluminum alloy AA5083-O friction stir welding process," *J. Mater. Process. Technol.*, vol. 252, no. September, pp. 13–24, 2018.

[69] P. Okon, G. Dearden, K. Watkins, M. Sharp, and P. French, "Laser welding of aluminium alloy 5083," *Proc. Int. Congr. Appl. Lasers Electro-Optics (Laser Inst. Am. 2002)*, vol. 54, no. Icaleo, p. 258, 1969.

[70] ASM International, "Properties and Characteristics of Aluminum and Aluminum Alloys,"

2016.

[71]   K. Y. Benyounis, A. G. Olabi, and M. S. J. Hashmi, "Effect of laser welding parameters on the heat input and weld-bead profile," *J. Mater. Process. Technol.*, vol. 164–165, pp. 978–985, 2005.

[72]   A. Ancona *et al.*, "Comparison of two different nozzles for laser beam welding of AA5083 aluminium alloy," *J. Mater. Process. Technol.*, vol. 164–165, pp. 971–977, 2005.

[73]   T. Sibillano, A. Ancona, V. Berardi, and P. M. Lugarà, "Real-time monitoring of laser welding by correlation analysis: The case of AA5083," *Opt. Lasers Eng.*, vol. 45, no. 10, pp. 1005–1009, 2007.

[74]   G. Magudeeswaran, S. R. Nair, L. Sundar, and N. Harikannan, "Optimization of process parameters of the activated tungsten inert gas welding for aspect ratio of UNS S32205 duplex stainless steel welds," *Def. Technol.*, vol. 10, no. 3, pp. 251–260, 2014.

[75]   A. Internationational, "Weld Solidification *," vol. 6, 1997.

[76]   A. Mishra, "Friction Stir Welding of Dissimilar Metal: A," no. January, 2018.

Appendix-A

```fortran
SUBROUTINE DFLUX(FLUX,SOL,KSTEP,KINC,TIME,NOEL,NPT,COORDS,
     1 JLTYP,TEMP,PRESS,SNAME)
C
      INCLUDE 'ABA_PARAM.INC'
C
      DIMENSION FLUX(2), TIME(2), COORDS(3)
      CHARACTER*80 SNAME
      REAL :: x,y,z
      REAL :: v,t
      REAL :: zl,xl
      REAL :: P,nom_power
      REAL :: re,ri,ye,yi,rc
      Double precision : : ro

C     Define laser parameter
      re=0.00069
      ri=0.0003
      ye=0.000
      yi=-0.0027
      P=3000.0

C     Get coordinates of current point
          x=COORDS(1)
          y=COORDS(2)
          z=COORDS(3)

C     Current time
      t=TIME(2)

C     Fixed position of laser (x)
      xl=0
C     Changing position of laser (y)
      zl=triag(t)

C     Distance of current point from laser center

      ro=0.00069+(0.1444444444)*y

      nom_power= 5.4701E12

      rc=SQRT((x-xl)**2+(z-zl)**2)
      IF  (ro>0)  THEN

      FLUX(1)=nom_power*exp(-3*rc**2/ro**2)

      ELSE
      FLUX(1)=0

      END IF

C     Flux temperature derivative
      FLUX(2)=0
      RETURN
      END
C
```

Block-1

Block-2

Block-3

Block-4

```fortran
C     Triangle wave function
C
      REAL FUNCTION triag(t)
C     Length, velocity and phase need to be defined
C     Phase: pi/2->start->y=0, -pi->start->-L/2, pi->start->L/2
      REAL :: t
      REAL, parameter :: M_PI =
    1 3.14159265358979323846264338327950290d0
      REAL :: L, period,v,phi
      L=0.05
      v=0.14167
      period=2*L/v
      phi=-M_PI
      triag = L/2*((abs(mod(abs(2*M_PI*t/period-phi),2.0*M_PI)-M_PI)/
    1 M_PI*2.0d0)-1d0)
      END function triag
```

Block-5

130

Appendix B

```fortran
      SUBROUTINE DFLUX(FLUX,SOL,KSTEP,KINC,TIME,NOEL,NPT,COORDS,
     1 JLTYP,TEMP,PRESS,SNAME)
C
      INCLUDE 'ABA_PARAM.INC'
C
      DIMENSION FLUX(2), TIME(2), COORDS(3)
      CHARACTER*80 SNAME
      REAL :: x,y,z
      REAL :: v,t
      REAL :: zl,xl
      REAL :: P,nom_power
      REAL :: re,ri,ye,yi,rc
      Double precision : : ro

C     Define laser parameter
      re=0.0006
      ri=0.00054
      ye=0.000
      yi=-0.002
      P=2500
      absorptivity=100




C     Get coordinates of current point
      x=COORDS(1)
      y=COORDS(2)
      z=COORDS(3)

C     Current time
      t=TIME(2)

C     Fixed position of laser (x)
      zl=triag(t)
C     Changing position of laser (y)
      xl=0

C     Distance of current point from laser center

      ro=0.0006+(0.02)*y

      nom_power=2.210485321e12

      rc=SQRT((x-xl)**2+(z-zl)**2)
      IF  (ro>0)  THEN

      FLUX(1)=nom_power*exp(-3*rc**2/ro**2)

      ELSE
      FLUX(1)=0

      END IF

C     Flux temperature derivative
      FLUX(2)=0
```

Block-1

Block-2

Block-3

Block-4

131

```fortran
      RETURN
      END
C
C     Triangle wave function
C
      REAL FUNCTION triag(t)
C     Length, velocity and phase need to be defined
C     Phase: pi/2->start->y=0, -pi->start->-L/2, pi->start->L/2
      REAL :: t
      REAL, parameter :: M_PI =
     1  3.141592653589793238462643383279502d0
      REAL :: L, period,v,phi
      L=0.05
      v=0.1
      period=2*L/v
      phi=-M_PI
      triag = L/2*((abs(mod(abs(2*M_PI*t/period-phi),2.0*M_PI)-M_PI)/
     1 M_PI*2.0d0)-1d0)
      END function triag
```

Block-5